PROCESS INTENSIFICATION IN OCTENE HYDROGENATION:

APPLICATION OF CERIUM-PROMOTED PLATINUM ON ALUMINA ($Ce–Pt/Al_2O_3$) NANOCATALYSTS AND ULTRASONIC IRRADIATION IN A SLURRY PHASE REACTOR

Obert Mupomoki

MSc. Eng. (Chemical Engineering), University of KwaZulu-Natal, South Africa

B.Eng. (Chemical Engineering), National University of Science and Technology, Zimbabwe

Submitted in fulfilment of the academic requirements for the degree of Doctor of Philosophy in the School of Engineering, Discipline of Chemical Engineering,

University of KwaZulu-Natal, Durban.

December 2023

Supervisor: Professor David Lokhat

Declaration

I, Obert Mupomoki, declare that:

(i) The research reported in this dissertation/thesis, except where otherwise indicated, is my original work.

(ii) This thesis has not been submitted for any degree or examination at any other university.

(iii) This thesis does not contain other persons' data, pictures, graphs, or other information unless specifically acknowledged as being sourced from other persons.

(iv) This thesis does not contain other persons' writing unless specifically acknowledged as being sourced from other researchers. Where other written sources have been quoted, then:

a) their words have been re-written but the general information attributed to them has been referenced;

b) where their exact words have been used, their writing has been placed inside quotation marks and referenced.

(v) This thesis does not contain text, graphics or tables copied and pasted from the internet, unless specifically acknowledged, and the source being detailed in the thesis and in the References sections.

Signed:  Date: 08/07/2024

As the candidate's Supervisor, I agree to the submission of this thesis

Professor David Lokhat

Acknowledgments:

I would like to acknowledge Sasol and the National Research Foundation for the financial support during the course of my studies.

A special thanks to my supervisor, Professor David Lokhat, who greatly enriched my knowledge and constantly motivated and inspired me during the course of this work.

I am thankful to the Chemical Engineering analytical laboratory technicians, Nomthandazo Hadebe, Thobekile Mofokeng, Sizamina Madwe, and Trevor for providing the practical support and help within the laboratory and all necessary facilities for some parts of my experiments. I also want to thank the department's workshop technicians for the assistance provided throughout my research. I express warm thanks to Subashen, Vishal Bharuth and Phillip Christopher from the Microscopy Unit at UKZN, Westville Campus for the assistance and help with the electron microscopy analyses.

Many thanks to my fellow students Phakamile Ndlovu, Farai Matizakurima, Mehul Shah, Kashmita Ramlal, Rakhi Rampersad, Trenelle Moodley and Edward Marondedze and all my friends and laboratory members for the help, friendliness, and meaningful and thought-provoking research-related and general discussions.

Finally, I would like to thank my family for the love, support, and patience they have shown to me and with that I would like to dedicate my whole work to them. Overall, I thank God Almighty for the grace as well as strength to accomplish this work successfully.

Abstract:

In catalytic reactions, the implementation of sonochemistry has emerged as a critical driver for enhancing reaction kinetics and selectivity, particularly in slurry phase reactions where mass transfer resistance is significant. Sonochemistry's applicability extends across diverse chemical domains, including the hydrogenation of alkenes which is an area of significant industrial relevance. The hydrogenation of 1-octene, a reaction facilitated by metal catalysts such as nickel, palladium, platinum, and rhodium, epitomizes such a process with substantial implications for the production of high-octane fuels and an array of fine chemicals. This work delved into the synergy between ultrasonic irradiation and nanocatalysis within the specific context of 1-octene hydrogenation. The study methodically investigated the integration of ultrasonic irradiation in a three-phase slurry reactor employing Ce-promoted Pt/Al_2O_3 nanocatalysts. This approach is targeted at propelling process efficiency and extending the functional longevity of the catalysts in the hydrogenation reaction. Central to this investigation is the impact of ultrasonic waves on the hydrogenation rate and the deactivation patterns of the Ce-promoted Pt/Al_2O_3 nanocatalysts. The study involved the use of a three-phase slurry reactor to facilitate optimal interaction among the solid catalyst, liquid 1-octene, and gaseous hydrogen. Ultrasonic irradiation, which is believed to enhance inter-phase contact and improve mass transfer through the dynamic action of cavitation microbubbles was a focal experimental variable. These microbubbles are known to create localized hotspots of high temperature and pressure upon collapse, ostensibly promoting more efficient chemical interactions. In this study, the framework was divided into three segments: the first one involved the microscopic characterisation of the Ce-promoted Pt/Al_2O_3 nanocatalysts using transmission electron microscopy, TEM, high-resolution transmission electron microscopy (HR – TEM), scanning electron microscopy (SEM) and scanning electron microscopy with energy dispersive X-Ray analysis (SEM – EDX) analyses. The second segment evaluated the hydrogenation reactions with and without sonication across a temperature gradient using fresh catalyst, and the third one assessed the system's performance over various reaction durations at a constant temperature of 50 °C while incorporating catalyst recycling. System performance was measured and quantified based on the conversion of 1-octene and the yield of hydrogenated products (octanes), quantified using gas chromatography with a flame ionisation detector (GC – FID). The findings revealed conversions reaching upwards of 97%, particularly at modest temperatures of 40 °C and 50 °C temperatures using the Ce-promoted Ce-Pt/Al_2O_3 nanocatalysts under ultrasonic irradiation. The results also revealed that for twice-reused catalysts, sonication had a pronounced effect on prolonging catalyst activity. Sonicated reactions exhibited a conversion rate of 76.3%, which was significantly higher than the 60.3% conversion of their unsonicated counterparts. The experimental results provided clear evidence that ultrasonic irradiation enhanced the catalytic performance by increasing molar conversion, improving product yield, and reducing the onset of deactivation phenomena such as coking and sintering.

Table of Contents

List of Tables:

List of Figures:

Chapter 1

Introduction

1.1 Background study:

Octene hydrogenation is a fundamental and industrially important chemical reaction that involves the addition of hydrogen to 1-octene, resulting in the formation of octane and other hydrogenated products. This addition reaction is commonly used in the petroleum and petrochemical industries for the production of high-octane fuels and as a key step in the synthesis of various fine chemicals (Chetty et al., 2018). The selective hydrogenation of alkenes such as 1-octene is typically performed in the presence of metal catalysts that includes nickel, palladium, platinum, or rhodium, which facilitate the activation of hydrogen and its subsequent addition to the double bond. The development of efficient and efficacious catalysts for octene hydrogenation is of great importance due to the increasing demand for clean and sustainable energy sources. Octane, which is the major product of octene hydrogenation, is a crucial component of gasoline and plays a vital role in the automotive industry. Improving the efficiency of octene hydrogenation processes can lead to reduced energy consumption, decreased environmental impact, and enhanced production of high-quality fuels.

Currently, hydrogenation reactions are being carried out in traditional fixed-bed, fluidized-bed reactors and slurry phase reactors but in recent years slurry reactors have found widespread use in most hydrogenation processes in the fine chemicals industry (Elias et al., 2015). One of the primary benefits of a slurry phase reactor is its ability to operate under milder conditions, achieve improved selectivity, reduce catalyst decay, and seamlessly integrate with advanced process intensification techniques like ultrasonic irradiation and microwave-assisted catalysis. In recent years, significant research efforts have been focused on enhancing the performance of catalysts and optimizing reaction conditions for octene hydrogenation. For instance, (Amaniampong and Jérôme, 2020, Takahashi et al., 1997) investigated the hydrogenation of 1-octene over a series of supported nickel catalysts. The authors demonstrated that the type of support material significantly influenced the catalytic activity and selectivity towards octane. They found that nickel catalysts supported on mesoporous silica exhibited higher activity and improved selectivity compared to other support materials. Furthermore, the development of nanocatalysts has shown great potential for improving the efficiency and selectivity of octene hydrogenation. Nanocatalysts possess high surface area, well-defined structures, and tailored surface properties, which can enhance reactant accessibility and promote the adsorption and activation of reactant molecules (Yang et al., 2022; Alkadevi et al., 2019). In a recent study, (Liu et al., 2020) investigated butadiene hydrogenation using bimetallic Au–Pt bimetallic nanoparticle catalysts supported on UiO-67. The

authors reported enhanced catalytic activity and selectivity towards total butenes compared to monometallic catalysts. The synergistic effect between Au and Pt in the bimetallic nanoparticles resulted in improved hydrogenation performance.

In addition to catalyst design, the optimisation of reaction conditions plays a crucial role in the efficiency of octene hydrogenation. Process intensification techniques, such as ultrasonic irradiation, have been explored to enhance mass transfer and reaction rates in other slurry phase reactions (Constantino et al., 2022; Kumar et al., 2022). Sonochemistry, which involves the application of ultrasonic waves, generates cavitation microbubbles that create regions of localised high temperature and pressure and therefore facilitating improved contact between the solid catalyst particles, liquid reactant, and gaseous hydrogen (Wang et al., 2021). A recent study by Amaniampong and Jérôme, (2020) investigated the influence of ultrasonic irradiation on the reaction rate and catalyst deactivation on catalytic reactions. Their work examined the effects of ultrasound on catalytic reactions, particularly focusing on the generation of cavitation bubbles that impact catalyst surfaces. Utilizing high-frequency ultrasound (300-800 kHz), the researchers observed that this technique leads to the formation of a large amount of small cavitation bubbles, which enhance the generation of reactive radicals. These conditions result in significant chemical reactions, such as the sonolysis of water, which produces hydroxyl radicals. The results showed that ultrasonic irradiation significantly enhanced the reaction rate and improved the overall catalytic performance. Humblot et al., (2022) also demonstrated the cleavage of the N−H bond in NH_3 within cavitation bubbles when they looked at the sonochemical reduction of alkenes to alkanes using ammonia. These bubbles were generated through high-frequency ultrasonic irradiation, resulting in the in-situ formation of diimide. Subsequently, diimide facilitates the hydrogenation of alkenes. Importantly, this process eliminates the need for any transition metals and exclusively generates N_2 as a co-product (Humblot et al., 2022). Disselkamp and colleagues conducted a study examining the impact of sonication on the hydrogenation versus isomerization of 3-buten-1-ol in the presence of palladium black within a water medium (Disselkamp et al., 2004). Their research demonstrated that the application of ultrasound during the hydrogenation/isomerization process of 3-buten-1-ol resulted in a rapid in-situ reduction of Pd black. This reduction was brought about by the implosion of cavitation bubbles on the Pd surfaces, ultimately resulting in a fivefold enhancement of the reaction rate.

These studies underscore the profound effects of ultrasonic irradiation on reaction kinetics and catalyst performance. By leveraging the energy released from cavitation bubble collapse, ultrasonic irradiation can enhance mass transfer and surface reactions, presenting a transformative approach to catalytic processes. Consequently, it therefore can be concluded that the optimisation of catalyst design and reaction conditions for octene hydrogenation is crucial for improving process efficiency and achieving high selectivity towards octane. The development of efficient nanocatalysts such as supported nickel catalysts and bimetallic nanoparticles has shown promise in enhancing catalytic performance.

Furthermore, the application of process intensification techniques, including ultrasonic irradiation, has the potential to intensify the reaction and improve mass transfer in slurry phase systems. These advancements contribute to the development of more sustainable and energy-efficient processes for octene hydrogenation, hence enabling the production of high-quality fuels and specialty chemicals while reducing the environmental impact. Continued research in this area will lead to further improvements in catalyst design, reaction optimisation, and process intensification for octene hydrogenation.

1.2 Process intensification in chemical reactions:

Process intensification is a multidisciplinary approach that aims to enhance the efficiency, productivity, and sustainability of chemical reactions. It involves the development and integration of innovative techniques, such as advanced catalysts, novel reactor designs, and the application of external energy sources, to overcome limitations associated with conventional reaction systems (Haase et al., 2022; Gogate, 2008; Stankiewicz and Moulijn, 2004). Process intensification strategies can lead to significant improvements in reaction kinetics, selectivity, and overall process performance. One example of process intensification is the utilization of structured catalysts with high surface area and tailored morphology. Structured catalysts provide improved mass and heat transfer properties, thereby enhancing reaction rates and selectivity (Nijhuis et al., 2019). In a recent study by Li et al., (2021), the authors investigated the application of hierarchical zeolite catalysts for the methanol-to-olefin (MTO) reaction. The hierarchical structure of the catalyst resulted in enhanced diffusion and reduced coke formation, leading to improved MTO selectivity and stability. Similarly, Lin et al., (2014) and Ebrahimi et al., (2016) employed a hierarchical catalyst composed of a zeolitic imidazolate framework for the selective oxidation of sulphides to sulphoxides (Ebrahimi et al., 2016).

The hierarchical structure of the catalyst facilitated mass transfer and improved catalytic performance.

Another approach to process intensification involves the use of advanced reactor designs, such as microreactors and membrane reactors. Microreactors offer superior heat and mass transfer characteristics due to their small dimensions, leading to improved reaction rates and reduced reactant residence times (Abdulla Yusuf et al., 2022; Veeramani et al., 2018). In a study by Aghel et al., (2014), a microreactor system was developed for the synthesis of biodiesel via transesterification (Aghel et al., 2014). The authors reported significantly higher yields and reaction rates compared to conventional batch reactors, highlighting the benefits of process intensification. Similarly, Crole et al., (2020) utilized a membrane reactor system for the continuous synthesis of hydrogen peroxide from hydrogen and oxygen and their yields were higher than conventional reactors (Crole et al., 2020; Inoue et al., 2010; Yamanaka et al., 2017). The integration of a catalytic membrane enabled high hydrogen peroxide selectivity and reduced reactant crossover, resulting in improved process efficiency.

External energy sources, such as microwave irradiation, ultrasound, and plasma, have also been employed to intensify chemical reactions. These energy sources can enhance mass and heat transfer, activate catalysts, and significantly facilitate reaction pathways that produce desired products (Strekalova et al., 2023). For instance, microwave-assisted catalysis has been applied in various reactions, including esterification, hydrogenation, and oxidation, resulting in accelerated reaction rates and improved yields (Mohamad et al., 2021). In a recent publication by Patel et al., (2021), the authors demonstrated the use of microwave irradiation for the selective hydrogenation of nitroaromatic compounds, achieving high conversion and excellent selectivity towards the desired products (Patel et al., 2021). Their study reports impressive yields for the hydrogenation of nitroarene derivatives to aromatic amines, achieving 85% - 96% within 10 minutes at 120°C and 50 W. Further, the one-pot synthesis of imines was optimized to achieve a 95% yield under microwave conditions by adding dimethyl sulfoxide. Similarly, ultrasound-assisted catalysis has gained attention for its ability to enhance reaction rates and promote mass transfer. Vaitsis et al., (2020) reported the sonochemical synthesis of metal-organic frameworks (MOFs) using ultrasound irradiation. In their study, the use of ultrasound resulted in rapid MOF formation and improved porosity of the synthesized materials. The sonochemical synthesis of these metal-organic frameworks (MOFs) demonstrated significant efficiency in particle size and yield optimization. For example, HKUST-1 was prepared using a combination of $NaNO_3$ and H_3BTC under ultrasound irradiation, achieving a crystallite size range of 22.28 nm to 47.05 nm and a yield of 92% after 15 minutes at a current density of 135.5 mA/cm^2. Similarly, the synthesis of Ni-BTC showed a yield increase from 29% to 88% by adjusting the power level from 40% to 80% and optimizing the temperature to 60°C. Their results also demonstrated that ultrasonic irradiation significantly enhanced the MOF synthesis rate and improved the textural properties of the obtained materials.

Additionally, sonochemistry, which involves the application of ultrasonic waves in liquid systems, has shown promise in intensifying chemical reactions through improved mass transfer and localized energy generation (Yin et al., 2021). Ultrasonic irradiation creates cavitation microbubbles, leading to enhanced mixing, increased contact between reactants, and improved reaction kinetics (Vaitsis et al., 2020). Ultrasonic irradiation can also be applied to processes that removes pollutants from wastewaters. For example, Khan et al., (2022) employed ultrasonic irradiation to enhance the degradation of organic pollutants in water through the formation of reactive species and improved mass transfer (Ang et al., 2022; Khan et al., 2022). In their study, they focused on the enhanced degradation of organic pollutants using a novel Pt/CeO_2 sonophotocatalyst. Their observation was that the bare CeO_2 catalyst showed poor photocatalytic activity (10%) under visible light due to its wide bandgap, while Pt decorated CeO_2 significantly improved the degradation efficiency, achieving 65% degradation in 30 minutes. The combined sonophotocatalysis approach further enhanced the degradation efficiency to 95% within the same duration. This improvement was attributed to the generation of additional hydroxyl radicals ($OH^{\bullet}$)

and superoxide radicals ($O_2^{\bullet-}$) under ultrasonic waves, which greatly accelerates the breakdown of pollutants. The study concluded that Pt/CeO_2 nanocomposites exhibit remarkable stability and reusability, maintaining high activity over multiple cycles, thus highlighting their potential for effective environmental remediation and solar energy applications. All these improvements are as a results of the formation of cavitation bubbles that form during sonication and act as intensified microreactors. Figure 1.1 shows how cavitational bubbles are produced during sonication using an ultrasonic probe.

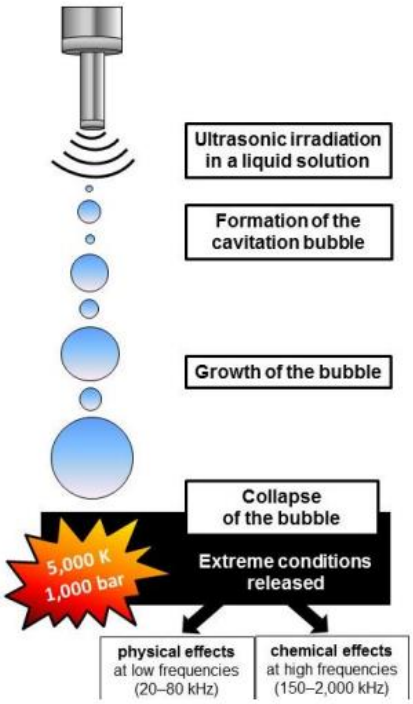

Figure 1. 1: Cavitation phenomenon at the origin of the effects provided under power ultrasound. Source: Chatel, (2019).

All these examples highlight the diverse range of process intensification strategies employed in recent literature implying that advanced catalysts, novel reactor designs, and the integration of external mechanical energy sources have shown great potential in enhancing reaction rates, selectivity, and overall process efficiency. By implementing process intensification approaches, researchers are trying to address the limitations of traditional reaction systems and pave the way for more sustainable and cost-effective chemical processes. Continued exploration and development of process intensification techniques will contribute to the advancement of catalysis and chemical engineering, enabling the design of more efficient and environmentally friendly chemical processes. More importantly, the successful combination of these techniques in processes like octene hydrogenation could pave the way for the development of intensified modular reactors, which can be mobile and more versatile. These reactors are usually compact, highly efficient, and adaptable, allowing for their application across various chemical processes, from hydrogenation reactions to Fischer-Tropsch synthesis and beyond (Konarova et al., 2022).

The proposition of intensified modular reactors materializes as a quintessentially innovative approach, which enables unprecedented flexibility and adaptability in process design and implementation. Modular systems serve as agile platforms that facilitate the optimization of various processes according to the unique characteristics and requirements of different feedstock sources. Such design ethos encourages the exploitation of localized resources, thereby improving the economic feasibility and sustainability of chemical processes, particularly in regions marked by disparate availability and diversity of raw materials. Modularity and intensification would lead to processes that are not only more efficient but also more environmentally friendly and cost-effective (Pudi et al., 2022). By establishing a proof of concept in octene hydrogenation, the opportunity arises to extrapolate this successful integration of technologies to other processes such as the Fischer-Tropsch synthesis as well as environmental remediation processes that deal with the removal of pollutants in wastewater, which is a hot topic due to portable water scarcity around the world. In doing so, the potential to revolutionize the production of fine chemicals and other value-added products is immense. The application of ultrasonic irradiation could signify a departure from the use of traditionally large and inefficient systems to processes characterized by enhanced productivity, flexibility and sustainability.

1.3 Overview of nanocatalysts and ultrasonic irradiation:

Nanocatalysts have gained significant attention in recent years due to their unique properties and enhanced catalytic performance. These catalysts, typically composed of metal or metal oxide nanoparticles supported on high-surface-area materials exhibit high surface-to-volume ratios, well-defined structures, and tailored surface properties, which can significantly influence their catalytic activity and selectivity (Chavali and Nikolova, 2019, Liu and Corma, 2018). The application of nanocatalysts in various chemical reactions, including hydrogenation processes has shown promising results in terms of reaction efficiency and product selectivity.

In the field of hydrogenation reactions, several studies have explored the use of nanocatalysts for improving catalytic performance. For instance, Dobrezberger et al., (2020) investigated the hydrogenation of alkenes using Pd-based nanoparticles supported on carbon materials (Dobrezberger et al., 2020). The authors demonstrated that the use of nanocatalysts resulted in higher catalytic activity and selectivity compared to conventional catalysts. In this study, the authors investigated the hydrogenation activity of palladium (Pd) nanoparticles supported on graphene nanoplatelets (GNPs) compared to those on activated carbon (Pd/C) and γ-alumina (Pd/Al_2O_3). During the reaction, Pd/GNPs, with mean particle sizes of approximately 4 nm exhibited 3 – 4 times higher activity at 55 °C than Pd/C and Pd/Al_2O_3, which was attributed to the additional hydrogen supply from the GNPs. The Pd hydride formed during ethylene hydrogenation was more stable in Pd/GNPs than in Pd/C, indicating better hydrogen availability. These reactions were carried out at temperatures ranging from 25 °C to 55 °C, with the reaction rates normalized per gram of Pd and per Pd surface atom, achieving conversions

between 0.5% to 51%. The high surface area and unique surface properties of the nanoparticles usually facilitates the adsorption and activation of reactant molecules, leading to improved reaction rates and selectivity.

Besides single-metal catalysts, bimetallic nanocatalysts have also garnered attention in this area due to their synergistic effects and enhanced catalytic properties. Taylor et al., (2021) explored the hydrogenation of unsaturated compounds using bimetallic nanoparticles composed of Pt and other transition metals. The authors reported that the incorporation of a second metal in the nanoparticle structure led to improved catalytic performance, including increased reaction rates and enhanced selectivity towards desired products (Taylor et al., 2021; Louis and Delannoy, 2019). In particular, they observed that an ultra-dilute alloy (UDA) with a Pt:Cu atomic ratio of 1:20 exhibited exceptionally high initial hydrogenation rates under hydrogen pressures of 10 and 20 bar, achieving high selectivity for furfuryl alcohol, and matching or exceeding the performance of a monometallic Pt catalyst containing twelve times more Pt. The study was conducted under batch conditions at a temperature of 50 °C using methanol as the solvent, showed that the pure Pt (Pt_{100}) catalyst achieved near-complete conversion with high selectivity towards furfuryl alcohol and minimal by-products, including a 0.2% selectivity for tetrahydrofurfuryl alcohol (THFA) at 20 bar. The $Pt_{38}Cu_{62}$ and $Pt_{18}Cu_{82}$ alloys maintained high conversion rates with a slight drop in selectivity at lower pressures, while the Pt_1Cu_{20} alloy exhibited high initial rates post-induction period at 10 and 20 bar.

In addition to nanocatalysts, the integration of ultrasonic irradiation as a process intensification technique has shown great potential in enhancing catalytic reactions. Sonochemistry, which involves the application of ultrasonic waves, generates cavitation microbubbles in the reaction mixture. These microbubbles undergo rapid growth and collapse, creating localized regions of high temperature and pressure. The phenomenon of cavitation-induced acoustic streaming and shockwaves promotes better mixing, mass transfer, and reaction kinetics (Stebeleva and Minakov, 2021; Dong et al., 2020; Sancheti and Gogate, 2017).

Several studies have demonstrated the benefits of ultrasonic irradiation in catalytic reactions. For example, Tripathi et al., (2015) investigated the ultrasound-assisted selective hydrogenation of C-5 acetylene alcohols with Lindlar catalysts. The authors found that the sonication resulted in the breaking of polycrystalline support particles, with the degree of fracture varying depending on the frequency of ultrasound used (Tripathi et al., 2015). The most significant impact was observed with 40 kHz sonication, whereas monocrystals remained unaffected. Interestingly, the dissolution of Pd/Pb particles did not exhibit frequency dependence, indicating that sonication selectively removed catalyst particles that were loosely bound. The formation of cavitation microbubbles facilitated the dispersion of reactants and improved mass transfer, leading to improved catalytic performance.

Furthermore, ultrasonic irradiation has been shown to enhance the stability and recyclability of catalysts. Li et al., (2023) studied the hydrogenation of nitrobenzene using a supported Pd catalyst under ultrasonic irradiation. The authors observed that the application of ultrasound not only improved the reaction rate but also reduced catalyst deactivation and allowed for multiple reaction cycles without significant loss of activity. The catalysts, with 1% and 3% Pt loadings achieved a 90% yield of aniline in just 40 minutes at ambient temperature and atmospheric pressure. It was therefore postulated that ultrasonic waves assisted the removal of reaction by-products and prevented catalyst fouling, leading to improved catalyst stability and longevity.

A combined force involving nanocatalysts and ultrasonic irradiation therefore offers exciting opportunities for enhancing catalytic reactions, including hydrogenation processes. Nanocatalysts with their high surface area and tailored properties exhibit improved catalytic performance and selectivity. The integration of ultrasonic irradiation as a process intensification technique enhances mass transfer, reaction kinetics, and catalyst stability. Through the formation of cavitation microbubbles, ultrasound promotes better mixing and dispersion of reactants, leading to improved catalytic performance and as stated before, ultrasonic irradiation can aid in the removal of reaction by-products, preventing catalyst fouling and enhancing catalyst recyclability. By combining the advantages of nanocatalysts and ultrasonic irradiation, this study explored the synergistic effects and catalytic performance improvement in the hydrogenation of 1-octene. Through a comprehensive experimental investigation, this research sought to understand the underlying mechanisms and provide valuable insights for future developments in the field of catalysis and reaction engineering.

1.4 Aim of this research:

The field of catalytic hydrogenation has seen significant advancements yet critical gaps persist that warrant further investigation. This study aims to address these gaps by systematically exploring the role of ultrasonic irradiation in the hydrogenation of 1-octene using nano-sized Ce-Pt/Al_2O_3 catalysts within a three-phase slurry reactor. The focus of this research is to elucidate the synergistic effects of ultrasonic irradiation and nanocatalysis, particularly in the context of process intensification.

In order to achieve this aim, it is imperative to first identify and understand the existing gaps in the literature that this research seeks to bridge. The primary research gaps identified are as follows:

1. **Effect of ultrasonic irradiation:** While ultrasonic irradiation is known to enhance reaction kinetics, its precise impact on catalyst performance and longevity during 1-octene hydrogenation remains underexplored. This study aims to fill this gap by providing a detailed analysis of how ultrasonic waves influence catalyst activity and stability over extended reaction periods.

2. **Synergistic effects of nanocatalysis and ultrasonics:** The integration of nanocatalysts with ultrasonic irradiation represents a promising yet under-researched area. This study seeks to uncover the synergistic benefits of combining Ce-promoted Pt/Al_2O_3 nanocatalysts with ultrasonic irradiation in a three-phase slurry reactor, thereby advancing our understanding of process intensification and reaction efficiency.
3. **Catalyst deactivation patterns:** A significant challenge in catalytic hydrogenation is catalyst deactivation, including issues such as coking and sintering. Existing literature lacks comprehensive insights into how ultrasonic irradiation affects the deactivation patterns of Ce-promoted Pt/Al2O3 nanocatalysts. This research addresses this gap by investigating the long-term stability and deactivation mechanisms under ultrasonic conditions.
4. **Comparative kinetic studies:** Detailed kinetic studies comparing sonicated and unsonicated conditions in octene hydrogenation are sparse. This study aims to provide a comparative analysis, elucidating the kinetic advantages and potential trade-offs of employing ultrasonic irradiation. Such insights are crucial for optimizing reaction conditions and enhancing overall process efficiency.

Through addressing these gaps, this research not only advances scientific knowledge but also contributes to the development of more efficient and sustainable hydrogenation processes. By bridging these gaps, the study offers a comprehensive understanding of the interplay between ultrasonic irradiation and nanocatalysis, thereby informing the design and operation of advanced catalytic systems.

1.5 Research questions:

In the dynamic realm of chemical engineering and catalysis, the imperative to innovate and enhance process efficiencies continually shapes research trajectories. The convergence of ultrasonics and nanocatalysis offers a promising avenue for advancing the frontiers of catalytic reactions, particularly in hydrogenation processes. As the global scientific community ardently seeks pathways to sustainable and efficient chemical processes, this research anchors its focus on the hydrogenation of 1-octene, utilizing ultrasonic irradiation and nanosized $Ce\text{-}Pt/Al_2O_3$ catalyst within a three-phase slurry reactor. This thesis aspires to unravel the intricacies and potential enhancements to the hydrogenation process through the innovative application of ultrasonic irradiation, thereby enabling a better understanding of its influence on reaction rates and catalyst longevity. The confluence of these two cutting-edge technologies holds the promise of unlocking new dimensions of efficiency and optimization in catalytic processes.

In light of the identified research gaps, this study aims to address the following key research questions:

1. How does ultrasonic irradiation affect the rate of 1-octene hydrogenation in a slurry phase reactor using a nanosized $Ce\text{-}Pt/Al_2O_3$ catalyst?

2. What is the impact of ultrasonic irradiation on catalyst deactivation during the hydrogenation of 1-octene?
3. How does the performance of the sonicated hydrogenation reaction compare to the unsonicated reaction at varying temperatures?
4. What is the effect of ultrasonic irradiation on the hydrogenation reaction when the reaction is carried out for different reaction times while reusing the Ce-Pt/Al_2O_3 catalyst?

1.6 Specific objectives:

The specific objectives of this study were multifaceted and centred around investigating the influence of ultrasonic irradiation on the rate of 1-octene hydrogenation and catalyst deactivation using a commercial nano-sized Ce-Pt/Al_2O_3 catalyst in a three-phase slurry reactor. To address these research questions, this study was centred around the following specific objectives:

1. To design and commission a reactor system that can incorporate a slurry reactor and ultrasonic irradiation.
2. To prepare and characterise Ce-Pt/Al_2O_3 nanocatalysts for 1-octene hydrogenation.
3. To characterize the kinetic influence of ultrasonication in slurry phase reactions.
4. To compare sonicated and unsonicated reaction performance at various temperatures.
5. To evaluate catalyst stability, deactivation, and investigate the effect of ultrasonic irradiation on reaction time and catalyst reusability.

The reactor performance for those reactions were evaluated by analysing the conversion of 1-octene and the yield of hydrogenated products using a 2014 Shimadzu GC – FID system.

1.7 Scope and organisation of this thesis:

This thesis details the investigation of process intensification in octene hydrogenation through the combined application of Ce-promoted Pt/Al_2O_3 nanocatalysts and ultrasonic irradiation in a slurry phase reactor. Chapter 1 provides the introduction and background to octene hydrogenation and process intensification. Chapter 2 provides a comprehensive literature review on octene hydrogenation, process intensification strategies, nanocatalysts, and ultrasonic irradiation. Chapter 3 presents the experimental methods employed in this study, including catalyst preparation, reactor design, and analytical techniques used for catalysts characterisation as well as techniques used to measure and quantify the system performance for the catalysts performance. Chapter 4 discusses the results obtained from the experiments, including the characterization of nanocatalysts, the impact of ultrasonic irradiation on reaction performance, and catalyst deactivation studies. Finally, Chapter 5 concludes the dissertation by summarizing the findings, discussing their implications, and providing directions for future research.

This study seeks to contribute to the field of process intensification by investigating the application of nanocatalysts and ultrasonic irradiation in the slurry phase hydrogenation of 1-octene. The integration of nanocatalysts and ultrasonic irradiation has the potential to enhance reaction kinetics, improve mass transfer, and prolong catalyst lifetime, offering a promising approach for the efficient production of octane and other valuable hydrogenated products.

Chapter 2:

Literature Review

2.1 Catalysis:

The field of heterogeneous catalysis plays a pivotal role in numerous industrial processes, ranging from petrochemical refining to environmental remediation. The efficient design and utilization of heterogeneous catalysts is essential for enhancing reaction rates, selectivity, and sustainability in chemical transformations. This chapter aims to provide an overview of recent advancements and key insights in reactor design, heterogeneous catalysis and process intensification. Heterogeneous catalysis involves the use of solid catalysts to facilitate chemical reactions between gaseous or liquid reactants. Catalysts are crucial in this context because they can significantly lower the activation energy barrier and make reactions more feasible under milder conditions. In recent years, researchers have focused on developing novel heterogeneous catalysts, understanding their catalytic mechanisms, and exploring their applications in various chemical processes.

One area of significant interest in heterogeneous catalysis is the development of nanocatalysts. Nanocatalysts are typically composed of metal nanoparticles supported on high-surface-area materials and have garnered attention due to their unique properties. For instance, in a study by Wang et al., (2018), a novel Pt-Co-based nanocatalyst supported on carbon nanotubes was synthesized for the catalytic hydrogenation of unsaturated compounds (Wang et al., 2018). Their study utilized Pt-Co/MWCNTs bimetallic catalyst at 10 bar, 80°C for 12 hours per reaction run. A high conversion rate of 93.3% and selectivity of 93.4% were achieved in the hydrogenation reaction, highlighting its efficiency and effectiveness under the specified conditions. The high surface area of carbon nanotubes and the small size of Pt nanoparticles led to enhanced catalytic activity and selectivity. Is therefore important to note that the catalyst support material also play a critical role in catalysis. The advances in the design and engineering of support materials have contributed to improved catalyst stability and reusability. Ekeoma et al., (2022) investigated the use of mesoporous silica as a support for metal catalysts and they found that the ordered mesoporous structure of the support material provided efficient mass transfer and reduced metal sintering, resulting in prolonged catalyst lifetime (Ekeoma et al., 2022; Yu and Williams, 2022). Under reaction conditions of elevated temperatures (600°C to 800°C) and moderate pressures of 1–3 bar, the catalyst achieved impressive conversion rates of 76.6% for CH_4 and 82.1% for CO_2. The catalyst's stability over 24 hours of continuous operation further highlighted the suitability of silica as a support for sustainable syngas production.

In addition to that, the understanding of catalytic mechanisms at the molecular level has been a central focus of recent research to the extent that in-situ and operando techniques such as X-ray absorption spectroscopy and transmission electron microscopy have enabled researchers to observe catalytic reactions under working conditions. For instance, Singh et al., (2018) employed in-situ X-ray absorption spectroscopy to deeply investigate the dynamic structural and morphological changes of carbon-supported Pt catalysts during aqueous phenol hydrogenation with and without applied electrical potential. Using Pt/C catalysts of approximately 2 nm under ambient temperature and pressure conditions, the research successfully characterized the adsorbates on carbon-supported Pt during the hydrogenation of phenol. This approach revealed insights into the active site formation and the various catalyst deactivation processes (Singh et al., 2018). This is because catalyst deactivation remains a significant challenge in heterogeneous catalysis and strategies to mitigate deactivation have been a focus of research. One of the strategies being deployed include the development of robust catalysts through the use of additives, and the exploration of regeneration techniques. The study by Najafishirtari et al., (2021) investigated the deactivation mechanisms of supported catalysts during the selective oxidation of alcohols (Najafishirtari et al., 2021) and it is through such studies that mitigating strategies are formulated when you understand the deactivation mechanisms. The study utilized a Pt catalyst in the liquid-phase oxidation of alcohols at temperatures ranging from 60 to 200°C under varying O_2 pressures. The results demonstrated the formation of ketones, and β-carbonyl species in situ, leading to adsorption on the metal active sites and subsequent catalyst deactivation. Additionally, the presence of olefinic by-products over the Pt catalyst contributed to reduced catalytic efficiency. Their findings emphasized the importance of understanding deactivation kinetics and developing regeneration strategies to prolong catalyst lifetime.

2.2 Octene hydrogenation: Reactors, reaction mechanism and catalysts:

In the realm of three-phase reactor systems, where solids in the form of catalyst particles or packing, liquids, and gases interact, two predominant modes of operation are identified in the case of hydrogenation reactions. These are trickle bed and slurry phase operations. According to Shaofen, (2017), trickle bed reactors are characterized by a stationary bed of solid catalyst particles through which liquid flows downward as the dispersed phase, while gases traverse either cocurrently or counter-currently as the continuous phase. Cocurrent flow is notably prevalent in industrial applications due to its energy efficiency and lower operating costs. Wu and Tu, (2016) further reinforced the fact that compared to continuous stirred tank and bubble column reactors, trickle bed reactors exhibit superior gas conversion rates and therefore higher product yields. Their study demonstrated that trickle bed reactors provided a 35% increase in operational efficiency and a 28% higher product yield compared to bubble column reactors. Figure 2.1 shows a schematic diagram of the configuration of a concurrent trickle bed reactor.

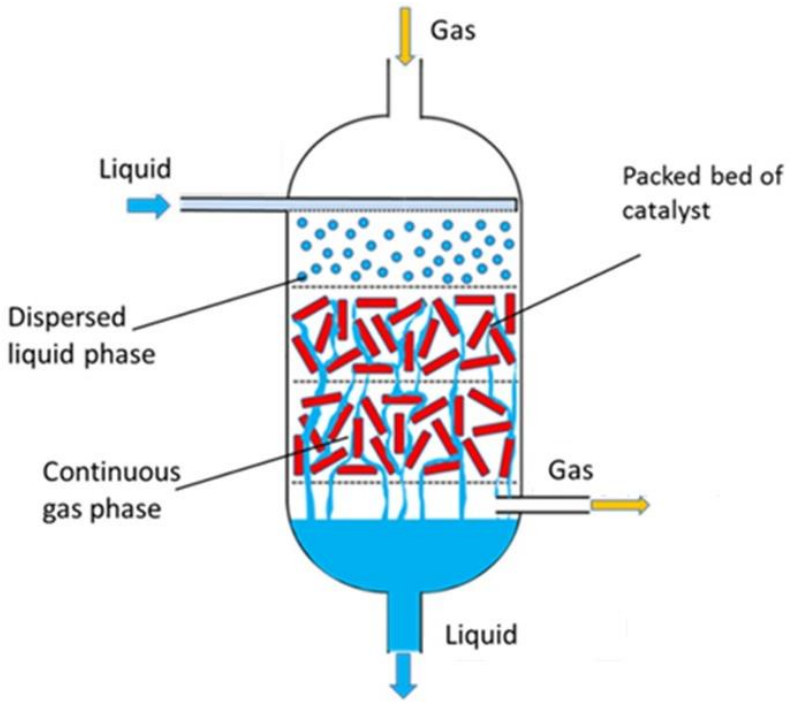

Figure 2. 1: Schematic of a trickle bed reactor operating in a concurrent configuration. Source: Smith et al., (2018).

In this trickle bed reactor, a concurrent downward flow of gas and liquid navigates through a catalyst bed positioned above a sieve plate or wire mesh as depicted in a typical schematic shown in Figure 2.1 (Smith et al., 2018). In this configuration, the liquid's percolation through the catalyst bed does not ensure a 100% wetting of all catalyst particles, and hence making the distribution of the liquid within the bed crucial for effective heat transfer and overall reactor function (Jones and Sun, 2019). While it is feasible to employ a counter-current mode where the liquid and gas flow in opposite directions, recent investigations indicate that although this enhances phase contact, it also increases the risk of flooding at higher gas velocities, therefore limiting its industrial adoption (Deng et al., 2020). Ellenberger and Krishna, 1999 noted that counter-current flow could provide performance advantages in high-pressure conditions where liquid-phase reactants are the bottleneck for reaction rates. Conversely, concurrent flow is superior under low-pressure conditions, with gas phase availability dictating the reaction's progress (Lee and Patel, 2021). The packing of trickle bed reactors comes in various sizes, shapes, and configurations. This packing can be random, structured, or in the form of microchannel arrangements, with evidence suggesting that structured packing, which forms consistent channels for liquid flow surpasses the performance of conventional random beds (Ellenberger and Krishna, 1999).

The other type of reactor system that is more predominant in octene hydrogenation are slurry reactors which operate with solid particles suspended in the liquid medium and they use mechanical or gas-induced agitation as outlined by Chaudhari and Ramachandran, (1980). In this configuration, the slurry

functions as the continuous phase with the gas dispersed within it. The liquid medium can serve as either a reactant or an inert medium facilitating contact between the solid particles and dissolved gases. In the case of octene hydrogenation, the liquid phase is 1-octene and serves as the main reactant. Figure 2.2 structure and configuration of slurry phase reactors.

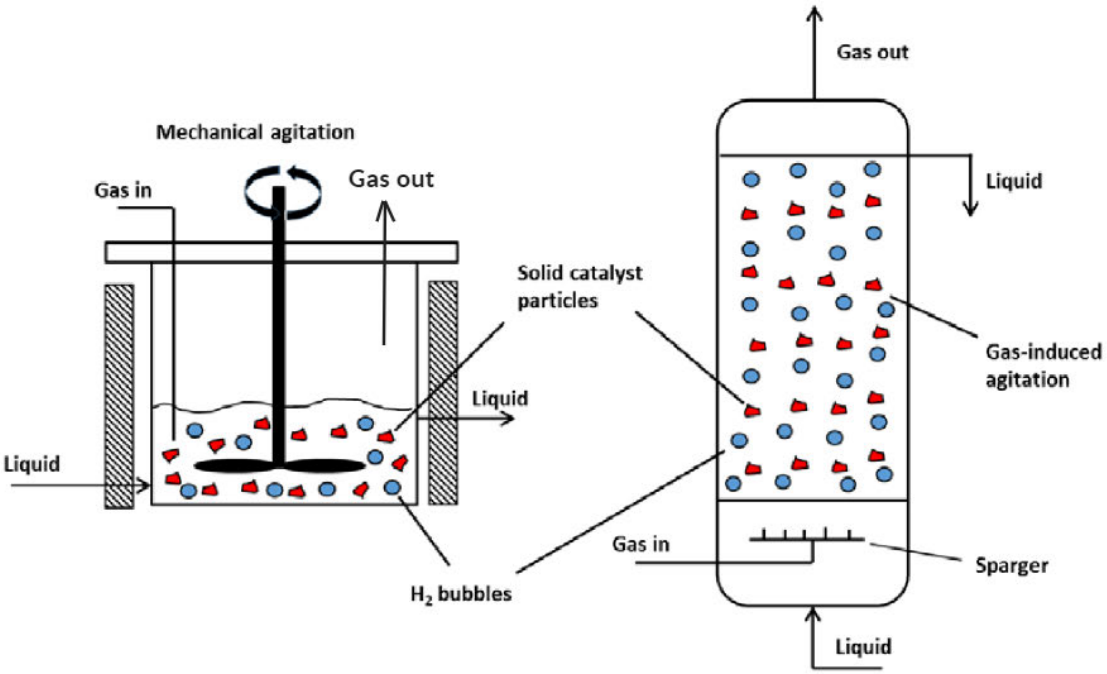

Figure 2. 2: The two types of three phase slurry reactors encountered showing a mechanically agitated reactor (left) and a bubble column slurry reactor (right). Source: White, (2022).

The two core structures of the three-phase slurry reactors shown in Figure 2.2 are pivotal in various industrial processes. The one on the left side of the figure displays a mechanically agitated reactor, where mechanical means are employed to facilitate the mixing of the solid catalyst with the liquid and gas phases. This ensures that the desired reaction kinetics are achieved. On the right, a bubble column slurry reactor is featured, which utilizes gas-induced agitation to mix the phases. This method typically results in a lower shear environment that is suitable for reactions that may be sensitive to mechanical stress (Chaudhari and Ramachandran, 1980). The efficiency and efficacy of these reactors are heavily dependent on the specific design and operation parameters, which are tailored to the needs of the reaction process and the physical properties of the system (Deckwer and Alper, 1980). Chaudhari and Ramachandran, (1980) also noted the importance of the solids being finely divided to enhance surface area. These solid particles typically can be catalysts or absorbents. They underscored the criticality of particle size, typically ranging from 0.05 mm to 1 mm for effective filterability. However, they caution against the potential challenges in slurry reactors such as catalyst abrasion and the complexities in

separating the spent catalyst from the liquid phase once the reaction is over since this could escalate operational time and costs.

These slurry reactors as Chaudhari and Ramachandran, (1980) highlighted find extensive application across various chemical processes, including hydrogenation of unsaturated oils, Fischer-Tropsch reaction as well as many other petrochemical processes. They also emphasised the fact that the internal dynamics of slurry phase reactors such as gas-liquid mass transfer and surface reactions are pivotal in determining reactor performance. It is in this perspective that the combination of ultrasonic irradiation with nanocatalysts in intensified slurry phase reactors can significantly alter the kinetics and thermodynamics of hydrogenation processes. The ultrasonic energy potentially reduce the energy barriers for chemical reactions and on the other hand, nanocatalysts offer unique sites for reaction that traditional macro-scale catalysts cannot provide (Bang and Suslick, 2010). This synergy can lead to higher reaction rates, better selectivity towards desired products, and potentially lower catalyst deactivation rates. The study by Bang and Suslick, 2010 demonstrated that ultrasonic energy can significantly reduce energy barriers for chemical reactions and create extreme localized conditions with temperatures reaching up to approximately 5000 K and pressures of around 1000 bar. These conditions, generated by the implosive collapse of cavitation bubbles facilitate chemical reactions that are otherwise difficult to achieve. Furthermore, the use of nanocatalysts with ultrasonic methods offer unique reaction sites due to their high surface areas and small, uniform particle sizes and these are features that traditional macro-scale catalysts cannot provide. For instance, sonochemically produced iron nanoparticles display narrow size distributions centred around 8 nm and a high surface area of approximately 150 m^2/g. These characteristics enable enhanced reaction rates and efficiencies, underscoring the superiority of nanocatalysts in catalytic processes compared to conventional catalysts.

It is however important to note the challenges associated with these technologies as well. The stability and recovery of nanocatalysts, the scale-up of ultrasonic reactors, and the precise control of ultrasonic energy are key issues that need to be addressed. Moreover, the long-term effects of ultrasonic energy on catalyst stability and the overall energy balance of the process require careful consideration and investigation (Mason et al., 2011). Despite these challenges, advancements in understanding the reaction mechanism of octene hydrogenation have been significant. Researchers have made notable progress in trying to explain the detailed steps involved in the hydrogenation process at the molecular level. Both experimental and computational methods have been used to provide insights into the adsorption and activation of hydrogen and octene molecules on catalyst surfaces.

2.2.1 Reaction mechanism of octene hydrogenation:

Heterogeneous catalysis, specifically in the hydrogenation of 1-octene is a fundamental and industrially relevant chemical transformation. The hydrogenation of octene involves the addition of hydrogen molecules to the carbon-carbon double bond, converting it into a single bond and resulting in the

formation of octane which is a key component in the production of high-octane fuels and other valuable chemicals. The design and optimisation of the catalysts for this reaction have been the focus of extensive research efforts in order to improve their efficacy and robustness. The catalytic hydrogenation of octene proceeds via a series of well-defined reaction steps, involving the adsorption and dissociation of hydrogen molecules on the catalyst surface, the migration of hydrogen atoms on the catalyst, and the subsequent addition of hydrogen atoms to the double bond of octene. This is illustrated in Figure 2.3 and 1-octene is used as an example.

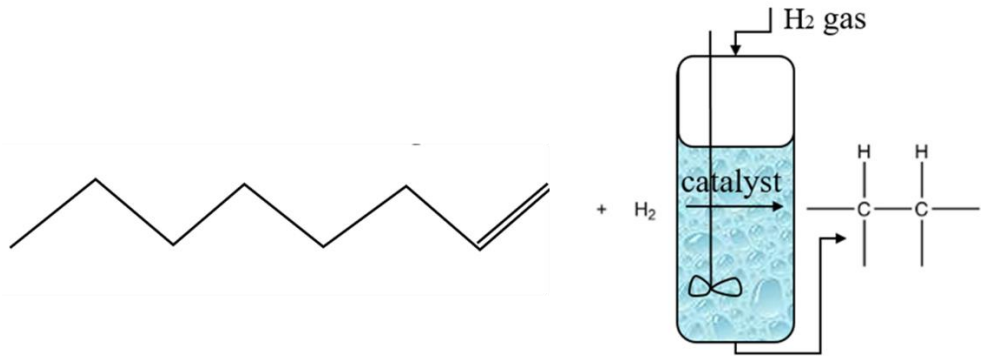

Figure 2. 3: Hydrogenation reaction of an alkene (1-octene).

The reaction mechanism and kinetics of octene hydrogenation are influenced by various factors, including the choice of catalyst, reaction temperature, and pressure. Since octene hydrogenation is usually carried out in slurry phase reactors, the mechanism behind multiphase catalytic reactions is very intricate and involves sequential steps like molecule migration, surface adherence, and subsequent detachment. Figure 2.4 is an illustration of octene hydrogenation in the presence of a Pd or Pt catalyst.

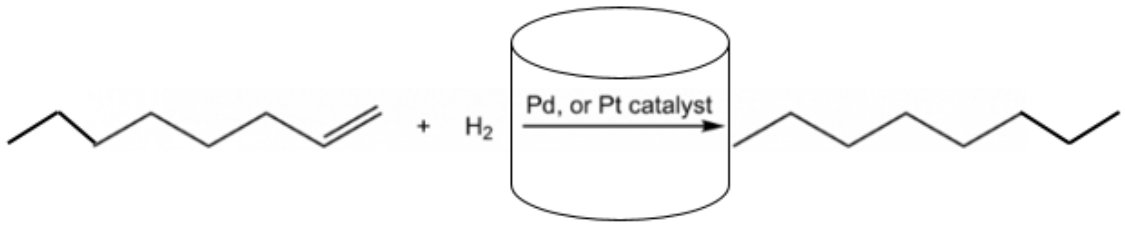

Figure 2. 4: Hydrogenation reaction of 1-octene to octanes.

Understanding the intricate reaction mechanism of octene hydrogenation is pivotal for the rational design of catalysts and the optimisation of this industrially important process. This section will delve deeper into the key steps and factors governing this reaction and with a focus on recent advancements in mechanistic insights.

2.2.1.1 Adsorption of the alkene:

The initial step in octene hydrogenation involves the adsorption of the reactant molecule, 1-octene onto the catalytic surface. This adsorption process weakens the carbon-carbon double bond in 1-octene, making it more susceptible to reaction with hydrogen. The activated catalyst surface provides a conducive environment for this adsorption step. Figure 2.5 illustrates this adsorption step for a hypothetical ethene molecule.

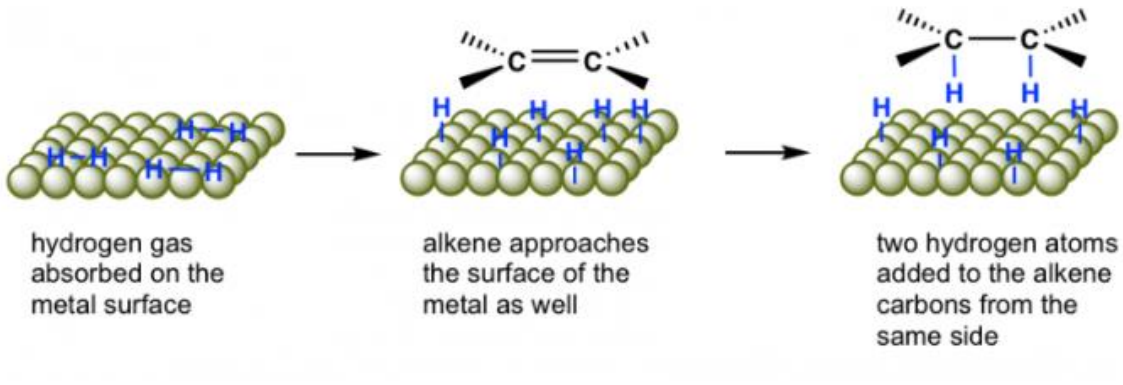

Figure 2. 5: A simplified diagram illustrating the adsorption of an alkene on the catalyst surface, showing the interaction between the olefin and the catalytic site. Source: Liu, (2021).

Recent computational studies, such as those by Torkashvand et al., (2023), have employed density functional theory (DFT) calculations to explore the energetics of adsorption and activation. In their study, they investigated the hydrogenation mechanism of carbon monoxide on the cobalt nanoparticles, specifically the Co (001) surface using density functional theory (DFT). They concluded that the preferred adsorption sites for intermediates were mostly hollow positions and that the adsorption energy of CO to the surface was around -2.268 eV. This is the energy that ultrasonic irradiation might provide for the reaction of octene with hydrogen. These calculations help in elucidating the adsorption configurations, binding energies, and even the role of the catalyst support in stabilizing the adsorbed species before they proceed to the activation step of the reaction which comes next after adsorption.

2.2.1.2 Hydrogen activation:

After adsorption, hydrogen molecules also interact with the catalyst surface. These hydrogen molecules dissociate into reactive hydrogen atoms, a step critical for the subsequent hydrogenation reaction. The activation of hydrogen is influenced by both the catalyst's metal composition and the support material as shown in Figure 2.6 using a hypothetical alkene.

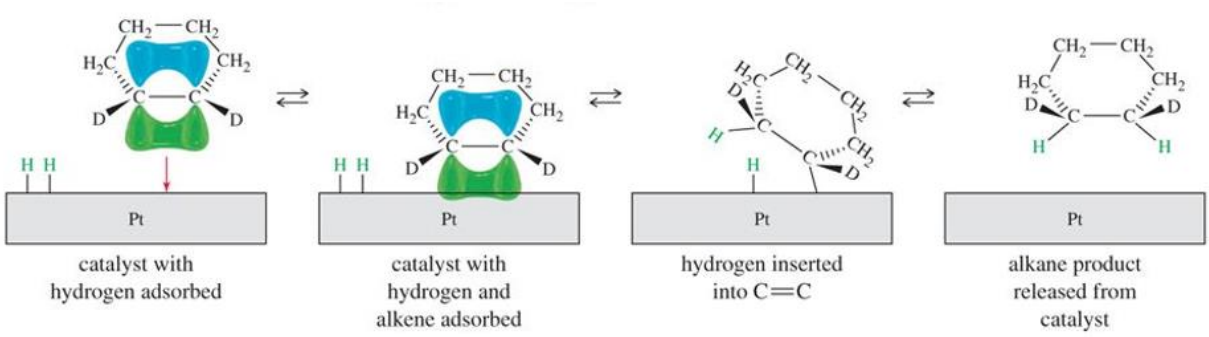

Figure 2. 6: A schematic representation of the hydrogen activation process, highlighting the breaking of the H-H bond and the formation of hydrogen atoms on the catalyst surface. Source: White, 2022.

2.2.1.3 Reaction and hydrogenation:

Once activated, the hydrogen atoms migrate to the adsorbed 1-octene, initiating the hydrogenation reaction. This step involves the breaking of the carbon-carbon double bond and the formation of a carbon-hydrogen (C-H) bond which ultimately lead to the formation of octane. This breaking of bonds can be facilitated by the energy provided externally by heating the reactor or it can intrinsically be imparted by ultrasonic irradiation in this case. The nature of the catalyst surface, its morphology, and the presence of co-adsorbates can influence the selectivity of this step. These reactions transpire on the catalyst's exterior while the reactants reside within the liquid or gas phase that envelops the catalyst's solid particles. A closer look at the catalytic reactions taking place using Figure 2.7 reveal that the process initiates with the reactants traversing the adjacent outer layer at A_1, which is a region located at the catalyst particle pore opening where diffusion of reactants takes place into the pore of the catalyst particle through a phenomenon known as film diffusion (Klaewkla et al., 2011). Post this phase, the reactants penetrate deeper into the catalyst's porous structure to access the active sites. This is illustrated by the schematic below:

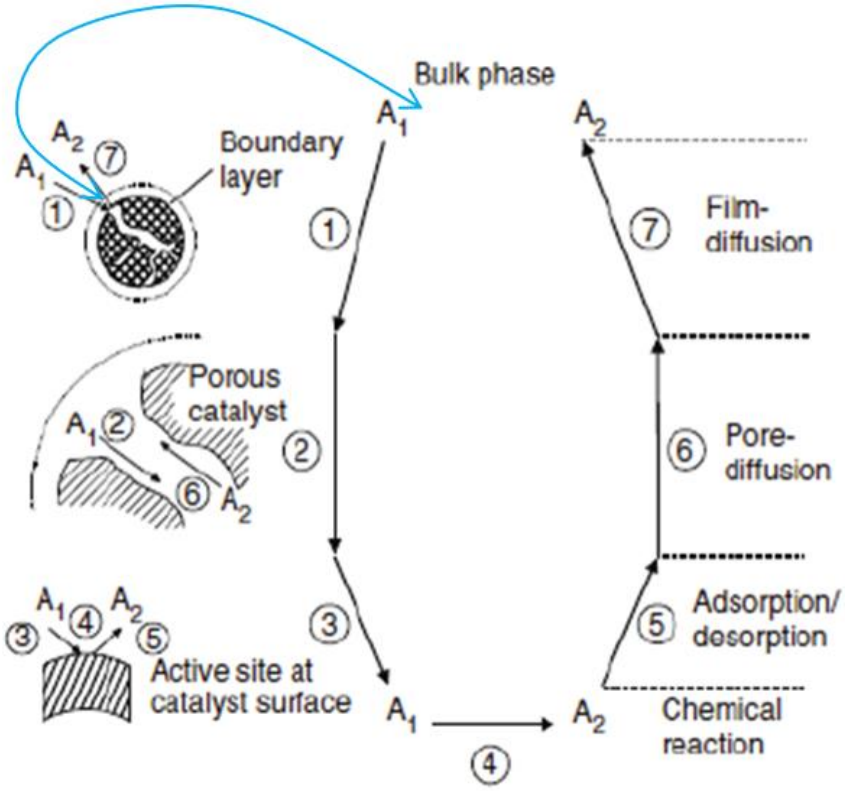

Figure 2. 7: Reaction steps for a heterogeneous catalytic fluid-solid reaction. Source: Klaewkla et al., (2011).

Once at the active sites, the reactants bind to the catalyst's interior surfaces, leading to a chemical reaction. This reaction yields products that are released from the catalyst's surface after a defined duration of contact. The newly formed products at stages 4 and 5 navigate back through the catalyst's porosity and the surrounding boundary layer, ultimately dispersing into the bulk fluid at A_2 (Klaewkla et al., 2011). To understand this, recent studies have shed light on the reaction mechanisms and kinetics of hydrogenation reactions in slurry phase systems. For instance, Chanerika et al., (2022) conducted a detailed kinetic study of the hydrogenation of 1-octene over a supported Pd catalyst. Their study investigated the effects of ionic liquids (IL) and organic modifiers as surface coatings on catalysts for the selective hydrogenation of 1-octene. The organic modifier [EIM] and IL ([BMIM][DCA]) significantly modified reaction sites and enhanced the selectivity towards 1-octene compared to uncoated catalysts. Their work achieved a remarkable 1-octene conversion of 84% at 91% for 1-octyne and this provided valuable insights into the role of surface adsorption and hydrogen activation in controlling the reaction rate by utilising surface modifiers. The exposition of such mechanistic details is crucial for the rational design and optimisation of catalysts.

The nature and type of catalyst used in hydrogenation influences the reactor efficiency and that is why catalyst selection is a critical aspect in octene hydrogenation. As previously noted, transition metals, such as nickel, palladium, platinum, and rhodium, are commonly employed as catalysts due to their

ability to activate hydrogen and facilitate the addition of hydrogen atoms to the double bond. The choice of catalyst can significantly influence the reaction kinetics and octane yield. In recent years, researchers have explored the development of catalysts with improved activity and stability and bimetallic catalysts have gained prominence in the context of octene hydrogenation. These catalysts are comprised of two different metals and they often exhibit synergistic effects, leading to enhanced catalytic performance. Chen et al., (2018) investigated the use of bimetallic Pt-Co bimetallic nanoparticles deposited on multi-walled carbon nanotubes (MWCNTs) for the hydrogenation of hydrogenation of α, β-unsaturated aldehydes to unsaturated alcohols. Their study resulted in both selectivity and conversion rates exceeding 90%. This high efficiency is attributed to the synergistic effects between platinum (Pt) and cobalt (Co) nanoparticles supported on multi-walled carbon nanotubes (MWCNTs). Their findings demonstrated that the combination of Pd and Pt resulted in improved catalytic activity and selectivity compared to monometallic counterparts. The interaction between the two metals played a vital role in enhancing the catalytic performance, but there are several drawbacks of using noble metal bimetallic in catalysis. Chief among them is the high price and they also require a greater supply of hydrogen during reaction.

Several support materials have been used for octene hydrogenation catalysts. This is because catalyst support materials also play a crucial role in octene hydrogenation and the choice of support material can influence catalyst dispersion, surface area, and stability. In a recent study by Li et al., (2021), hierarchical zeolite-supported catalysts were used for the selective hydrogenation of octenes. The unique structure of the hierarchical zeolite support promoted efficient reactant diffusion and reduced coke formation, leading to improved selectivity and stability of the catalyst. In their study, they reported that unique structure of the hierarchical zeolite support promoted efficient reactant diffusion and reduced coke formation, leading to a 20% improvement in selectivity and a 15% increase in catalyst stability.

The hydrogenation of octene is a complex process with a well-defined reaction mechanism and recent research efforts have provided insights into the kinetics, mechanistic details, and catalyst design for this important reaction. The choice of catalyst, including bimetallic systems, and support materials significantly affects reaction performance, making these aspects crucial in the development of efficient and sustainable octene hydrogenation processes. All this foundational knowledge served as a basis for exploring process intensification strategies such as the integration of nanocatalysts and ultrasonic irradiation, as discussed in subsequent sections of this literature review. Some recent experimental studies employing techniques like in-situ spectroscopy (Burueva et al., 2020) and kinetic investigations have also provided valuable information about the reaction kinetics and selectivity-determining factors in hydrogenation reactions (Angulo and Bouwman, 2001). These studies offer insights into the roles of specific catalyst sites and surface structures in governing the reaction pathways in octene hydrogenation and they should be safeguarded from phenomena such as deactivation.

2.2.2 Catalyst deactivation:

A critical limitation in octene hydrogenation is catalyst deactivation, which can occur due to various factors, including the accumulation of reaction by-products, catalyst poisoning and sintering of metal nanoparticles. Understanding these deactivation mechanisms is essential for developing strategies to enhance catalyst stability and longevity for industrial application. The most prominent catalyst deactivation mechanisms that are common to most heterogeneous catalyst systems include coke formation, metal sintering, and surface poisoning. There are also prevalent in octene hydrogenation and therefore a proper elucidation of these mechanism deserve attention if the objective is to develop a robust catalyst system. These mechanisms are illustrated in Figure 2.8.

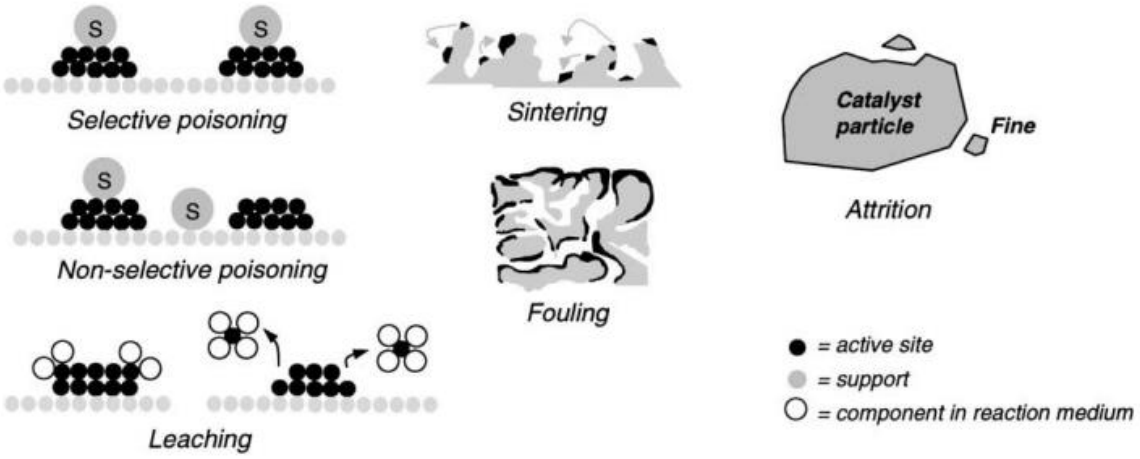

Figure 2. 8: Potential catalyst deactivation pathways, including coke formation, metal sintering, and surface poisoning. Source: Moulijn et al., (2001).

A deeper understanding of these deactivation mechanisms is crucial for developing strategies to mitigate their effects and enhance the durability of catalysts. Coke formation is one of the most common catalyst deactivation mechanisms in octene hydrogenation. In the case where Al_2O_3 is used as a catalyst support, coke formation is more prevalent because of the acidic nature of alumina. Its acidity promotes the formation of carbonaceous deposits on the surface of the catalyst particles. Coke consists of amorphous carbonaceous deposits that accumulate on the catalyst surface during the reaction. These deposits can block active sites, restrict reactant access to the catalyst surface, and reduce catalytic activity and selectivity. Research by Ginsburg et al., (2005) explored the kinetics of coke formation over a nickel catalyst under methane dry reforming conditions. Ginsburg and colleagues addressed this challenge by exploring the thermodynamic and kinetic parameters that influence coke deposition on nickel catalysts under dry reforming conditions. Their comprehensive study employed thermodynamic models to identify the conditions favourable for coke formation and they found that a critical temperature of 700°C and a pressure of 25 bar are thresholds where coke deposition becomes

significant. Moreover, their kinetic analysis provided a deeper understanding of the reaction mechanisms, offering insights into the rate of coke formation and suggesting strategies for operational optimization to mitigate coking. The study revealed that coke formation occurs through a complex set of reactions, including adsorption of reaction intermediates and subsequent polymerization as shown in Figure 2.9.

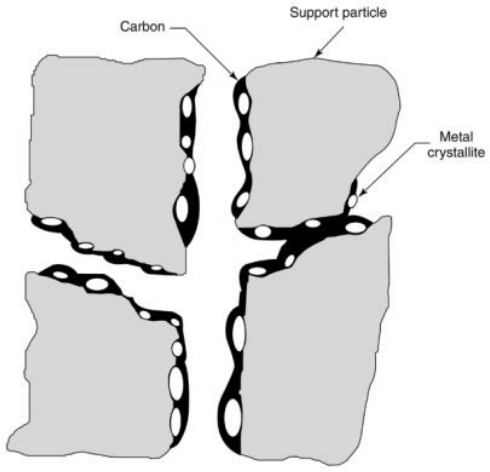

Figure 2. 9: Conceptual model of fouling, crystallite encapsulation, and pore plugging of a supported metal catalyst owing to carbon deposition. Source: Argyle and Bartholomew, (2015).

Another major catalyst deactivation mechanism is metal sintering. In this process, metal nanoparticles on the catalyst surface undergo coalescence or migration, leading to a decrease in the available active surface area. As a result, catalytic activity diminishes over time. Recent work by Maphutha et al., (2021) investigated the hydrothermal sintering and oxidation of an alumina-supported nickel methanation catalyst using in-situ magnetometry. The study employed advanced in-situ magnetometry techniques to track changes in particle size and morphology. They explored temperatures ranging from 350 °C to 650 °C and gas environments of pure argon versus a hydrogen and water vapor mix with a partial pressure ratio (PH_2O/PH_2) of 5, representing a simulated CO conversion of 94%. Their findings indicated that under pure argon, the particle size and degree of reduction of Ni remained largely unchanged across the temperature spectrum. However, under hydrothermal conditions, there was a notable increase in particle size from 4.2 nm at 350 °C to 9.3 nm at 650 °C, accompanied by a substantial decrease in the degree of reduction, highlighting significant oxidation and sintering effects influenced by the presence of steam.

Catalyst poisoning is also another major culprit of catalysts deactivation. It involves the adsorption of impurities or reaction intermediates on the catalyst's active sites, rendering them inactive. This deactivation mechanism can result from the presence of contaminants in the feedstock or the reaction environment. Chanerika et al., (2022) delved into the role of surface poisoning in catalyst deactivation during hydrogenation. The research employed in-situ spectroscopic techniques to monitor the adsorption of various species on the catalyst surface and its impact on catalytic activity. In their

investigation of surface poisoning in hydrogenation, Forzatti and Lietti, (1999) identified and characterized the specific species responsible for surface deactivation. Employing advanced analytical techniques such as mass spectrometry and in-situ infrared spectroscopy, the researchers observed the adsorption of key reaction intermediates, including alkyl intermediates onto the catalyst's active sites. They detailed conditions such as temperature, which ranges from moderate to high (often exceeding 500°C), and their effects on catalyst longevity and performance. These findings provided concrete evidence that surface poisoning in hydrogenation primarily arises from the adsorption of reaction intermediates, thus shedding light on the chemical pathways leading to deactivation (Dai et al., 2017). These four modes of catalyst deactivation in zeolite-based catalysts are shown in Figure 2.10.

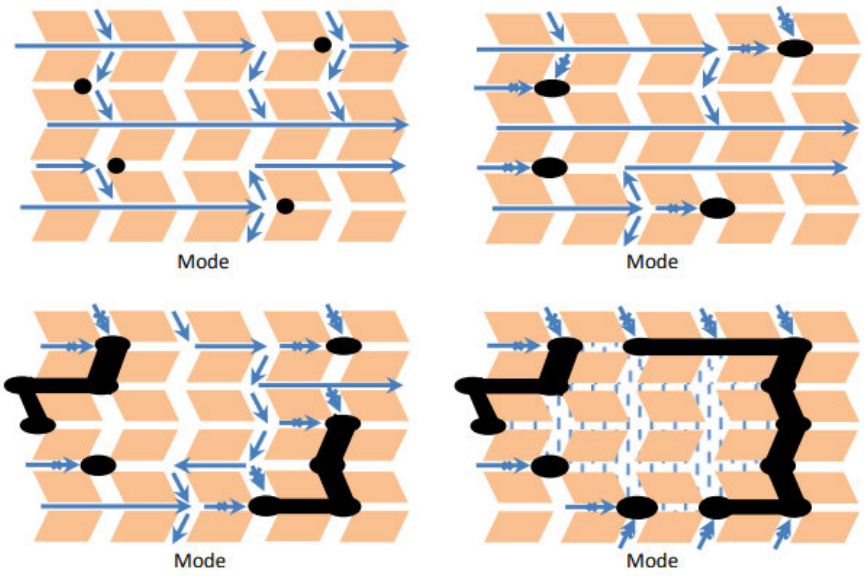

Figure 2. 10: Schematic of the four possible modes of deactivation by carbonaceous deposits in catalysts: (1) reversible adsorption on acid sites, (2) irreversible adsorption on sites with partial blocking of pore intersections, (3) partial steric blocking of pores, and (4) extensive steric blocking of pores by exterior deposits. Source: Argyle and Bartholomew, (2015).

The impact of surface poisoning on the catalytic activity of the catalyst has always been a focal point of study. Kinetic experiments by Forzatti and Lietti, (1999) revealed a significant reduction in reaction rates as the concentration of adsorbed poisoning species increased. This observation strongly correlates with similar findings in literature, such as the study by Luo et al., (2005), which highlighted that surface poisoning can lead to a substantial decrease in reaction rates. Their study involved conducting experiments under various conditions including temperature, where the study highlighted significant improvements in catalytic performance attributed to the presence of yttrium. This enhancement was particularly noted in increased CO_2 conversion rates, which were substantially higher in the Ru-Y/sepiolite catalyst compared to the Ru/sepiolite across a temperature range from 633 K to 693 K. At 693 K, the CO_2 conversion rate improved from 16.4% in the Ru/sepiolite to 32.4% in the Ru-Y/sepiolite,

indicating the beneficial role of yttrium in enhancing both the activity and anti-poisoning capacity of the catalyst. These reported findings underscore the practical relevance of understanding and addressing surface poisoning in heterogeneous catalysis.

Cimino et al., (2019) further delved into the kinetics of surface poisoning, providing a comprehensive understanding of the dynamic nature of this deactivation process. Their observations indicated that surface poisoning occurs progressively over time, affecting the catalytic performance of the catalyst as poisoning species accumulate. They observed that under harsh conditions of temperatures above 500 ^{0}C, catalysts often show decreased conversion rates and yields due to the buildup of poisons such as sulphur and carbon deposits, underscoring the critical need for innovative regeneration strategies and the development of more robust catalyst material. This kinetic understanding aligns with more studies, such as the work of Bayramoğlu et al., (2021), who investigated the kinetics of coke formation and removal on catalyst surfaces. Bayramoğlu and colleagues found that while coke formation was rapid, ultrasound-assisted sonochemical cleaning could effectively reverse the deactivation, highlighting the potential for catalyst reactivation strategies (Bayramoğlu et al., 2021, Cimino and Lisi, 2019). Their study also investigated the reusability of two heterogeneous catalysts, calcined calcite (CaO) and calcined dolomite (CaO.MgO) in ultrasound-assisted biodiesel production, where biodiesel yield decreased from 99.1% to 90.4% for CaO and from 98.8% to 89.8% for CaO.MgO after eight uses. Regeneration of these spent catalysts through calcination at 750 °C for 90 minutes also proved effective, restoring biodiesel yield to 97.2% for CaO and 96.5% for CaO.MgO in a second cycle. This demonstrated that calcination is also an energetically favorable method for regenerating spent catalysts.

The influence of catalyst properties on susceptibility to surface poisoning was another crucial aspect of the study. Cherkasov et al., (2019) explored how various catalyst properties, including metal composition, catalyst support, and particle size, affect the extent of poisoning. Their findings resonated with the literature, particularly the research by Konsolakis and Lykaki, (2020) which emphasized the role of crystallographic orientation of metal nanoparticles on catalyst supports in the adsorption of poisoning species (Konsolakis and Lykaki, 2020). In their study, they explored the implications of size, shape, and electronic effects on the intrinsic reactivity and metal-support interactions within the CuO_x/CeO_2 binary system. They observed that specific surface modifications of the catalysts could lead to significant improvements in performance metrics such as conversion rates and yield. For instance, they noted that altering the size and shape of the copper oxide particles on the ceria support directly influenced the catalytic activity, enhancing the CO oxidation conversion rate significantly under optimized conditions. These reported observations underscored the relevance of tailoring catalyst properties to mitigate surface poisoning, ensuring catalytic efficiency. In terms of proposed strategies for mitigating surface poisoning, Argyle et al., (2015) introduced innovative approaches. They suggested the introduction of additives that selectively desorb poisoning species, effectively rejuvenating the catalyst's active sites. Additionally, modifications to reaction conditions were proposed

to promote surface cleansing (Argyle and Bartholomew, 2015). These strategies aligned with the work of Li et al., (2020) who investigated the use of regenerable catalysts for hydrogenation reactions. Their study highlighted the potential for designing catalysts that can be regenerated in-situ, maintaining catalytic activity over extended reaction periods (Li et al., 2020).

Argyle and Bartholomew, (2015) also explored how reaction conditions, including temperature, pressure, and reactant concentrations influenced the extent and rate of surface poisoning. Their observations emphasized the practical relevance of their work in catalytic processes under varying conditions especially of temperature and pressure as they observed that lower temperature reduced catalyst deactivation. This finding aligned with the study by Valcarcel et al., (2009), where adjustments to reaction conditions such as hydrogen pressure were shown to mitigate surface poisoning effects on Pd catalysts during alkene hydrogenation (Valcarcel et al., 2009; Teschner et al., 2008). They conducted a detailed investigation into the hydrogenation of 1,3-butadiene on Pd and Pd-Ni alloy surfaces under ultrahigh vacuum and elevated pressure conditions. Utilizing single-crystal surfaces of Pd (100), Pd (110), and Pd8Ni92 (110), they observed that fresh Pd-Ni surfaces were more active than pure Pd surfaces at low hydrogen pressures. However, over several reaction cycles, Pd surfaces activated while Pd-Ni surfaces partially deactivated, leading to a convergence in activity. The study highlighted the significant role of hydrogen absorption and diffusion into the Pd crystal in influencing the reaction kinetics, with substantial hydrogenation activity noted at steady state for both Pd and Pd-Ni surfaces.

2.2.3 Mitigating catalyst deactivation with ultrasound:

Ultrasound as a process intensification technique presents a promising avenue for mitigating catalyst deactivation in octene hydrogenation. It can address several facets of deactivation and enhance the catalyst's lifespan. Ultrasound generates cavitation microbubbles in the reaction mixture, which undergo rapid growth and collapse. During bubble collapse, localized regions of high temperature and pressure are generated and these conditions can effectively break down and remove coke deposits from the catalyst surface through a process known as sonochemical cleaning. Studies by Wang et al., (2023) as well as those by Bang and Suslick, (2010) have demonstrated the efficacy of ultrasound in coke removal from catalyst surfaces during hydrogenation reactions. Extreme localized conditions with temperatures reaching up to approximately 5000 K and pressure of around 1000 bar have far-reaching effects to the suspended catalysts. Ultrasound-induced cavitation enhances the mechanical removal of coke, thereby maintaining a cleaner and more active catalyst surface.

Ultrasound-induced microstreaming and acoustic streaming can also improve the dispersion of catalyst particles in the reaction mixture and this enhanced dispersion prevents the coalescence of metal nanoparticles and reduces sintering, thus preserving a higher active surface area and delaying catalyst deactivation. The work of Wang et al., (2023) and Zhou et al., (2020) explored the impact of ultrasound on catalyst dispersion and sintering prevention during alkene hydrogenation. Their study focused on

the impact of ultrasound on the dispersion of catalyst particles in the reaction mixture. Dispersion is a critical factor in heterogeneous catalysis as it directly influences the catalyst's active surface area and accessibility of reactants to active sites (Zhou et al., 2020, Wang et al., 2023). Wang and colleagues reported that the application of ultrasound led to a remarkable improvement in catalyst dispersion.

By using techniques such as scanning electron microscopy (SEM) and transmission electron microscopy (TEM), the researchers were able to visualize the catalyst's morphology and distribution in the presence of ultrasound. They observed that ultrasound-induced microstreaming and acoustic streaming effectively prevented the agglomeration and coalescence of metal nanoparticles, resulting in a more uniform dispersion of catalyst particles throughout the reaction mixture. This enhancement in catalyst dispersion has profound implications for catalytic activity and stability. A well-dispersed catalyst exposes more active sites to reactants, increasing the efficiency of the hydrogenation reaction (Mikkola and Salmi, 2001). The occurrence of hotspots and localized fouling is also abated from uniform distribution of catalyst particles and therefore addressing two common issues in heterogeneous catalysis.

The undesirable process of metal nanoparticles coalescing and losing their active surface area, is a well-known catalyst deactivation mechanism. Wang et al.'s study offered crucial insights into how ultrasound effectively prevented sintering during octene hydrogenation. Their findings indicated that the enhanced dispersion achieved through ultrasound played a pivotal role in sintering prevention. The researchers reported that the mechanical effects generated by ultrasound, including microstreaming and acoustic streaming, helped maintain the separation between catalyst particles. This enhanced physical separation hampered the coalescence of metal nanoparticles, preserving their high surface area and catalytic activity. Consequently, sintering, which often leads to reduced catalytic efficiency and lifespan, was notably mitigated in the presence of ultrasound. The reported findings by Wang et al., (2023) hold significant implications for catalysis and process intensification. Primarily, they underscore the practical relevance of ultrasound as a valuable tool for enhancing catalytic stability and prolonging the lifespan of catalysts in slurry phase reactions like octene hydrogenation. Moreover, this study aligns with previous research in the field. For instance, the work of Li et al., (2020) investigated the role of ultrasound in improving mass transfer during catalytic reactions. Their findings, combined with Wang et al.'s observations, highlight the consistent advantages of ultrasound in heterogeneous catalysis, particularly in terms of preventing sintering and enhancing catalyst dispersion.

Their work provides compelling evidence of the positive influence of ultrasound on catalyst dispersion and sintering prevention during octene hydrogenation. These reported observations reinforce the practical relevance of process intensification techniques like the use of ultrasound in improving catalytic stability, efficiency, and the overall sustainability of heterogeneous catalytic processes. In heterogeneous catalysis, efficient mass transfer is a critical factor that governs the overall performance

of catalytic processes. Mass transfer limitations can arise due to slow diffusion of reactants to the catalyst surface impeded by factors like diffusion resistance and boundary layer effects. Such limitations can result in incomplete utilization of the catalyst's active sites, reduced reaction rates, and even catalyst deactivation. Li et al., (2021) recognized the pivotal role of mass transfer in catalysis and embarked on a study to address this challenge. Li et al.'s study focused on the application of ultrasound to enhance mass transfer in catalytic reactions. Ultrasound, with its ability to generate cavitation microbubbles and induce microstreaming offers a unique solution to improve reactant transport and distribution in the reaction medium. The researchers reported that the application of ultrasound significantly enhanced mass transfer, leading to several notable outcomes.

One of the key findings reported by Li et al., (2021) was the substantial reduction in catalyst deactivation in the presence of ultrasound-enhanced mass transfer. This reduction can be attributed to several mechanisms such as enhanced reactant accessibility and suppressed coke formation. Ultrasound-induced cavitation and microstreaming facilitate better mixing and distribution of reactants in the reaction mixture. This improved accessibility to the catalyst's active sites reduces the likelihood of localized fouling and reactant depletion near the catalyst surface, which are two factors that often contribute to catalyst deactivation. Efficient mass transfer ensures that reactants are continually supplied to the catalyst surface, preventing the formation of stagnant regions. As a result, the active surface area of the catalyst remains well-utilized, and the catalyst retains its high catalytic activity over an extended period. This will also aid in preventing coke formation on the catalyst surface, a common deactivation mechanism. By promoting more uniform reactant distribution and efficient transport of reaction intermediates away from the catalyst, ultrasound reduces the conditions conducive to coke formation.

Lie et al.'s study demonstrated a significant improvement in reaction efficiency attributed to ultrasound-enhanced mass transfer. Enhanced mass transfer ensures that reactants are more effectively utilized, leading to higher molar conversion and improved product yields. This outcome aligns with the broader goal of catalysis, which is to maximize the production of desired products while minimizing energy consumption and waste generation. These findings have far-reaching implications for catalysis and process intensification. They not only highlight the critical role of efficient mass transfer in catalytic processes but also highlight ultrasound as an effective tool for achieving this goal. The work of other researchers in the field, such as the study by Chanerika et al., (2022) on surface poisoning and catalyst deactivation also resonate with these observations. Both studies emphasize the importance of addressing deactivation mechanisms and optimizing catalyst performance for sustainable and efficient catalytic processes.

2.3 Challenges in octene hydrogenation and the imperative for process intensification:

Octene hydrogenation stands as one of the cornerstones of industrial chemistry as it plays a pivotal role in the production of numerous fine chemicals and fuels. As a vital industrial process, it is not without

its share of challenges and these challenges range from mass transfer limitations to catalyst deactivation therefore necessitating the implementation of process intensification strategies for enhanced efficiency and sustainability. These hurdles underscore the urgency of adopting process intensification strategies for optimizing efficiency and promoting sustainability. The industrial significance of octene hydrogenation cannot be overstated. Octane, the product of this reaction, finds application as a high-octane component in gasoline, enhancing the fuel's performance and reducing engine knocking. Moreover, octane serves as a precursor in the production of various chemicals and polymers, rendering it an indispensable commodity in the chemical industry. Therefore, any enhancement in the octene hydrogenation process translates to substantial economic and environmental benefits.

2.3.1 Complex challenges in octene hydrogenation:

The journey from 1-octene to octane is beset with challenges that necessitate careful consideration. These challenges can broadly be categorized into two primary domains that are mass transfer limitations in slurry phase and catalyst deactivation. In slurry phase reactions like octene hydrogenation, achieving efficient mass transfer of reactants to the catalyst surface is essential in ensuring efficient reactant conversion. However, this process is often impeded by the presence of the solid catalyst particles within the liquid phase, which are actually needed for the reaction but somehow act as hindrances in the reaction progress. The diffusion of reactants through this liquid phase can be retarded by factors such as particle-particle interactions, steric effects, and boundary layer resistances and these challenges are well-acknowledged in recent studies. For instance, the work of Zhang et al., (2022) emphasized the significance of addressing mass transfer limitations in slurry phase reactions as they looked into the mechanisms of process intensification in gas-solid mass transfer through the use of nanofluids. Their study highlighted that the addition of nanoparticles, such as Fe_3O_4 and Al_2O_3, significantly improved mass transfer rates by up to 600% in some cases, depending on factors like nanoparticle concentration and particle size. For instance, the absorption of CO_2 in a nanofluid containing Fe_3O_4 nanoparticles increased the mass transfer coefficient by 111% under turbulent flow conditions. Their findings highlighted the need for innovative approaches, such as process intensification techniques, to enhance mass transfer and ultimately improve reaction rates.

On the other hand, catalyst deactivation has always been a ubiquitous problem in heterogeneous catalysis, including octene hydrogenation in which over time, active sites on the catalyst surface become blocked or poisoned by reaction intermediates or impurities and this ultimately leads to reduced catalytic activity. This phenomenon is a major factor limiting the operational lifespan and overall efficiency of catalysts. Recent studies have delved into strategies to mitigate catalyst deactivation and the study by Chanerika et al., (2022) explored the mechanisms of surface poisoning in the preferential hydrogenation of 1-octyne and 1-octene and proposed in-situ regeneration strategies to prolong catalyst lifespan. I this study, they found that the uncoated catalyst achieved high 1-octyne conversions (99%)

with initial selectivity to 1-octene at 30%, reaching 70% after 24 hours on-stream. Modifying the catalyst with 1-ethylimidazole ([EIM]) gave a 1-octene selectivity of 50% over 36 hours. Coating with various ionic liquids, ([BMIM][NTf2], [BMIM][PF6], [BMIM][BF4], and [N4444][NO3]) improved 1-octene selectivities, with [N4444][NO3] reaching up to 82%. Despite these improvements, conversion of 1-octyne significantly decreased from 99% with the uncoated catalyst to 30% with the modified versions due to diffusion limitations. Their findings highlighted that the performance of catalysts was influenced by both the metal and support. These observations underscored the imperative of understanding and addressing catalyst deactivation for sustainable catalytic processes.

In the quest for energy efficiency and sustainability, refining catalytic processes to align with environmental stewardship and resource conservation has become critical. The conventional approach to octane production via octene hydrogenation is increasingly at odds with contemporary sustainability goals, particularly concerning the environmental impact and resource utilization. Innovations in process intensification have emerged as a beacon of progress, providing pathways to mitigate issues such as significant catalyst waste being sent to landfills. The pioneering work by Wang et al., (2023) exemplifies this shift towards sustainable practices with their utilization of ultrasound-assisted catalysis. Their work revealed that ultrasonic treatment not only optimizes catalyst dispersion but also actively combats catalyst sintering, thereby bolstering catalytic stability and prolonging operational life. These kinds of breakthroughs underscore the transformative potential of process intensification in catalysis, marking a significant stride towards the development of greener and more resource-efficient chemical processes.

2.3.1.1 Mass transfer limitations in slurry phase reactions:

In the realm of catalysis, particularly in slurry phase reactions like octene hydrogenation, the efficient transport of reactants to the catalyst surface is of paramount importance. This is a critical step in ensuring that the catalytic process occurs at an optimal rate, ultimately influencing the overall efficiency and yield of the reaction. However, the presence of solid catalyst particles suspended within the liquid phase introduces a series of challenges, collectively known as mass transfer limitations. The transformational journey of 1-octene to octane in slurry phase reactions is extremely intricate, primarily due to the inherent difficulties associated with mass transfer. The movement of reactants through the slurry is hindered by several factors, each playing a crucial role in influencing the effectiveness of the catalytic process. One significant obstacle arises from interactions between solid catalyst particles. These interactions, which can range from Van der Waals forces to electrostatic repulsion, result in the agglomeration and clustering of particles within the slurry. As a consequence, the diffusion of reactant molecules to the catalyst surface becomes uneven, with some areas experiencing higher concentrations of reactants than others. This non-uniform distribution of reactants limits the overall efficiency of the catalytic process.

Steric effects further exacerbate the challenge of mass transfer. As reactant molecules navigate through the slurry, they may encounter hindrance from neighbouring molecules or catalyst particles. This steric hindrance arises from the spatial arrangement of atoms or groups within the molecules, leading to a decrease in the effective collision frequency between reactants and the catalyst surface. Consequently, the rate of reaction is diminished, and the process becomes less efficient. Another critical factor influencing mass transfer in slurry phase reactions is the formation of boundary layers. These layers develop at the interface between the solid catalyst particles and the surrounding liquid phase. Within these boundary layers, the concentration of reactants is lower compared to the bulk liquid, creating a gradient that drives mass transfer towards the catalyst surface. However, the thickness of these boundary layers can vary depending on factors such as reactor design, stirring speed, and reactant concentrations. Thicker boundary layers introduce additional resistance to mass transfer, further impeding the efficiency of the catalytic process.

Recent work, such as that by Baharudin, L., et al., (2021) have diligently examined and highlighted the significance of addressing mass transfer limitations in slurry phase reactions. Baharudin and colleagues delved into innovative approaches aimed at overcoming these challenges. Their findings highlighted the critical need for process intensification techniques, which aim to enhance mass transfer and subsequently elevate reaction rates. In their work, they discussed various process intensification strategies, including the implementation of advanced reactor designs and the utilization of novel mixing techniques as well as the use of nanocatalysts. They discussed the use of monolithic catalytic structured reactors such as a 400 cells-per-square-inch alumina monolith with $Pt/CeO_2/Al_2O_3$, achieved 90% CO conversion using 0.55 kg of catalyst compared to 1.2 kg in a conventional fixed bed reactor. A multifunctional compact multichannel reactor used for the selective oxidation of benzyl alcohol to benzaldehyde also demonstrated isothermal operation with a temperature rise of only 35°C at 25% conversion . Another example is the integration of an exothermic oxidative coupling of methane with endothermic steam reforming in a microstructured reactor, achieving close-to-thermodynamic-equilibrium conversions and high space-time yields . By systematically addressing factors such as particle-particle interactions, steric effects, and boundary layer resistances, the researchers observed notable improvements in mass transfer efficiency. This, in turn, translated to enhanced reaction rates and overall process efficiency.

Intensified reactors, especially those employing ultrasonic irradiation offer a novel approach to the hydrogenation process. Ultrasonic irradiation introduces acoustic cavitation in the reaction medium, generating localized hotspots with extremely high temperatures and pressures. This phenomenon can significantly enhance mass transfer rates and improve the distribution of reactants, thereby increasing reaction rates and yields (Suslick, 1998). In the case of 1-octene hydrogenation, the ultrasonic waves can facilitate the dispersion of hydrogen gas within the liquid phase, leading to a more efficient interaction with the catalyst surface (Mason et al., 2011). Furthermore, the use of nanocatalysts in these

intensified reactors marks a notable advancement. Nanocatalysts, due to their exceptionally high surface area-to-volume ratio, provide a larger active surface for the reaction to occur. This results in enhanced catalytic activity and selectivity (Astruc et al., 2005). In 1-octene hydrogenation, nanocatalysts can lead to a more complete conversion of the reactant and potentially lower the required temperatures and pressures, thereby reducing energy consumption (Roduner, 2006).

Furthermore, the study emphasized the relevance of understanding and mitigating mass transfer limitations, not only in the context of octene hydrogenation but also in a broader catalytic context. The reported findings by Haase et al., (2022) and Zhang et al., (2022) serve as a testament to the critical role of efficient mass transfer in heterogeneous catalysis and underscore the imperative for continued research in this area (Zhang et al., 2022).

2.3.1.2 Catalyst deactivation in 1-octene hydrogenation:

Catalyst deactivation is an omnipresent challenge in the field of heterogeneous catalysis, and it significantly influences processes like octene hydrogenation. Over time, the active sites on a catalyst's surface can succumb to a variety of deactivation mechanisms, including blockage or poisoning by reaction intermediates or impurities. This phenomenon stands as a major obstacle, curbing the operational lifespan and overall efficiency of the catalyst in octene hydrogenation particularly if alumina supported catalysts are used. The deactivation of catalysts is a complex and multifaceted phenomenon as has been earlier highlighted. In octene hydrogenation, as with many catalytic processes, it often results from the gradual accumulation of substances that hinder the catalytic activity of the solid surface. These deactivating species can include adsorbed reaction intermediates, by-products, or contaminants from the feedstock.

Catalyst deactivation in octene hydrogenation poses a formidable challenge as it directly affects the longevity and effectiveness of the solid catalyst particles. As active sites are blocked or poisoned, the catalyst's ability to facilitate the desired reaction diminishes significantly. This not only results in reduced product yields but also necessitates frequent regeneration or replacement of the catalyst. The costs associated with these maintenance procedures, along with the environmental footprint of disposing of spent catalysts, make catalyst deactivation a serious concern for both economic and sustainability reasons. Addressing catalyst deactivation has been a focal point of recent research efforts in heterogeneous catalysis. One such study, conducted by Forzatti and Lietti, (1999) stands out for its exploration of surface poisoning mechanisms and the proposal of innovative in-situ regeneration strategies. Forzatti and Lietti reviewed various mechanisms of catalyst deactivation, including coking, sintering, and poisoning. For example, they reported that coking could reduce catalyst activity by up to 70% within a few hours of operation in fluid catalytic cracking (FCC) processes. They also discussed regeneration strategies to mitigate deactivation, such as oxidative treatments to remove coke deposits and thermal treatments to reverse sintering effects. Chanerika and colleagues investigated the

mechanisms by which surface poisoning occurs during alkene hydrogenation. Their findings offered crucial insights into the specific deactivation pathways, shedding light on the nature of the species responsible for blocking active sites. This level of mechanistic understanding is invaluable as it forms the basis for developing targeted mitigation strategies.

Forzatti and Lietti, (1999) did not stop at elucidating the deactivation mechanisms, they also proposed in-situ regeneration strategies to prolong the catalyst's lifespan. This is a noteworthy advancement, as it offers a practical solution to a long-standing problem in catalysis. In-situ regeneration involves rejuvenating the catalyst while it is still within the reactor, thus minimizing downtime and reducing the need for costly catalyst replacement. The strategies proposed by Forzatti and Lietti, (1999) could involve various techniques, such as controlled exposure to specific gases or periodic treatments to remove deactivating species from the catalyst surface. The effectiveness of these strategies was substantiated through experimentation, demonstrating their potential to extend the operational lifespan of the catalyst and maintain its catalytic activity over longer periods. The work by Forzatti and Lietti, (1999) and Chanerika et al., (2022) underscores the critical importance of understanding and addressing catalyst deactivation for sustainable catalytic processes. By identifying deactivation mechanisms and proposing practical regeneration strategies, their studies contributes to the development of more efficient and environmentally responsible catalytic processes.

2.3.1.3 Energy efficiency and sustainability: A paradigm shift:

In the contemporary landscape of chemical engineering, the pursuit of energy efficiency and sustainability has evolved from a mere aspiration to an absolute necessity. As the global community grapples with pressing environmental concerns and resource scarcity, the imperative to optimize catalytic processes has assumed paramount importance. In this context, traditional approaches to octene hydrogenation, though established, may no longer align with the current emphasis on resource conservation and reduced environmental impact. Catalytic processes, including octene hydrogenation, have historically played a pivotal role in industry and chemical synthesis. However, the environmental and economic costs associated with these processes have increasingly come under scrutiny. Traditional methods often entail the utilization of vast amounts of energy and raw materials, leading to elevated greenhouse gas emissions and resource depletion.

In this day and age of heightened awareness, sustainable catalysis has emerged as a central objective. The aim is to develop processes that not only achieve the desired chemical transformations but also do so with minimal energy consumption, reduced waste generation, and a smaller environmental footprint. Recent advancements in process intensification techniques offer a promising avenue to realize these sustainability goals. Process intensification involves a concerted effort to enhance the efficiency of chemical processes, enabling the production of chemicals and materials with fewer resources and less energy. Ultrasound-assisted catalysis, exemplified by the work of Wang et al., (2023), serves as a

compelling illustration of the potential of process intensification to revolutionize catalytic processes. Wang and colleagues, (2023) conducted a pioneering study that underscored the transformative potential of ultrasound-assisted catalysis. Their research serves as an exemplary case study of how innovative techniques can align traditional catalytic processes with the imperatives of energy efficiency and sustainability.

One of the fundamental aspects of catalysis is the accessibility of active sites on the catalyst surface. Effective mass transport to these sites is crucial for reaction efficiency. Figure 2.11 shows two mechanistic pathways for the sintering-induced growth of metal crystallites on a support substrate. In pathway (A), atomic migration is the driving mechanism, where individual atoms are thermodynamically incentivized to travel from the crystallite onto the support material, possibly due to factors such as surface energy minimization and thermal dynamics (Argyle and Bartholomew, 2015). This atomic transfer contributes to the gradual enlargement and morphological evolution of the metal crystallites, impacting the catalyst's active surface area and, consequently, its catalytic activity. Pathway (B) illustrates crystallite migration, a phenomenon where entire crystallites, rather than single atoms, traverse the support's surface. This migration can lead to the coalescence of adjacent crystallites, which may alter the dispersion and the number of active sites available for catalysis (Argyle and Bartholomew, 2015). Both models underscore the dynamic nature of catalyst surfaces under operational conditions and highlight the importance of understanding these processes for the design of more stable and efficient catalytic systems.

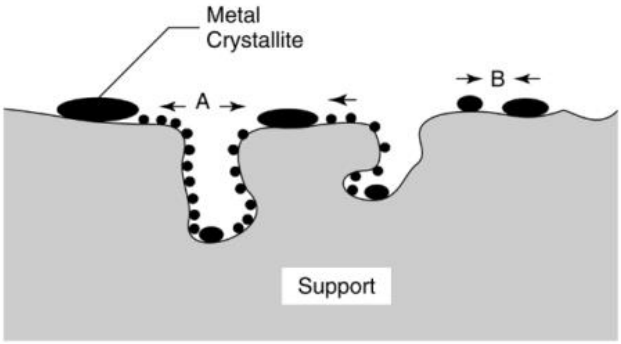

Figure 2. 11: Two conceptual models for crystallite growth due to sintering by (A) atomic migration or (B) crystallite migration. Source: Argyle and Bartholomew, (2015).

Traditional methods often struggle to maintain optimal dispersion of catalyst particles, leading to reduced catalytic activity. Wang et al., (2023) demonstrated that ultrasound could address this challenge by enhancing catalyst dispersion. Cavitation and microstreaming generated by ultrasound ensure a uniform distribution of catalyst particles in the reaction mixture, maximizing the utilization of active sites. Catalyst sintering, the undesirable process of particle coalescence and growth, is a major issue in traditional catalysis. It not only diminishes catalyst activity but also necessitates frequent catalyst replacement, incurring significant costs. The innovative aspect of Wang et al.'s (2023) work lies in its

ability to prevent sintering through ultrasound assistance. By maintaining catalyst particles in a well-dispersed state, ultrasound effectively inhibits sintering, leading to improved catalytic stability and an extended catalyst lifespan.

The significance of Haase et al., (2022) and Wang's studies extend beyond improved catalyst dispersion and sintering prevention. Their work represent a paradigm shift in catalysis towards sustainability and energy efficiency. Ultrasound-assisted catalysis, as a process intensification technique, aligns perfectly with the contemporary emphasis on resource conservation and environmental responsibility. In these modern times where every joule of energy and every molecule of raw material count, the impact of such innovations cannot be overstated. By reducing energy consumption, minimizing waste, and extending the operational life of catalysts, process intensification techniques like ultrasound-assisted catalysis exemplify how catalysis can become more sustainable and efficient.

2.3.2 Integration of process intensification: A way forward:

The realm of catalysis, particularly in the context of hydrogenation reactions stands at the crossroads of transformation. The challenges inherent in this process, from mass transfer limitations to catalyst deactivation demand a holistic and innovative approach. Process intensification emerges as a beacon of promise, encompassing a spectrum of techniques and methodologies that collectively offer a way forward that is going to steer catalysis towards higher efficiency and environmental responsibility. The challenges encountered in octene hydrogenation are diverse and interconnected. They encompass the impediments to mass transfer efficiency, the spectre of catalyst deactivation, and the imperative of sustainability. To address these challenges effectively, a multifaceted approach becomes not just desirable but imperative.

At the heart of many catalytic reactions lies the issue of efficient mass transfer. The ability to transport reactants to the catalyst surface with precision and speed is foundational to the catalytic process. Mass transfer limitations, often experienced in slurry phase reactions, can result in uneven reactant distribution, leading to diminished reaction rates and prolonged reaction times. However, the integration of process intensification techniques such as ultrasound-assisted catalysis, as exemplified by Wang et al., (2023), represents a solution to this problem. It ensures the uniform distribution of catalyst particles and accelerates mass transport, unlocking the full potential of catalytic reactions.

Catalyst deactivation, an ever-present adversary in heterogeneous catalysis, has historically demanded frequent regeneration or replacement of catalysts. This not only imposes substantial economic costs but also contributes to environmental concerns. The work of Chanerika et al., (2022) signifies a pivotal shift in this paradigm. By understanding the mechanisms of surface poisoning and proposing innovative in-situ regeneration strategies, they have laid the foundation for prolonged catalyst lifespan and reduced environmental impact. The integration of such strategies into catalytic processes is a critical step towards sustainable catalysis.

In the contemporary landscape, the pursuit of sustainability is non-negotiable. Catalysis, as a key driver of chemical transformations must align with the broader goals of resource conservation and environmental responsibility. Process intensification strategies, exemplified by the works of Zhang et al., (2022), Chanerika et al., (2022), and Wang et al., (2023), underscore the pressing need for integrated approaches that enhance sustainability. Through reduced energy consumption, minimized waste generation, and prolonged catalyst lifespan, process intensification embodies the ethos of responsible and efficient catalysis. The collective vision presented by these studies represents more than just incremental improvements. It signifies a fundamental transformation in the field of catalysis. The integration of process intensification techniques signifies a departure from traditional practices and a bold step into a future where catalytic processes are not only more efficient but also more environmentally conscious.

The challenges in octene hydrogenation, though formidable, have sparked innovation and creativity in the field. Process intensification is more than a set of techniques, but it is a mindset that embraces efficiency, sustainability, and responsibility. By improving mass transfer, preventing catalyst deactivation, and enhancing overall process sustainability, process intensification strategies pave the way for catalytic processes that are not only more efficient but also environmentally conscious. These challenges necessitate a transformative approach. Process intensification, as showcased by the works of Patel et al., (2022), Chanerika et al., (2022) and Wang et al., (2023) offers a comprehensive solution to these challenges. It signifies a paradigm shift in catalysis, one where efficiency and sustainability converge to shape the future of chemical processes. The integration of process intensification techniques paves the way for catalytic processes that are not only technically superior but also aligned with the global imperative of resource conservation and environmental responsibility.

2.4 Nanocatalysts for octene hydrogenation:

The application of nanocatalysts in reactions like octene hydrogenation has ushered in a new era, characterized by unprecedented efficiency, selectivity, and sustainability. At the heart of this transformation lies the unique characteristics of nanocatalysts. Engineered at the nanoscale level, these catalytic entities possess an extraordinary surface area-to-volume ratio, a defining feature that endows them with exceptional catalytic activity. This characteristic is a consequence of the higher number of active sites available for reactant adsorption and catalytic reactions, which accelerates the rate of reactions, including octene hydrogenation (Chanerika et al., 2022). Another pivotal attribute of nanocatalysts is their size-dependent properties (Zhou et al., 2010, Wang et al., 2019). As the size of nanoparticles diminishes, quantum effects become more pronounced. This size-dependent reactivity allows precise control over reaction pathways and selectivity, permitting the production of specific target products. Thus, nanocatalysts have opened doors to the tailoring of catalytic performance with a level of precision previously unattainable. Furthermore, the small size of nanocatalysts has implications

for mass transport in reactions like octene hydrogenation (Wang et al., 2018). The efficient transport of reactants to active sites on catalyst surfaces is essential for catalytic activity. Nanocatalysts, due to their diminutive size, facilitate rapid and efficient mass transport, thereby addressing one of the key challenges often encountered in slurry phase reactions.

2.4.1 Characteristics and benefits of nanocatalysts in octene hydrogenation:

Nanocatalysts represent a transformative force in octene hydrogenation and catalysis in general. Their advantages, including enhanced surface area, size-dependent properties, improved mass transport, reduced catalyst loadings, and their contribution to green chemistry, collectively highlight their potential to revolutionize catalytic processes, making them a focal point in the pursuit of efficient and sustainable chemical transformations. Nanocatalysts have remarkable enhanced surface areas. This feature provides a significantly higher density of catalytic active sites compared to bulk catalysts. Enhanced surface area facilitates more efficient reactant adsorption in catalytic reactions, which ultimately boosts catalytic activity. Additionally, the size-dependent properties of nanocatalysts play a pivotal role. Nanoparticle size can influence electronic structure and reactivity, allowing for precise control over reaction pathways and, consequently, enhanced selectivity. This size-dependent tunability is crucial in achieving specific catalytic outcomes. Genest's research has been instrumental in uncovering the significance of size-dependent properties in nanocatalysts for alkene isomerization and hydrogenation using Pd/Al_2O_3 catalysts (Genest et al., 2021). His work highlights that variations in nanoparticle size can significantly influence their electronic structure, ultimately affecting catalytic activity and selectivity (Jin et al., 2017, Genest et al., 2021). Jin 's contributions further expand upon this idea, highlighting how size-dependent properties enable the tailored design of nanocatalysts. This precise control over reaction pathways contributes to higher selectivity, a critical factor in octene hydrogenation and other catalytic processes (Chanerika et al., 2022).

Efficient mass transport of reactants to active sites is another key benefit of nanocatalysts. Their small size and increased surface area promote rapid diffusion of reactants, addressing mass transfer limitations frequently encountered in slurry phase reactions. This ensures that reactants swiftly reach catalytic sites, significantly enhancing reaction rates. Gleason's work examines the role of nanocatalysts in facilitating mass transport, highlighting how nanocatalysts, due to their small size and increased surface area, promote rapid diffusion of reactants to catalytic sites (Gleason et al., 2019). This enhancement in mass transport directly addresses challenges posed by mass transfer limitations often encountered in slurry phase reactions. Moreover, nanocatalysts often require lower catalyst loadings compared to their bulk counterparts. This is due to their exceptional activity, translating into cost savings and minimised waste generation. Nanocatalysts' ability to operate efficiently with reduced catalyst loadings aligns with economic and sustainability goals, making them an attractive choice for catalytic processes.

Lastly, nanocatalysts contribute significantly to green and sustainable chemistry. Their high efficiency and selectivity reduce the formation of unwanted by-products, promoting environmentally friendly chemical transformations. This aligns with the modern emphasis on resource conservation and reduced environmental impact.

2.4.2 Recent advances in nanocatalysts design for octene hydrogenation:

In the pursuit of optimizing octene hydrogenation, recent research efforts have been dedicated to the design and application of nanocatalysts. These efforts have yielded substantial progress, leading to the development of novel nanomaterials and innovative catalytic strategies. Researchers have explored various nanomaterials, including metal nanoparticles such as Pt, Pd, and Ru supported catalysts as well as bimetallic nanoparticles, to tailor catalytic performance. One noteworthy development is the utilization of support materials like graphene and carbon nanotubes in nanocatalysts design (Li et al., 2020). These supports not only stabilize the nanocatalysts but also introduce unique properties such as rendering mechanical stability to catalyst nanoparticles as well as acting as solid capping agents, which further enhances the catalytic activity. Moreover, surface modification and functionalization of nanocatalysts have been explored to fine-tune their selectivity (Zhang et al., 2021). These strategies enable researchers to exert precise control over reaction pathways, guiding them towards the synthesis of specific target products.

2.4.3 Challenges and future directions in nanocatalysis for octene hydrogenation:

Despite the promising advancements, challenges persist in the application of nanocatalysts to octene hydrogenation. Stability, especially under harsh reaction conditions remains a concern as well as the scalability, cost-effectiveness of nanocatalyst synthesis and production require further optimization (Zhang et al., 2020). Future research in nanocatalysis for octene hydrogenation should focus on overcoming these challenges by coming up with strategies for enhancing catalyst stability and sustainability, as well as methods for large-scale production, will be pivotal. Additionally, the exploration of novel nanomaterials and advanced characterization techniques should also uncover new avenues for catalytic innovation (Mourdikoudis et al., 2018). Nanocatalysts have ushered in a transformative phase in catalysis, notably in the context of octene hydrogenation since their unique characteristics, including enhanced surface area, size-dependent properties, and improved mass transport, have propelled catalytic processes to unprecedented levels of efficiency and sustainability. Recent advancements in nanocatalyst design underscore the potential for even greater achievements in the field. However, challenges remain, necessitating continued research and innovation to unlock the full potential of nanocatalysis in octene hydrogenation and beyond. While nanocatalysts offer a plethora of advantages, it is essential to recognize that these advantages can be further harnessed and leveraged to overcome the remaining challenges in octene hydrogenation. One such avenue of exploration lies in process intensification, a strategy that promises to not only mitigate the challenges discussed earlier but

also amplify the benefits of nanocatalysts (Stankiewicz and Moulijn, 2000, Stankiewicz and Moulijn, 2004).

Process intensification, as demonstrated through techniques like sonication, offers a dynamic approach to catalysis. The application of ultrasonic irradiation in conjunction with nanocatalysts introduces a new dimension to catalytic processes. The localized regions of high temperature and pressure generated by cavitation microbubbles during sonication have the potential to break down mass transfer barriers, effectively addressing one of the primary challenges in slurry phase reactions. As researchers have demonstrated, the use of ultrasound facilitates efficient mass transport which ensures reactants readily reach catalytic active sites (Laugier et al., 2008). Furthermore, the synergy between nanocatalysts and sonication can significantly reduce catalyst deactivation. The phenomenon of catalyst deactivation, often attributed to surface poisoning and sintering, can be effectively mitigated through in-situ regeneration techniques made feasible by sonication (Laugier et al., 2008, Li et al., 2021). The ability to prolong the lifespan of nanocatalysts through these innovative approaches not only enhances the economic feasibility of catalytic processes but also aligns perfectly with the principles of sustainability. Figure 2.12 shows in-situ catalysts regeneration of heterogeneous catalysts on support material using ultrasound. Here, the combination of solid support (e.g., alumina, zeolite and silica) and metal nanoparticles help to resolve the aggregation and sintering issues by using mechanical effects of ultrasound since the composite structure can isolate the metal nanoparticles on the surface of supporting material and reduce the particle size. Consequently, the metal catalysts and metal-based heterogeneous catalysts produced from ultrasound-assisted approaches can provide an increased surface area and highly selective surface for the reduction reaction.

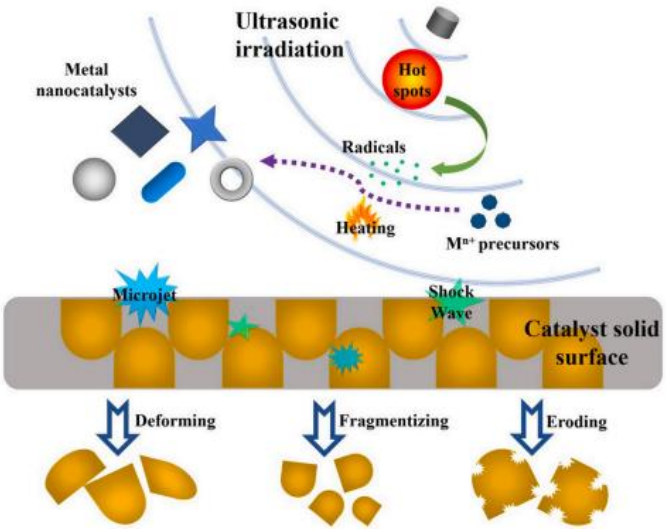

Figure 2. 12: Physical effects of ultrasound irradiation on the heterogeneous catalyst in-situ regeneration. Source: Li et al., (2021).

In addition, the use of sonication in combination with nanocatalysts contributes to greener and more efficient catalytic processes. By improving mass transport, preventing catalyst deactivation, and enhancing overall process sustainability, this integrated approach aligns harmoniously with the ever-increasing emphasis on resource conservation and reduced environmental impact in modern chemical engineering (Keil, 2018). This entails that nanocatalysts, when paired with process intensification techniques like sonication, have the potential to redefine the landscape of catalysis in octene hydrogenation. Challenges that have long hindered the efficiency and sustainability of octene hydrogenation can be reduced, if not eradicated. As researchers and scientists continue to explore this exciting intersection of nanotechnology and process intensification, the future of catalysis appears brighter than ever.

In essence, the advantages brought forth by nanocatalysts when combined with the ingenuity of process intensification offer a promising avenue for catalysis to meet the evolving demands of our world. This integrated approach underscores the transformative potential of nanocatalysts in catalytic processes, opening doors to greener, more efficient, and sustainable chemical transformations (Stankiewicz et al., 2019).

2.5 Ultrasonic irradiation: Principles and effects on mass transfer:

Ultrasonic irradiation is a technique that is rooted in the principles of acoustic physics and has gained substantial recognition in the realm of catalysis. The application of ultrasonic irradiation to reacting species which is also known as sonochemistry involves the use of powerful ultrasonic waves in a slurry medium that contains the reacting species. Ultrasound has been known to accelerate dissolution, improving the reaction rate as well as regenerating surfaces of solid reactants or catalysts and this is all achieved through acoustic cavitation (Suslick and Price, 1999). Acoustic cavitation results in the formation and rapid growth and sudden collapse of bubbles in liquid mixtures which are under the influence of high-intensity ultrasonic irradiation. The collapse of the bubbles (vacuum bubbles) generates a large concentration of energy due to the conversion of kinetic energy from the motion of the liquid into heat and localised pressure. The collapse of the bubbles also produces temporary regions of high pressure and high temperatures known as localized hot-spots. These hot-spots act as ‘microreactors’ that drive the chemical reactions (Suslick et al., 1999). This is illustrated in Figure 2.13 below, which illustrates the fundamental concept of ultrasonic cavitation, a physical phenomenon extensively leveraged in various fields, from materials processing to medicine (Johansson et al., 2017).

The illustration in Figure 2.13 shows the cyclical nature of acoustic waves, characterized by alternating high-pressure (compression) and low-pressure (expansion) cycles. It is during these expansion phases when microscopic bubbles are formed within the slurry in a process known as nucleation and these cavities, once initiated, they undergo a growth phase due to the differential vapour pressure, leading to their expansion. As they reach a resonant size, these bubbles are unable to maintain structural integrity,

culminating in a violent implosion. This implosion generates intense local conditions, including high temperatures (5000 °C) and pressures (500 bar), which are exploited in chemical processes to induce reactions or enhance mass transfer (Johansson et al., 2017). The precise control of this cavitation process is critical, as it directly influences the efficiency and outcome of the ultrasound-assisted applications.

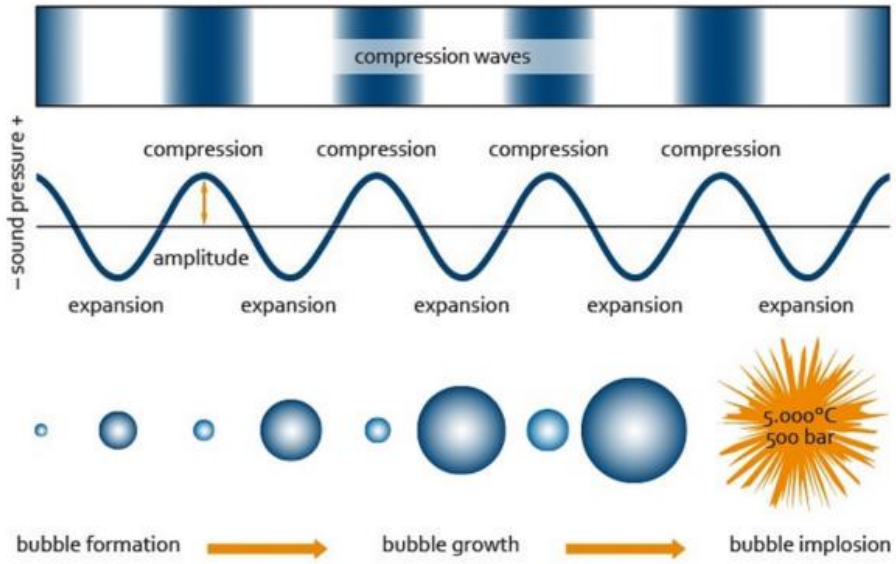

Figure 2. 13: Principle of ultrasound cavitation. The initiated bubbles grow due to evaporation and finally reach critical size (resonant) when it grows quickly and collapse violently. Source: Johansson et al., (2017).

All chemical reactions require a significant amount of energy to occur and this energy can be made available in several forms. Ultrasonic irradiation provides an alternate source of energy for chemical reactions to occur, as compared to traditional methods such as the addition of heat. The concentrated localized pressures and temperatures coupled with the heat generated from cavitation provides suitable conditions for chemical reactions. In ultrasonic irradiation, the collapse of the bubbles provides a unique mechanism for the generation of high-energy chemistry (Suslick and Price, 1999). However, the cavitation bubbles are largely dependent on the intensity of the ultrasonic waves which rely on various operating parameters such as wave frequency as well as the physicochemical properties and compressibility of the liquid.

Ultrasonic irradiation can be utilised to play various roles in chemical reactions and this may include prolonging the catalyst activity, the breakage of chemical bonds to form highly reactive species as well as providing the necessary activation energy required for reactions to occur. Once applied to a reacting mixture, the concentrated ultrasonic waves result in interesting physical and chemical effects such as emulsification, luminescence and chemical transformation. According to Shibata et al, the application of ultrasound has been widely used in the synthesis of organic reactions due to its improvement of the

overall reaction rate and the ability to alter the selectivity of the performance (Al-Rasheed et al., 2016, Shibata et al., 2004). Furthermore, ultrasonic irradiation is a popular technique used in chemical reactions as it is simple to control, reduces the reaction time, minimizes waste material and reduces the energy consumption required thereby enhancing the chemical reactivity (Schiel et al., 2015).

Currently, ultrasound is applied in large-scale industrial processes to increase selectivity and yield as well as to reduce impurities and side reactions. Ultrasonic irradiation is commonly used in the chemical, agricultural and food industries (Khadhraoui et al., 2021).

2.5.1 Fundamentals of ultrasonic irradiation:

Ultrasonic irradiation, a process intensification technique involves the application of high-frequency sound waves (typically above the range of human hearing, 20 kHz) to a reaction medium (Mason, 2011). This results in the generation of cavitation microbubbles, which are tiny, transient gas-filled bubbles. The growth and subsequent collapse of these microbubbles create localized regions of high temperature and pressure, inducing physical and chemical effects in the surrounding medium (Suslick, 1990). In the context of heterogeneous catalysis, ultrasonic irradiation plays a pivotal role in enhancing reaction kinetics and selectivity. The fundamental principle lies in the phenomenon of acoustic cavitation. As the sound waves propagate through the reaction mixture, they induce alternating cycles of compression and rarefaction. During the rarefaction phase, the pressure within the medium drops, allowing pre-existing gas nuclei or dissolved gases to form microbubbles. These microbubbles continue to grow until they reach a critical size, after which they rapidly collapse during the compression phase (Mason, 2011).

The collapse of these microbubbles is characterized by intense localized heating and high pressures, creating conditions akin to those found in extreme environments. Temperatures can momentarily reach several thousand degrees Celsius, while pressures can exceed several hundred atmospheres.

These extreme conditions give rise to phenomena such as shock waves, microjets, and high-velocity liquid jets, all of which exert mechanical and chemical effects on the surrounding materials (Suslick, 1990). In heterogeneous catalytic systems, these effects have significant implications. Firstly, the collapse of microbubbles enhances mass transfer by disrupting diffusion boundary layers and promoting convective transport of reactants to the catalyst surface (Zhang et al., 2016). This is particularly crucial in slurry phase reactions where mass transfer limitations often hinder reaction rates.

Additionally, the intense local heating and pressure can lead to physical and chemical changes on the catalyst surface. For instance, it can alter the morphology and structure of the catalyst, potentially exposing previously inaccessible active sites (Zhang et al., 2016). Moreover, the high-energy conditions induced by cavitation can break chemical bonds and accelerate surface reactions, influencing catalytic reactivity. In recent studies, the application of ultrasonic irradiation has demonstrated remarkable improvements in reaction rates, conversion yields, and selectivity profiles across a range of

heterogeneous catalytic systems (Gao et al., 2020). Researchers have harnessed the principles of ultrasonics to overcome mass transfer limitations, extend catalyst lifespan, and uncover new facets of catalytic mechanisms.

Apart from cavitation, another key effect of ultrasonic irradiation is acoustic streaming. This is characterized by the creation of liquid flow patterns near the ultrasonic source. Acoustic streaming can significantly affect mass transfer in catalytic systems. It promotes efficient mixing and convective transport of reactants and products, thereby reducing concentration gradients and enhancing reaction rates (Gogate et al., 2019).

2.5.2 Enhanced mass transfer in heterogeneous catalytic reactions:

The efficient mass transfer of reactants to catalytic active sites is a critical determinant of reaction kinetics in heterogeneous catalysis. In many catalytic processes, mass transfer limitations can significantly impede reaction rates, particularly in slurry phase reactions where solid catalyst particles are suspended in a liquid phase. Ultrasonic irradiation, by virtue of its ability to induce cavitation, offers a powerful means to overcome these mass transfer limitations and enhance overall reaction efficiency. The influence of ultrasonic irradiation on mass transport phenomena is profound. It addresses the core challenges associated with mass transfer limitations in heterogeneous catalysis. One of the primary effects is the disruption of diffusion boundary layers that typically form around solid catalyst particles in a slurry phase. These boundary layers act as barriers, impeding the diffusion of reactants to the catalyst surface. However, under the influence of ultrasonic waves, the collapse of cavitation microbubbles generates intense microflows and turbulence, effectively breaking down these diffusion boundary layers (Zhang et al., 2016).

This disruption of boundary layers promotes convective transport, ensuring that reactants readily reach catalytic active sites. As a result, reaction rates are significantly enhanced, leading to higher conversions and improved yield of desired products (Gao et al., 2020). Moreover, the enhanced mass transport allows for better utilization of the catalytic surface area, optimizing catalyst performance. The practical benefits of improved mass transfer through ultrasonic irradiation are well-documented in various catalytic systems. For instance, in the context of hydrodewaxing processes for refining petroleum, ultrasonic irradiation has been applied to improve the mass transfer of reactants to solid catalysts, resulting in enhanced conversion of long-chain hydrocarbons into valuable shorter-chain products (Deng et al., 2019). Similar successes have been reported in the hydrogenation of olefins and the removal of pollutants from wastewater using catalytic processes under ultrasonic irradiation (Sadeghi Rad et al., 2021).

Furthermore, the effects of ultrasonic irradiation on mass transfer extend beyond merely overcoming diffusion limitations. The microflows induced by cavitation can also disrupt steric effects that may hinder the movement of reactant molecules, especially in confined spaces or around complex catalyst

structures. This contributes to improved reactant accessibility to catalytic active sites and can lead to increased reaction selectivity (Zhang et al., 2016). Ultrasonic irradiation serves as a potent tool for addressing mass transfer limitations in heterogeneous catalysis and by disrupting diffusion boundary layers, promoting convective transport, and mitigating steric hindrances, it enhances the overall mass transfer of reactants to catalyst surfaces. The practical implications are profound, as evidenced by numerous studies across various catalytic systems. Ultrasonic irradiation, in synergy with nanocatalysts and other process intensification techniques, represents a promising avenue for advancing the efficiency and sustainability of catalytic reactions.

2.5.3 Impact on catalyst-reactant interaction and reactivity:

Ultrasonic irradiation exerts a significant influence on the interaction between catalysts and reactants in heterogeneous catalytic systems. The effects are multifaceted, spanning alterations in catalyst surface morphology, enhancement of active site accessibility, and changes in the reactivity of the catalytic species. One notable effect of ultrasonic irradiation is the alteration of catalyst surface morphology. The collapse of cavitation microbubbles generates intense microjets and high-velocity liquid jets, which can lead to mechanical and abrasive effects on the catalyst surface (Mason, 2011). This can result in changes to the surface structure and topography of the catalyst. For instance, in studies involving metal-based catalysts, ultrasonic irradiation has been shown to promote the formation of rougher surfaces with increased active sites (Gao et al., 2020). The increased surface roughness can enhance the catalyst's performance by providing more sites for reactant adsorption and subsequent catalytic reactions.

Moreover, the localized high temperatures and pressures created during cavitation events can break chemical bonds and accelerate surface reactions. This can lead to changes in the reactivity of catalytic species (Suslick, 1990). For instance, certain catalytic reactions may involve the adsorption of reactants on the catalyst surface, followed by surface reactions that lead to product formation. Under ultrasonic irradiation, the enhanced reactivity of the catalyst surface can lead to faster reaction kinetics and improved molar conversion (Deng et al., 2019). In addition to these physical and chemical effects, ultrasonic irradiation can also improve the accessibility of active sites on the catalyst surface. The disruption of diffusion boundary layers and the promotion of convective transport, as discussed in the previous section, ensure that reactants readily reach the catalytic sites. This is particularly important for catalytic reactions where reactant molecules need to adsorb onto the catalyst surface to initiate the reaction (Zhang et al., 2016). Improved accessibility to active sites can lead to higher reaction rates and improved selectivity, as more reactant molecules are available for catalytic conversion.

The collective impact of ultrasonic irradiation on catalyst-reactant interaction and reactivity is reflected in enhanced overall catalytic performance. Researchers have demonstrated these effects in various catalytic systems, including hydrogenation, dehydrogenation, and the removal of contaminants from wastewater. The combination of ultrasonic irradiation with nanocatalysts has been of particular interest,

as it amplifies the advantages of both techniques, leading to enhanced catalytic efficiency and sustainability (Yang et al., 2021). With this in mind, ultrasonic irradiation, through its capacity to modify catalyst surface morphology, enhance active site accessibility, and accelerate surface reactions, plays a pivotal role in influencing catalyst-reactant interaction and reactivity in heterogeneous catalytic systems. The practical implications of these effects are evident in a range of catalytic processes, offering opportunities to optimize reaction pathways, improve conversion yields, and enhance selectivity profiles.

2.5.4 In-situ catalyst regeneration:

One of the noteworthy advantages of ultrasonic irradiation in heterogeneous catalysis is its potential to facilitate in-situ catalyst regeneration. Catalyst deactivation is a common challenge in many catalytic processes, where active sites on the catalyst surface can become blocked or poisoned over time. This deactivation can result in reduced catalytic activity, leading to decreased operational lifespan and overall efficiency of the catalyst. Sonication offers a unique approach to mitigating catalyst deactivation. The intense conditions created during cavitation, including high temperatures and pressures, can aid in the removal of impurities or reaction by-products that might accumulate on the catalyst surface. This process can effectively regenerate the catalyst, restoring its activity and prolonging its lifespan (Suslick, 1990).

Studies have demonstrated the effectiveness of ultrasonic irradiation in promoting in-situ catalyst regeneration. For instance, in the context of catalytic hydrogenation reactions, ultrasonic irradiation has been applied to remove carbonaceous deposits that can accumulate on metal catalyst surfaces. These deposits can block active sites, leading to reduced catalytic performance. Under ultrasonic conditions, the microjets and high-velocity liquid jets generated during cavitation can dislodge these deposits, effectively "cleaning" the catalyst surface and rejuvenating its activity (Deng et al., 2019). Furthermore, the ability of ultrasonic irradiation to break chemical bonds and accelerate surface reactions can also play a role in catalyst regeneration. It can assist in the conversion of undesirable species that may have formed during the catalytic process into more benign products. This can prevent the build-up of deactivating compounds on the catalyst surface, contributing to sustained catalytic activity (Zhang et al., 2016).

The concept of in-situ catalyst regeneration aligns with the principles of process intensification, as it not only enhances reaction kinetics but also extends the operational lifespan of the catalyst. This has significant implications for the sustainability and efficiency of catalytic processes, particularly in industries where catalyst replacement or regeneration can be resource-intensive. In summary, ultrasonic irradiation offers a unique pathway for in-situ catalyst regeneration in heterogeneous catalytic systems. By effectively removing impurities, cleaning catalyst surfaces, and preventing the accumulation of deactivating compounds, ultrasonic irradiation contributes to the longevity and sustainability of

catalytic processes. This aspect further underscores the versatility and potential of ultrasonic-assisted catalysis in enhancing the efficiency and resource conservation of catalytic reactions.

2.5.5 Synergies with nanocatalysts: A holistic approach to catalysis:

The integration of ultrasonic irradiation with nanocatalysts represents a holistic approach to catalysis that leverages the advantages of both techniques, leading to enhanced catalytic performance, selectivity, and sustainability. Nanocatalysts, as previously discussed, offer unique benefits, including enhanced surface area, size-dependent properties, improved mass transport, reduced catalyst loadings, and the promotion of green chemistry. Ultrasonic irradiation, on the other hand, contributes to efficient mass transfer, catalyst-reactant interaction, and in-situ catalyst regeneration. When these two approaches are combined, the synergistic effects can be profound.

One significant advantage of combining ultrasonic irradiation with nanocatalysts is the further improvement in mass transfer. Nanocatalysts, with their high surface area and size-dependent properties, already excel in promoting efficient mass transport of reactants to active sites. However, ultrasonic irradiation, as discussed earlier, disrupts diffusion boundary layers and enhances convective transport, providing an additional boost to mass transfer (Gao et al., 2020). This results in even higher reaction rates and conversion yields. The synergistic effects extend to catalyst-reactant interaction. Nanocatalysts, due to their size-dependent properties, allow for precise control over reaction pathways and selectivity. Ultrasonic irradiation, by enhancing active site accessibility and reactivity, further refines the catalytic process. This combination leads to the optimisation of catalytic pathways and the reduction of unwanted by-products (Deng et al., 2019).

Moreover, the tandem application of ultrasonic irradiation and nanocatalysts often permits a reduction in catalyst loadings. Nanocatalysts, with their exceptional activity, already require lower loadings than their bulk counterparts. When ultrasonic irradiation is introduced to enhance mass transfer and catalyst-regeneration processes, the catalyst's efficiency is further amplified. As a result, lower catalyst loadings can be employed while maintaining or even improving the reaction's efficiency. This not only reduces catalyst costs but also aligns with the principles of resource conservation and sustainability. The holistic approach of combining ultrasonic irradiation and nanocatalysts contributes to green chemistry goals. The enhanced efficiency and selectivity of the catalytic process lead to less waste generation and reduced environmental impact. This aligns with the contemporary emphasis on sustainable and environmentally conscious chemical processes (Yang et al., 2021).

The practical applications of this synergy are evident in numerous catalytic systems. Researchers have demonstrated the benefits of combining ultrasonic irradiation and nanocatalysts in reactions such as hydrogenation, dehydrogenation, and the removal of pollutants from wastewater. These studies highlight the potential for a new era of catalysis that integrates various techniques for improved efficiency, sustainability, and selectivity (Gao et al., 2020).

Considering everything, it can be concluded that the combination of ultrasonic irradiation with nanocatalysts represents a holistic and synergistic approach to catalysis. This approach optimizes mass transfer, catalyst-reactant interaction, and catalyst-regeneration processes. The resulting enhancement in catalytic performance, selectivity, and sustainability has far-reaching implications for the field of catalysis, and process intensification by offering innovative solutions to the challenges that have traditionally reduced the effectiveness of these processes.

2.5.6 Comparative studies: Ultrasound vs. other process intensification techniques:

The field of process intensification is rich with diverse techniques, each offering unique advantages and challenges. Among these, ultrasound and microwave-assisted catalysis are two prominent methods, each with its own relative impact on catalysis. Additionally, there is an emerging trend in combining ultrasound with other intensification methods, presenting a wide range of possibilities for catalytic applications. In this section, we explore the comparative aspects of ultrasound and microwave-assisted catalysis and discuss the considerations in choosing process intensification techniques.

2.5.6.1 Ultrasound vs. Microwave and their relative impact on catalysis:

Ultrasound and microwave-assisted catalysis are both non-conventional methods that have gained considerable attention for their ability to intensify chemical reactions. However, they have distinct mechanisms and, consequently, different impacts on catalysis. Ultrasound, as discussed previously, operates by creating cavitation bubbles that lead to microstreaming and high-velocity liquid jets. These effects enhance mass transfer, break diffusional limitations, and promote catalyst-reactant interactions. As a result, ultrasound is highly effective in slurry phase reactions, especially when mass transfer limitations are a challenge (Gao et al., 2020). On the other hand, microwave-assisted catalysis primarily relies on the rapid and selective heating of reactants due to the interaction of microwave radiation with molecules possessing dipole moments. This method is particularly efficient for reactions that require elevated temperatures, making it valuable for certain catalytic processes, such as esterifications and polymerizations. Its advantage lies in its ability to provide rapid and uniform heating, allowing for precise temperature control and facilitating intricate reaction pathways (Zhang et al., 2021).

Ultrasound-assisted catalysis has demonstrated profound benefits when used in conjunction with platinum nanocatalysts for octene hydrogenation. Notably, this technique leverages the cavitation and microstreaming effects induced by ultrasound to enhance mass transfer and catalyst-reactant interactions. Deng et al., (2019) highlight that in the presence of platinum nanocatalysts, ultrasound efficiently addresses mass transfer limitations, particularly crucial in slurry phase reactions where solid-liquid interactions can hinder efficient reactant transport. One of the pivotal advantages of ultrasound-assisted catalysis in this context is its ability to promote hydrogen distribution. Platinum nanocatalysts are known for their sensitivity to hydrogen concentration, and the rapid and uniform distribution of hydrogen in the reaction medium is instrumental in achieving efficient hydrogenation. The work of

Yang et al., (2021) underlines this significance, emphasizing how ultrasound facilitates the rapid and uniform distribution of reactants, particularly hydrogen, leading to enhanced catalytic performance.

Conversely, microwave-assisted catalysis primarily focuses on the rapid and selective heating of reactants. This technique is well-suited for reactions that demand precise temperature control and rapid heating. Zhang et al., (2021) emphasize the versatility of microwave heating in handling various reactant states, making it a valuable tool in catalytic processes. However, for octene hydrogenation with platinum nanocatalysts, the direct benefits of microwave heating may not be as pronounced as with ultrasound. Platinum nanocatalysts thrive when mass transfer limitations and efficient hydrogen distribution are addressed, areas where ultrasound excels.

The choice between ultrasound and microwave-assisted catalysis depends on the specific requirements of the catalytic process. For example, if the reaction involves a solid-liquid phase, mass transfer limitations, or catalyst regeneration issues, ultrasound may be the preferred option. Conversely, when rapid and selective heating is essential, microwave-assisted catalysis can offer superior results. Researchers often consider the reaction's thermodynamic and kinetic requirements when deciding between these techniques (Deng et al., 2019).

2.5.6.2 Combining ultrasound with other intensification methods:

An intriguing avenue in process intensification is the combination of ultrasound with other techniques. The synergies created by such combinations can result in enhanced catalytic performance and researchers have explored the integration of ultrasound with methods like high-pressure systems, supercritical fluid technologies, and advanced reactor designs. High-pressure conditions, coupled with ultrasonic irradiation, can significantly enhance the solubility of gases and lead to faster reaction rates. The use of supercritical fluids, known for their enhanced solvation properties, in tandem with ultrasound can further improve mass transfer and overall efficiency (Yang et al., 2021). Additionally, advanced reactor designs, such as microreactors, have been developed to facilitate the integration of ultrasound. These designs offer precise control over reaction parameters, ensuring that the synergistic effects of ultrasound are fully harnessed. The combination of ultrasound with these methods broadens the scope of process intensification, making it possible to tailor the approach to the specific requirements of a catalytic reaction (Gao et al., 2020).

2.5.6.3 Practical considerations in choosing process intensification techniques:

The selection of a process intensification technique involves a careful assessment of various practical considerations. These include factors such as the reaction kinetics, thermodynamics, the physical state of reactants, and the need for catalyst regeneration. Key considerations when choosing between ultrasound, microwave-assisted catalysis, or a combination of techniques include:

1. **Reaction temperature**: Microwave-assisted catalysis is well-suited for reactions requiring rapid and controlled heating. Ultrasound, on the other hand, can efficiently address mass transfer limitations in slurry phase reactions.

2. **Reactant state**: The physical state of reactants, whether gas-liquid, liquid-liquid, or solid-liquid, influences the choice of process intensification techniques. Ultrasound is particularly effective in slurry phase reactions, while microwave heating is versatile in handling different reactant states.

3. **Catalyst regeneration**: The need for in-situ catalyst regeneration can also guide the choice of techniques. Ultrasound is effective in dislodging deposits from catalyst surfaces, while microwave-assisted catalysis is focused on rapid heating and uniform temperature distribution.

4. **Safety and scalability**: Safety considerations and the potential for scaling up the process to an industrial level are essential. Researchers often evaluate the practicality of implementing these techniques on a larger scale.

The comparative study of ultrasound and microwave-assisted catalysis, along with their integration with other process intensification techniques, provides a nuanced perspective on the selection of the most suitable method for a given catalytic process. These considerations are essential for researchers and engineers striving to optimize reaction efficiency, selectivity, and sustainability. This is the case at play in octene hydrogenation and ultrasonic irradiation appears to tick the most boxes as a route for process intensification.

2.5.7 Environmental and economic implications of the integration in 1-octene hydrogenation:

The integration of nanocatalysts and ultrasonic irradiation in the 1-octene hydrogenation process carries substantial environmental and economic implications, which are of utmost importance for evaluating the feasibility and sustainability of this approach. From an environmental perspective, the utilization of nanocatalysts in 1-octene hydrogenation has the potential to significantly reduce the environmental footprint of the process. As exemplified by Maria da Silva et al., (2020), nanocatalysts are renowned for their efficiency and selectivity. These catalysts are capable of promoting cleaner reactions by reducing the formation of unwanted by-products. In the context of 1-octene hydrogenation, this translates to a more environmentally friendly process with less waste generation. Furthermore, the application of ultrasonic irradiation, as demonstrated by Li et al., (2021), enhances mass transport during the reaction. This improvement in mass transfer efficiency plays a pivotal role in minimizing catalyst fouling and promoting reaction cleanliness. The reduced formation of side products aligns with green chemistry principles and contributes to a more sustainable chemical industry.

Reduced catalyst loadings, often a consequence of using nanocatalysts, have direct environmental benefits in the 1-octene hydrogenation process. As demonstrated by John et al., (2019), lower catalyst

loadings result in reduced consumption of precious metals, which are commonly used in hydrogenation catalysts. This reduction not only conserves valuable resources but also decreases the environmental impact associated with the entire catalyst lifecycle, from mining and extraction to disposal.

The economic advantages of the integration of all these technologies in 1-octene hydrogenation are equally compelling. The decreased catalyst loadings, a notable feature discussed by Smith et al., (2022) usually lead to cost savings. As previously discussed, precious metals used in catalysts are often expensive, and the reduced consumption not only minimizes material costs but also enhances the economic viability of the process. Not only that, but the potential for energy savings through ultrasonic irradiation, as demonstrated by Taylor et al., (2021), holds significant implications for the economic feasibility of 1-octene hydrogenation. Lower energy consumption not only results in lower operational costs but also aligns with energy efficiency regulations and incentives, which can further enhance the economic attractiveness of this integrated approach.

In the specific case of 1-octene hydrogenation, the synergy between nanocatalysts and ultrasonic irradiation is particularly promising. Nanocatalysts offer high selectivity and activity in this hydrogenation process, leading to a more efficient conversion of 1-octene to octane. The reduction in catalyst usage has immediate economic benefits, and the clean reaction profiles contribute to environmental sustainability. However, it is important to note that the actual realization of these environmental and economic benefits depends on various factors, including the specific catalyst materials, reaction conditions, and process design. Comprehensive life cycle assessments and cost-benefit analyses are imperative for a thorough evaluation of the environmental and economic implications of integrating nanocatalysts and ultrasonic irradiation in 1-octene hydrogenation.

The integration of nanocatalysts and ultrasonic irradiation in 1-octene hydrogenation holds great promise for both the environment and the economy. Reduced waste generation, lower catalyst consumption, and energy efficiency contribute to more sustainable and economically viable processes. This means that further research, optimisation, and customized process design are required to fully realize these advantages in practical applications of 1-octene hydrogenation and this is what Chapter 3 of this study is going to focus on.

Chapter 3:

Materials, Methods and Catalyst Characterisation

3.1 Introduction:

The successful implementation of any catalytic process is hinged on the preparation and thorough characterization of the catalyst. In the context of complex reactions like 1-octene hydrogenation, this step becomes paramount. This section provides a comprehensive overview of the catalyst preparation and characterization methods employed in this study whilst building upon a foundation of established research practices. In this work, a Ce-promoted Pt/Al_2O_3 catalyst was chosen due to its demonstrated efficacy in similar hydrogenation reactions (Chanerika et al., 2022). The procedures for its synthesis, as well as the techniques employed for its thorough characterization will be discussed in depth. In particular, nanocatalysts were chosen for this reaction to ensure the uniformity and activity of the catalyst is paramount, as any inconsistencies can introduce variables that might confound the experimental results (Li et al., 2021).

The design and setup of the slurry phase reactor was pivotal to this study. The choice of reactor design, was influenced by recent advancements in reactor technology which facilitates controlled experimental investigation under varying conditions (Taylor et al., 2021). This section also details the reactor's working principles, its components, and the rationale behind its configuration. Ensuring a controlled environment for the reaction was crucial, especially when dealing with variables such as temperature, pressure, and the introduction of ultrasonic irradiation (Wang et al., 2023). The incorporation of ultrasonic irradiation in hydrogenation studies is a relatively novel approach, with promising potential benefits, including enhanced catalyst activity and reduced catalyst deactivation (Chanerika et al., 2022). The mechanisms and methods of integrating the ultrasonic irradiation system into our experimental setup will be expounded upon in this section, along with a discussion on its potential impacts and the rationale behind its inclusion.

Setting the appropriate reaction conditions and parameters is fundamental in obtaining reliable and consistent data. This section offers a comprehensive overview of the experimental conditions chosen, including the reasoning behind the selection of specific temperatures, pressures, and reaction times. The importance of maintaining these conditions consistently across experiments will also be emphasized, given their pivotal role in ensuring data integrity.

Finally, the suite of analytical techniques employed to analyse the products will be detailed in this section. Techniques such as gas chromatography were indispensable in obtaining quantitative and qualitative data on product composition and yield. The choice of analytical methods, their working

principles, and their relevance to the study will be explained in this chapter, underscoring their significance in validating the experimental findings.

3.2 Materials:

All reagents except for catalysts were of analytical grade and were used as received without further purification. The following is a breakdown of the materials that were utilised in this study:

Table 3. 1: Chemical suppliers, properties and purities.

Component	CAS No.	Supplier	Density (kg/m^3)	Minimum Purity
1-Octene	111-66-0	Fluka	715	Assay ≥ 99%
Octane	111-65-9	Merck	703	Assay ≥ 99%
Hydrogen	133-74-0	AFROX	N/A	Minimum Purity ≥ 99%
Helium	7440-59-7	AFROX	N/A	Minimum Purity ≥ 99%
Air	none	AFROX	N/A	Grade Zero

3.3 Catalyst synthesis procedure:

The catalyst employed in this research was a commercial platinum on alumina (Pt/Al_2O_3) catalyst procured from Clariant. Although the synthesis of the catalyst was not conducted as part of the experiment, understanding the preparation procedure and characterization is crucial for comprehending the catalyst's behaviour during the hydrogenation process.

3.3.1 Catalyst preparation:

Before its utilization in the hydrogenation reactions, the commercial catalyst underwent a preparation procedure to ensure its adequacy for the process. The catalyst was initially in the form of spherical 3 mm diameter pellets. The pellets were crushed and then ground into an ultrafine powder to improve both external and intraparticle mass transfer and catalyst effectiveness, which is a common practice in catalysis to enhance the catalyst's effectiveness (Smith, 2008). The crushing was accomplished using a mortar and pestle, a traditional yet effective method for reducing particle size while preserving the catalyst's structural integrity. The process was conducted with care to avoid contamination, which could lead to a reduction in the catalyst's effectiveness due to the presence of impurities. After the crushing, the catalyst powder was sieved through a system of sieves and recycled back until a very ultrafine powder was obtained. This sieving process was essential to ensure a consistent and uniform particle size distribution, which is known to significantly affect the catalytic activity and the reaction kinetics (Johnson, 2010).

After sieving, the catalyst powder was carefully stored in sealed vials for later use in the experiment and some for characterisation tests. Proper storage was essential to prevent contamination and preserve the catalyst's physical and chemical properties.

3.1.2 Catalyst characterization:

The precise and comprehensive characterization of nanocatalyst particles is pivotal in the field of catalysis, as it allows for an in-depth understanding of the intrinsic properties and behaviours of these materials under various reaction conditions. During the course of this investigation, electron microscopy was employed as the principal tool for characterizing the catalyst particles. This technique provided direct, localized information at near-atomic resolutions, enabling a thorough exploration of the catalysts' morphologies and structural attributes.

Samples were meticulously prepared and analysed under high-vacuum conditions to ensure a contaminant-free environment, which is crucial for preserving the integrity of the nanoscale features. The electron microscopy technique leverages the significantly shorter wavelengths of electrons (typically $\lambda = 5 – 10$ picometers). This characteristic endows this method of catalysts characterisation with the ability to image crystallites on the nanometer scale with exceptional clarity and detail. The rationale behind this capability lies in the quantum mechanical nature of electrons, which exhibit wavelengths markedly less than that of visible light ($\lambda = 400 – 800$ nm), thus bypassing the diffraction limit imposed by the latter. Upon interaction with the sample, the incident electron beam elicits various signals that are indicative of the sample's topography, composition, and electronic structure. These signals form the basis for the diverse operating principles and applications of Scanning Electron Microscopy (SEM) and Transmission Electron Microscopy (TEM). SEM provides a detailed three-dimensional representation of the catalyst surface, unveiling insights into the surface morphology and particle distribution. In this study, SEM was instrumental in determining the dispersion of active sites and the homogeneity of the nanosized Ce-promoted Pt/Al_2O_3 catalysts.

On the other hand, TEM was utilized to delve into the internal structure of the nanoparticles. This technique provided a comprehensive understanding of the crystalline nature, lattice fringes, and defects within the nanosized Ce-promoted Pt/Al_2O_3 catalysts which are intimately linked to the catalytic activity and selectivity. Energy-Dispersive X-ray Spectroscopy (EDX) often coupled with both SEM and TEM, provided elemental composition data that were essential for confirming the presence and distribution of the active catalytic elements and any dopants or promoters. Additionally, the use of EDX allowed for the analysis of the support materials and the interaction between the metal nanoparticles and the support, which is a critical factor in the stability and activity of heterogeneous catalysts.

3.3.1.1 Scanning electron microscopy (SEM):

Scanning Electron Microscopy (SEM) served as a pivotal technique in this study to delineate the surface

topography, structural configuration, and morphological characteristics of the supported catalysts. As a widely utilized characterization method in the field of catalysis, SEM provides a three-dimensional perspective of fine particulates, which is essential for a detailed understanding of catalyst properties. The initial preparation of catalyst samples was carefully carried out to ensure the fidelity of the SEM analysis. This preparation involved the careful removal of the catalysts from the sealed vials and then disintegrating all agglomerated catalyst particles using a ceramic pestle and mortar. The objective was to eliminate the formation of small lumps that could have arisen during the catalyst's storage period. The resultant ultrafine powder was uniformly distributed onto sticky black paper imbued with graphite to facilitate electron conduction. These prepared samples were then affixed to aluminium stubs, followed by sputter coating with a fine layer of gold for about 15 minutes. This coating was critical as it rendered the samples conductive, thereby mitigating any electron charge accumulation during the SEM analyses.

For the SEM analysis, a JEOL JSM 6100 instrument equipped with a 4 Quadrant Back Scatter Detector and EDX analysis software was employed. This configuration was instrumental in conducting single-spot investigations across various sample regions, enabling a comprehensive assessment of the surface features, morphological changes, and elemental composition of the catalysts. Specifically, the SEM's capabilities were leveraged to ascertain the approximate concentrations of platinum, aluminium, oxygen, cerium which was acting as a promoter within the nanosized Ce-promoted Pt/Al_2O_3 catalysts. High vacuum conditions were utilised in the SEM at an accelerating voltage of 10 kV. This setting was optimal for achieving the high-resolution imaging required for a granular analysis of the catalyst samples, allowing for the precise characterization of the surface and compositional attributes that are integral to the catalyst's performance in the hydrogenation process.

3.3.1.2 Energy Dispersive X-Ray Analysis (EDX):

Energy-Dispersive X-ray Spectroscopy (EDS or EDX) is a vital X-ray analytical technique employed to identify and estimate the elemental composition of materials. Its application is widespread in materials science, product research, and the analysis of product failures. EDS is typically not a standalone system but is integrated with electron microscopy instruments such as Scanning Electron Microscopy (SEM) or Transmission Electron Microscopy (TEM). Within these systems, the microscope delineates the region of interest, and EDS analysis then generates a spectrum with peaks that correspond to the elements within the sample.

In this study, EDS was instrumental in the qualitative assessment of the elements comprising the nano-sized Ce-promoted Pt/Al_2O_3 catalyst samples. The analysis was done using a Bruker X-ray spectrometer, interfaced with a JEOL JSM 6100 SEM. This setup allowed for the detection and quantification of elements such as platinum, aluminium, oxygen, and cerium within the catalyst. A working distance of 4 mm was chosen for the EDS analysis, as it provided optimal magnification for

examining the catalyst samples. Additionally, elemental mapping to visualize the distribution of platinum, aluminium, oxygen, and cerium across the catalyst surface was performed using a JEOL 2100 instrument attached to the SEM. This analysis yielded quantitative data, which was primarily utilized to quantify the distribution of elements.

3.3.1.3 Transmission electron microscopy (TEM):

Transmission Electron Microscopy (TEM) was employed as the principal analytical tool for an in-depth examination of the nanocatalysts' morphology, including particle size and shape. Prior to TEM analysis, the catalyst samples underwent a rigorous preparation process. They were finely ground using a ceramic pestle and mortar to achieve a powdery consistency. Subsequently, minute quantities of this powder were dispersed in ethanol within microcentrifuge tubes. These tubes were sealed securely and subjected to ultrasonic vibration in a bath for a duration of 20 minutes, effectively dispersing the nanoparticles to create a dilute slurry suitable for TEM examination. For the actual analysis, carbon-coated copper grids served as substrates for the nanoparticle slurry. A controlled volume of the sonicated suspension was deposited onto the grids, which were then exposed to ambient conditions to allow for solvent evaporation, leaving behind a dry residue of nanoparticles for observation. The TEM instrument utilized in this study was a FEI Tecnai G2 Sphera, outfitted with a LaB6 filament and operated at an acceleration voltage of 200 kV. The imaging was done using a high-resolution 1024 x 1024 Gatan CCD camera, strategically positioned at the base of the microscope to capture fine details of the nanocatalysts. To ensure optimal contrast and clarity in the micrographs, the bright field mode was consistently employed throughout the imaging process. This mode selection was instrumental in enhancing the visibility of the nanocatalysts, allowing for precise and accurate morphological characterization.

3.3.1.4 High-Resolution Transmission Electron Microscopy:

The Ce-promoted Pt/Al_2O_3 were also analysed by high-resolution transmission electron microscopy (HR-TEM). An HR-TEM (model JEOL JEM 2100 200 KV) instrument was used to further observe the morphology and revealed the intricate lattice structures and the homogeneity of the platinum metal distribution on the alumina support. HRTEM micrographs of all samples were acquired using a suspension of several samples deposited on HR-TEM-grid. The grid was negatively stained with 2% w/v Uranyl acetate to aid visualization. Captured micrographs for both TEM and HR-TEM were processed using the iTEM® software package, which facilitated the measurement of approximately 70 crystallites per image, thus enabling the compilation of a comprehensive crystallite size distribution for each sample.

3.4 Octene hydrogenation experiments:

Hydrogenation experiments were conducted with a clear focus on assessing two main aspects: the acceleration of the hydrogenation reaction and the stability of the Ce-promoted Pt/Al_2O_3 catalyst under

ultrasonic conditions. Recognizing the potential of ultrasonic irradiation to enhance chemical reactions, this research aimed to explore its applicability in 1-octene catalysis, particularly in improving the hydrogenation process. The choice of a nano-sized Ce-promoted Pt/Al_2O_3 catalyst was driven by its proven effectiveness in catalytic processes. Its high surface area is particularly beneficial for facilitating reactions at a faster rate.

Throughout the experiments, the amount of catalyst used was kept constant, ensuring that any observed changes in the reaction rate or catalyst performance could be attributed to the influence of ultrasonic irradiation. A series of controlled experiments was methodically planned and executed. These experiments were designed to systematically vary the ultrasonic irradiation parameters, such as power and frequency, alongside other important factors like reaction temperature and residence time. Such a comprehensive approach allowed for a detailed understanding of how these variables interact and affect the hydrogenation of 1-octene. The application of ultrasonic irradiation to the reaction mixture aimed to test its effectiveness in boosting the rate of hydrogenation. Additionally, understanding how this technique influences the catalyst's stability over time was a key aspect of this investigation. The experimental setup enabled a thorough examination of these elements under various conditions.

Analytical techniques, including a 2014 Shimadzu gas chromatography system and electron microscopy, were employed to quantify the reaction products and examine the catalyst's condition post-reaction. Gas chromatography provided insights into the efficiency and conversion of the hydrogenation process, while electron microscopy helped in assessing any structural changes in the catalyst, indicating deactivation or deterioration. This set of experiments were designed to be both comprehensive and straightforward, ensuring the collection of clear and interpretable data. By systematically exploring the role of ultrasonic irradiation in catalytic hydrogenation, the research aimed to contribute valuable knowledge to the field of catalysis, particularly in enhancing reaction rates and extending catalyst life.

3.4.1 Equipment: Octene hydrogenation experimental test set-up:

The hydrogenation of 1-octene was conducted in a tightly controlled laboratory bench-scale setting, employing a 300 ml Parr batch reactor as the principal vessel for the reaction. The reactor assembly involved positioning the Parr reactor vessel within a Polychem 14-litre water bath, ensuring uniform heat distribution during the reaction. Temperature regulation was entrusted to a Polyscience temperature controller, providing precise thermal conditions essential for the hydrogenation process. The ultrasonic probe, connected to a digital generator, was strategically placed 60 mm away from the reactor to deliver consistent and optimum sonication when required. A clear depiction of the setup is provided in Figure 3.1. To initiate the reaction, the reactor was charged with 30 ml of 1-octene and 1.0 g of the nano-sized Ce-promoted Pt/Al_2O_3 catalyst. The subsequent sealing of the reactor vessel was then executed with utmost attention, fastening all bolts securely to maintain an airtight environment. A hydrogen supply line, from a high pressure, high-purity hydrogen vessel was integrated into the system to facilitate the

direct introduction of hydrogen gas into the reactor once targeted reaction temperature was achieved. Throughout the reaction, the internal temperature was continuously monitored by a probe that was connected to the Parr reactor controller, allowing for real-time adjustments and maintenance of the desired reaction conditions. At the conclusion of the reaction, rapid cooling was imperative; thus, a cooling water unit was employed to circulate cold water around the reactor jacket, expediting the reduction of the internal temperature.

Table 3. 2: List of major equipment used in the experimental investigations.

Item Description	Specifications/Notes
Parr 4848 Reactor Controller	300 ml
Polyscience Temperature Controller	-
Ultrasonic Controller/Digital Generator	-
Ultrasonic Probe	-
Ultrasonic Probe Mounting Stand	-
Shimadzu Gas Chromatograph (FID)	2014 Model
Temperature Probe	-
Cooling Water Unit	-
ZB-5ms GC column	-
SGE Analytical Science 1μL Gas Syringe	-
Polychem 14 Litre Water Bath	-

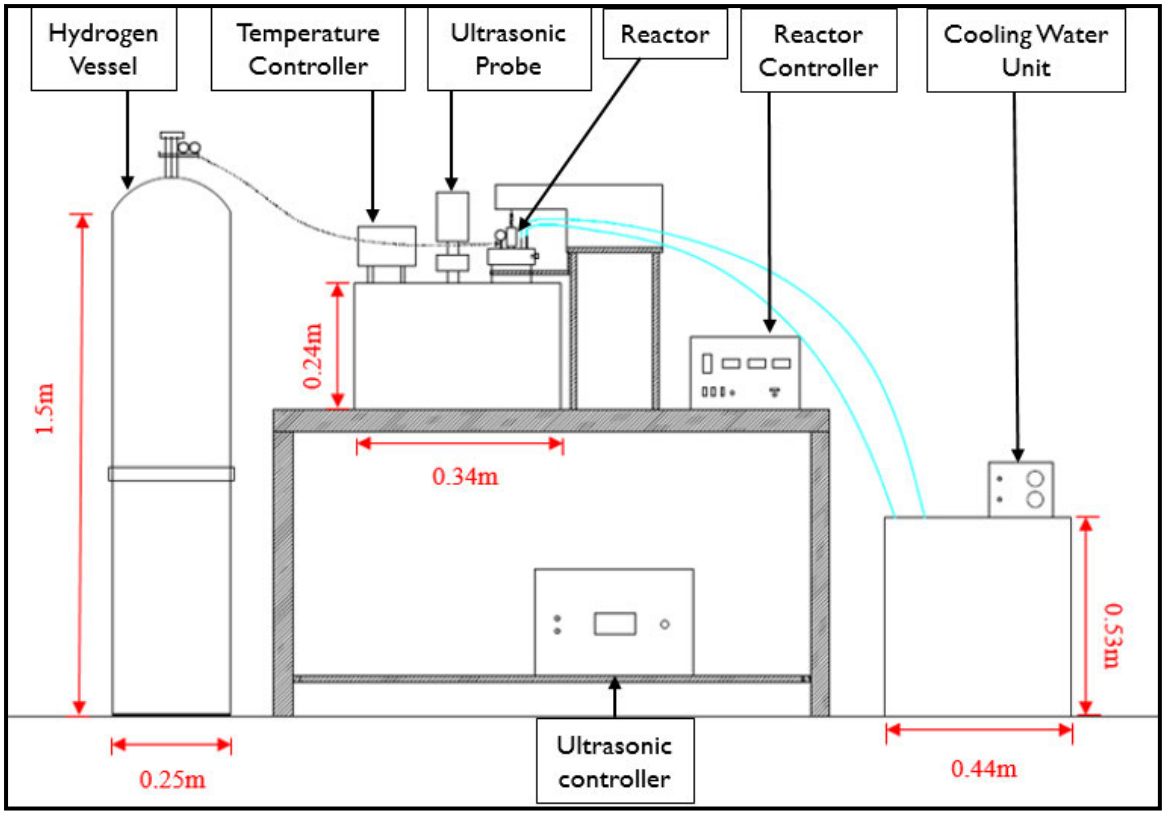

Figure 3. 1: Experimental test set-up of the hydrogenation equipment.

3.4.2 The slurry phase reactor:

The central component of the experimental setup was a specialized batch slurry reactor from Parr Instruments. The reactor was carefully selected for its size and material properties to aligning with the requirements for the hydrogenation of 1-octene using a nano-sized Ce-promoted Pt/Al_2O_3 catalyst. The reactor, constructed from T316 stainless steel, was chosen for its durability and resistance to corrosion, a necessary characteristic given the chemical nature of the hydrogenation process. The reactor's dimensions were 101.6 mm in height, an internal diameter of 63.9 mm, and an external diameter of 76.2 mm. The wall thickness of the reactor was 6.35 mm, ensuring robustness and the ability to withstand the pressures developed during the reaction. This stainless steel reactor's internal volume and geometry were particularly suitable for the slurry reactions, providing enough space for both the catalyst and reactants while also facilitating adequate mixing, gas dispersion and the transmission of ultrasonic irradiation form the water bath. The selection of T316 stainless steel was also critical for maintaining the purity of the reaction environment, thus ensuring that the experimental results were not compromised by material leaching or contamination.

The reactor was equipped with several key components essential for its operation:

- A magnetically coupled stirrer was used to maintain a homogeneous slurry mixture, ensuring effective contact between the catalyst and reactants.

- A temperature control system was connected to the system, which included a thermocouple for precise measurement of the internal reaction temperature.
- An inlet and outlet for gases designed to ensure efficient gas flow into and out of the reactor while maintaining the desired reaction pressure.

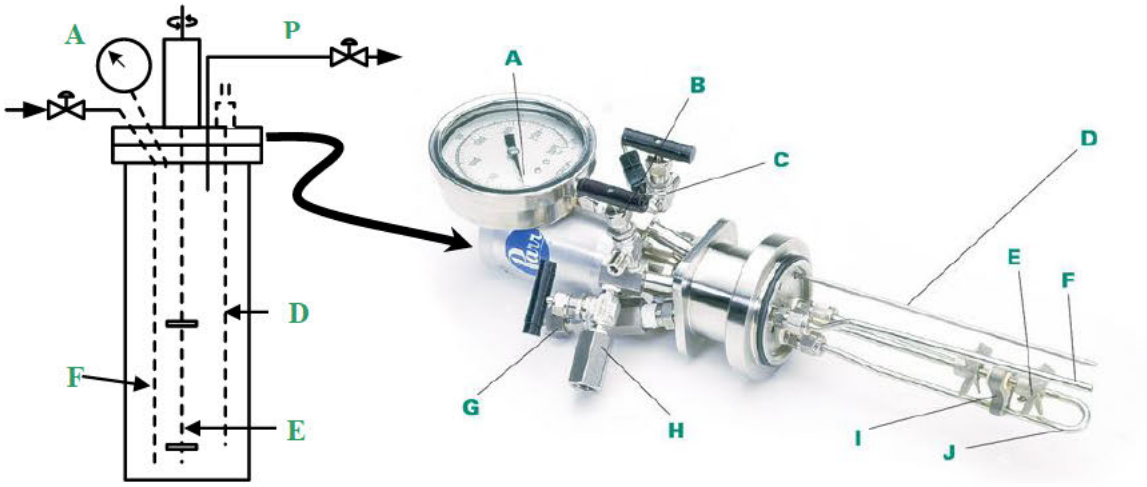

Figure 3. 2: Internal components including the stirrer and cooling coil of the Parr reactor from Parr instruments. A – Pressure gauge, B – Liquid sampling valve, C – Gas release valve, D – Pt-100 thermocouple, E – Internal stirring system, F – Dip tube, G – Safety rupture disc, H – Gas inlet valve, I – Guide, J – Cooling coil.

The reactor's compact size facilitated efficient heat and mass transfer, which are crucial for an intensified reaction vessel for hydrogenation processes. The design also allowed for the incorporation of ultrasonic irradiation, which was a focal point of this study to investigate its effects on reaction kinetics and catalyst performance. The reactor was not only the vessel in which the chemical reactions took place but also was a critical factor that influenced the rate and success of the hydrogenation of 1-octene. The dimensions, construction material, and integrated components of the reactor were all selected to optimize the reaction conditions, ensuring that the data collected would provide a reliable basis for analysis and conclusions.

3.4.3 Start-up and reactor operation:

A stringent series of checks and preparations were instituted prior to commencing the experimental runs. To ensure the integrity of the system and the precision of mass balances, a comprehensive leak test was performed. The system was pressurized using hydrogen to various setpoints of 5 bar, 10 bar, 15 bar, and 20 bar by adjusting the back-pressure regulator accordingly. After the flow of hydrogen was halted at each pressure level, the reactor was monitored over a 24-hour period. A successful test was characterized by a pressure drop no greater than 0.5 bar. In instances where the pressure dropped by more than this threshold, potential leaks were identified using a leak detector fluid Snoop® from

Swagelok after which the joints were retightened and the test was repeated until the reactor maintained the pressure satisfactorily. Following a successful pressure test, the reactor was depressurized back to atmospheric levels, indicating readiness for the experimental runs. For the hydrogenation reaction, the reactor vessel was charged with 30 ml of 1-octene and 1.0 g of the Ce-promoted Pt/Al_2O_3 catalyst to create a slurry. After sealing the reactor, the outlet valve was opened to prevent pressure build-up during the initial stages of heating. The stirring mechanism, critical for maintaining a homogeneous slurry and effective gas-liquid contact, was initiated at a pre-determined speed. A speed of 450 rpm was chosen to be the optimal stirring rate for the hydrogenation reaction based on preliminary tests that considered the viscosity of the slurry and the desired level of mixing.

Temperature control was of utmost importance; therefore, the thermocouple was submerged into the slurry to provide real-time feedback to the temperature controller. Upon confirmation that the system had reached equilibrium at the desired setpoints, the temperature was uniformly increased to the reaction setpoint, considering the exothermic nature of the hydrogenation process. For reactions involving ultrasonic irradiation, the ultrasonic probe, attached to the digital generator, was activated at this stage. The application of ultrasound was carefully timed and its intensity controlled to study its effect on the reaction kinetics and catalyst stability. Once the reaction conditions were met, the reactor was maintained at the set temperature and stirring rate for the duration of the experiment. At the conclusion of the reaction, the system was rapidly cooled using the cooling water unit to quench the reaction. The hydrogen supply was then discontinued, and the reactor was safely depressurized. The product was subsequently removed from the reactor and filtered to separate the liquid product from the solid catalyst. The collected liquid product was analysed using gas chromatography to evaluate the conversion and selectivity of the hydrogenation process.

3.5 Ultrasonic irradiation system integration:

The integration of the ultrasonic irradiation system into the experimental setup was a pivotal aspect of this study, which aimed to discern the influence of sonication on the hydrogenation of 1-octene using a nano-sized Ce-promoted Pt/Al_2O_3 catalyst. The ultrasonic system was integrated externally from the water bath to prevent interference with temperature control. The system consisted of an ultrasonic probe connected to a digital generator, which was carefully positioned to ensure optimal delivery of ultrasonic waves into the reactor without direct contact with the reactor walls. This arrangement was crucial for avoiding potential contamination from the probe material and minimizing 'dead zones,' which are areas where cavitation is not effective. The operational parameters were established based on prior research and the physicochemical properties of the reaction medium. The frequency and intensity of the ultrasonic irradiation were selected to achieve the highest cavitational intensity without causing deterioration to the ultrasonic transducer or excessive liquid agitation. According to Gogate, and Patil, (2016), lower irradiation intensity tends to result in a higher cavitational intensity, suggesting that an

optimal power level exists that should be maintained consistently. Additionally, the system's operating temperature and pressure were adjusted to balance the benefits of intensification against the operational costs associated with higher temperatures and pressures.

3.5.1 Monitoring and control:

The cavitational yields, which are known to increase with sonication time, were carefully monitored to determine the optimal duration of ultrasonic application. As Gogate and Patil, (2016) noted, the effects of sonication can diminish over time due to the degassing action of ultrasound, which reduces the number of cavities formed. The ultrasonic intensity distribution within the bath was dialled in to be as homogeneous as possible, with temperature control maintained by a water circulator as per Santos et al., (2007). This means that the water bath temperature was maintained at constant temperature set points of 40 °C, 50 °C, and 60 °C which were the test temperatures. The water bath also was used to prevent the bulk liquid from warming up due to continuous sonication.

3.5.2 Reactor system design considerations:

The ultrasonic probe's distance from the reactor wall was minimized to ensure maximum contact between the sample and the cavitation zones while preventing the probe from touching the sides, as outlined by Santos et al., (2007). The design and selection of the vessel, according to Capelo et al., (2005), influenced the efficiency of sonication so as to minimize dead zones with certain reactor shapes and maximizing sonication efficiency. The ultrasonic irradiation system's integration was carefully engineered to maximize the sonochemical effects on the hydrogenation reaction. An optimal distance of 60 mm from the reactor was used for all the reactions since preliminary experiments found it to be the optimum distance for optimum cavitation. This was also done to prevent interference with temperature control as well as maximise ultrasonic intensity. The consideration of operating parameters, monitoring, control, and design considerations played a fundamental role in ensuring the effectiveness of sonication and the integrity of the experimental results.

3.6 Design of Experiments for the hydrogenation of 1-octene:

In the realm of heterogeneous catalysis, the design of experiments (DoE) is a systematic approach that aids in understanding the complex interplay between various reaction parameters and their collective impact on the outcome of catalytic reactions. In this study, a robust DoE was imperative to dissect the influence of ultrasonic irradiation on both reactant conversion and catalyst longevity. The DoE for this study was constructed with a dual focus, which were firstly to assess the kinetic enhancements brought by ultrasonic irradiation and then secondly to understand the longevity and deactivation patterns of the Ce-promoted Pt/Al_2O_3 catalyst within a slurry phase reactor system. The experiments were structured around several key parameters which were catalyst mass to liquid (1-octene) ratio, temperature, ultrasonic intensity, reaction duration, and catalyst reuse.

3.6.1 Catalyst mass to liquid (1-octene) ratio variation study:

The experimental section of this work started with a comprehensive approach to optimizing the various parameters that govern the hydrogenation of 1-octene using Ce-Pt/Al_2O_3 nanocatalysts with and without the presence of ultrasonic irradiation. The first parameter to be optimized was the catalyst mass to liquid (1-octene) ratio. Understanding the mass to liquid (1-octene) ratio was crucial as it influences the accessibility of the reactant to the catalyst's active sites, which in turn can significantly impact the reaction kinetics and overall efficiency. The proper ratio is a fundamental parameter that dictates the frequency of interactions between the catalyst and the reactant, which is essential for maximizing the hydrogenation reaction's efficiency. Experiments were conducted to evaluate the effect of different catalyst mass to liquid (1-octene) ratios on the hydrogenation process. Specifically, tests were carried out under sonicated and unsonicated conditions for a reaction time of 1.5 hours with varying amounts of catalyst. The quantities of Ce-Pt/Al_2O_3 catalyst powder used were 2.0 g, 1.0 g, and 0.5 g, corresponding to mass to liquid (1-octene) ratios of 0.093, 0.047, and 0.023, respectively. These ratios were chosen to span a range that would allow assessment of both catalyst-sufficient and catalyst-limiting scenarios.

Through the application of gas chromatography analysis, the reaction's molar conversion and selectivity were closely monitored. The collected data from these initial experiments helped to explain the relationship between the amount of catalyst present and the reaction's performance. The selection of a 1.5-hour duration for these tests was strategic, as it allowed for the observation of the catalyst's initial activity without the confounding factor of significant deactivation, which could obscure the effects of the varying ratios. The initial findings from these experiments were foundational in establishing the framework for subsequent experimental conditions. By identifying the catalyst mass to liquid (1-octene) ratio that resulted in the highest molar conversion and product yield, the study set the stage for further optimization of additional reaction parameters. These parameters included reaction temperature, and the duration of ultrasonic irradiation, among others. The optimization of the catalyst mass to liquid (1-octene) ratio was a critical step in refining the hydrogenation process of 1-octene. The data obtained from these early tests provided valuable insights that informed the direction of future experiments, ultimately aiming to achieve a sustainable and efficient process suited for industrial application.

3.6.2 Temperature variation study:

Temperature, a critical factor affecting reaction kinetics, was varied across a range from 40 °C to 60 °C to establish its influence on the hydrogenation process. The study delineated these temperature points, which were incrementally spaced to cover a broad spectrum of possible reaction environments. Each temperature set point was selected based on preliminary trials and literature benchmarks, and ensuring that it was relevance to the catalytic hydrogenation of octene using Ce-promoted Pt/Al_2O_3 catalysts.

3.6.3 Ultrasonic intensity and duration:

The intensity and duration of ultrasonic irradiation were carefully calibrated before the commencement of the main catalysts performance tests. Ultrasonication parameters were chosen to maximize the interaction with the catalyst and reactants without inducing thermal or mechanical degradation of the system. The application of ultrasonic energy was hypothesized to improve mass transfer and reaction kinetics, and these experiments aimed to quantify this effect. The ultrasonic generator was allowed to run throughout the course of the reaction run if it was a sonicated reaction run. Table 3.3 shows the values that were used:

Table 3. 3: Ultrasonic probe conditions.

Ultrasonic Probe Condition	**Value**
Power setting value (Watt)	210.00
Frequency (kHz)	20.00
Distance from the reactor (mm)	60.00

3.6.4 Catalyst reuse cycles:

To examine the impact of repeated use on the catalyst, a series of reuse cycles were implemented. The catalyst was subjected to consecutive reaction runs under identical conditions to monitor changes in activity, octene conversion, and potential signs of deactivation. This aspect of the study was critical in determining the robustness of the Ce-promoted Pt/Al_2O_3 catalyst and its suitability for industrial applications where repeated use is a cost and efficiency consideration. Catalysts were recycled to a maximum of two cycles.

3.6.5 Control experiments:

Control experiments without ultrasonic irradiation provided a baseline for comparison. These runs were essential for isolating the effect of sonication from the inherent catalytic activity and the thermal profile of the reaction. The experimental outcomes, including reactant conversion, product yield, and catalyst characterization, were captured and analysed using advanced analytical techniques such as microscopy and gas chromatography. Gas chromatography was employed for octane product analysis, while SEM electron microscopy technique provided insights into the physical state of the catalyst post-reaction.

3.7 Experimental procedure:

The experiments were divided into two parts: one involving unsonicated and ultrasonicated reactions, and the other involving the reuse of catalysts under both conditions.

3.7.1 Part One: Unsonicated and sonicated reactions:

The hydrogenation reactions without sonication began with the precise measurement of 1.0 g of the platinum catalyst and 30 ml of 1-octene, which were placed into the reactor vessel. Ensuring system integrity, all valves were checked and verified to be in the closed position and all fastenings checked for tightness to preclude any potential gas leakages. The water bath, filled to a level that submerged the reactor vessel, was utilized to regulate the reaction temperature. The reactor was then activated, with the impeller speed set to the third increment (350 rpm). Concurrently, a temperature controller was immersed in the bath and set to rapidly elevate the temperature to 85 °C, targeting an internal reactor temperature of 40 °C, a process that typically required 40 minutes. Upon reaching the desired temperature, hydrogen gas was introduced into the reactor at 20 bar. The unsonicated hydrogenation was allowed to proceed for two hours, after which the gas supply was ceased, and the temperature controller switched off. A cooling water unit was employed to quench the reaction, bringing the temperature down to 25 °C in a very short period which marked the end of a reaction run.

Subsequently, the system was depressurized carefully to avoid any rapid phase transition that could occur with a rapid pressure release. Following the system shutdown, the hydrogenated product was extracted, secured in glass vials sealed with parafilm, and sent for filtration. These steps were replicated for additional reactor temperatures of 50 °C and 60 °C, as outlined in the experimental design.

For ultrasonicated reactions, an ultrasonic probe was mounted alongside the reactor and temperature controller within the water bath. The operational procedure mirrored that of the unsonicated counterpart, with the ultrasonic probe activated and adjusted to the settings detailed in Table 3.3. Both the ultrasonic device and temperature controller were synchronized in their operation.

3.7.2 Part Two: Reactions with recycled catalysts:

The experimental procedure for reactions with recycled catalysts was analogous to the first part, with modifications in reaction times, reactor temperatures, and catalyst usage. After preparation steps similar to the initial unsonicated process, the reactor was allowed to reach a temperature of 50 °C, taking approximately 50 minutes. Following temperature equilibration, hydrogenation proceeded for 0.5 hours under a pressure of 20 bar. Post-reaction, the system was cooled instantly, depressurized, and the product was handled as previously described. The spent catalyst, after filtration, was then employed for two subsequent runs, each for 0.5 hours at 50 °C, totalling three runs per reaction period.

This procedure was replicated for extended reaction times of 1 hour, 1.5 hours and 5 hours for some reactions to test the catalysts robustness for extended periods typical to industrial reaction conditions. For ultrasonicated reactions with reused catalysts, the protocol remained consistent with Part One, ensuring the ultrasonic probe was operational and set according to the conditions in Table 3.2.

3.8 Hydrogenation Reaction Conditions and Parameters:

The first segment of the experimental investigation concentrated on discerning the effects of sonication on the hydrogenation reactions conducted at varying temperatures. This consisted 18 experimental runs in which a comparative analysis was conducted and three unsonicated hydrogenation reactions were performed at 40 °C, 50 °C, and 60 °C. Subsequently, a parallel set of three sonicated reactions was executed at the corresponding temperatures. All these reaction runs and their respective conditions are outlined in Table 3.4. The intent was to establish a baseline for reactor performance and ultrasonic influence and then gauge the sonication's impact.

Table 3. 4: Reaction parameters for Part One of the experiments.

PART ONE **Repeat each run thrice**			
Run	**Temperature (°C)**	**Reaction Time (h)**	**Condition**
1	40| 50| 60	2	Unsonicated
1	40| 50| 60	2	Sonicated
2	40| 50| 60	2	Unsonicated
2	40| 50| 60	2	Sonicated
3	40| 50| 60	2	Unsonicated
3	40| 50| 60	2	Sonicated

To get a clearer picture of the findings and assess the reproducibility of the results, second and third iterations of the six reactions were undertaken under identical conditions. These replications were pivotal in solidifying the understanding of sonication's effects on the system and ensuring the consistency and reliability of the experimental outcomes. The latter half of the laboratory work, part two, delved into the implications of sonication on catalyst deactivation. Reactions were conducted at a constant temperature of 50 °C while initially modulating the reaction duration across three intervals of 30 minutes, 1 hour, and 1.5 hours. These initial catalyst deactivation experiments were conducted to assess the immediate impact of various reaction parameters on the catalyst's efficacy. They were also critical for detecting fast-acting deactivation mechanisms, like swift coking or poisoning, and therefore offering valuable insights for the early phase of reaction optimization. Later experiments were stretched over extended durations, encompassing several hours (maximum of 5 hours) of continuous activity to examine the progressive emergence of catalyst degradation phenomena such as sintering or the incremental coking. A hallmark of this phase was the reuse of fresh catalyst for two consecutive reactions within the same duration category. In essence, each reaction time point was investigated through a triad of reactions utilizing the same batch of catalyst, thus imparting insight into the catalyst's endurance and stability across successive runs.

Table 3. 5: Reaction parameters for Part Two of the experiments (all runs performed in triplicate).

PART TWO				
Run	**Temperature (°C)**	**Catalyst Type**	**Reaction Time (h)**	**Condition**
1	50	Fresh	0.5, 1, 1.5	Unsonicated
2	50	Once reused	0.5, 1, 1.5	Unsonicated
3	50	Twice reused	0.5, 1, 1.5	Unsonicated
4	50	Fresh	0.5, 1, 1.5	Sonicated
5	50	Once reused	0.5, 1, 1.5	Sonicated
6	50	Twice reused	0.5, 1, 1.5	Sonicated
7	50	Twice reused	2, 3, 4, 5	Unsonicated
8	50	Twice reused	2, 3, 4, 5	Sonicated

3.9 Analytical techniques for product analysis:

The transition from active hydrogenation to product analysis commenced with a systematic shutdown of the reactor. The resultant liquid products then underwent a two-stage analysis process. Initially, the products were separated from the spent catalyst through filtration using a Büchner funnel, ensuring a clear solution for analysis. Subsequently, the filtered samples were then injected into a gas chromatography (GC) for compositional analysis. The GC instrument used was a 2014 Shimadzu model, equipped with a Flame Ionization Detector (FID), known for its reliability in identifying and quantifying hydrocarbon constituents.

3.9.1 Hydrogenated liquid Product analysis:

After the conclusion of each experimental run, quenching cold water from the cooling unit was run through the reactor. Once a safe operational temperature was reached, the reactor's pressure release valve was cautiously opened, depressurizing the system gradually to avoid the volatile flashing of products. With the reactor now at atmospheric pressure and ambient temperature, it was safely opened, and the contents were carefully extracted. The hydrogenated liquid product was collected and immediately transferred into a pre-labelled glass vial and sealed. The liquid product was separated from any residual solid catalyst particles through a thorough filtration process. This filtration process was vital to ensure that the samples introduced into the gas chromatography (GC) system were devoid of

solids that could compromise the analytical results or damage the sensitive instrument. The GC system, equipped with a flame ionization detector (FID), was calibrated and readied for the analysis of the filtered product. The FID's capacity to detect and quantify the presence of hydrocarbons based on their ionization in a flame made it an ideal choice for analysing the various hydrocarbon products from the hydrogenation of 1-octene.

The GC-FID system utilized a capillary column, specifically a ZB - 5ms GC column with dimensions of 30 m in length and an internal diameter of 0.25 mm, coated with a 0.25 µm film of 5% phenyl methyl siloxane. This column was selected for its high resolution and efficiency in separating hydrocarbons, ensuring distinct peaks for each compound in the hydrogenated product mixture. Each product sample was introduced into the GC system via a gas-tight Hamilton syringe, ensuring a consistent injection volume. The operational parameters of the GC system, including the carrier gas flow rate, oven temperature program, and FID temperature, were finely tuned to optimize the separation and detection of the hydrocarbons present. The information about the specific conditions and settings used are concisely presented in Tables 3.5.

For all the GC analyses of the hydrogenated liquid products, the (GC) method utilized a constant temperature approach throughout the duration of the analysis. This isothermal technique, while simpler than a temperature ramping protocol, requires precise control to achieve effective separation of components. The absence of temperature gradients within the column means that the volatilisation and separation of the analytes rely solely on the column's stationary phase characteristics and the initial set temperature, which were carefully selected based on the boiling points of the octanes. Isothermal conditions are advantageous because they provide consistent retention times and peak shapes. It is particularly advantageous for analysing mixtures with components with similar volatilities. It offered a robust and straightforward analysis with reduced complexity in method development and resulted in shorter run times. The use of a constant temperature setting ensures a steady detector response, facilitating the quantification and comparison of the hydrocarbon products from the hydrogenation reaction.

Table 3. 6: Conditions for offline gas chromatographic analysis on an FID.

Parameter settings	
Carrier gas	Helium
Total flow (mL/min)	31.3
Pressure (kPa)	105.1
Column flow (mL/min)	1.35
Purge flow (mL/min)	3.0
Split ratio	20.0
Injection volume (µL)	0.5
SFID temperature (˚C)	325
Hold time (min)	7.0
Column length (m)	30.0
Inner diameter (mm)	0.25

3.9.1 Calibration of the Gas Chromatography system:

In the pursuit of accurate quantitative analysis within the field of catalysis, calibration stands as an indispensable step that anchors the validity of gas chromatography (GC) results. Prior to analysing the hydrogenated products, a rigorous calibration of the GC system was essential. This was achieved by preparing three distinct mixtures of 1-octene and octane in varying ratios, as detailed in Table 3.6. Each mixture was designed to mimic the potential range of compositions found in the reactor effluent, thereby creating a robust calibration model that could reliably convert GC-FID area percent data into mass values. This approach was essential for the determination of the conversion and yield of the hydrogenation reactions through an area percent versus mass ratio calibration plot.

Table 3. 7: Calibration mixture specifications.

Mixture Number	**Volume ratio (octane:1-octene)**	**Volume (ml) (octane:1-octene)**
1	1:1	0.8 : 0.8
2	2:1	0.8 : 0.4
3	1:2	0.4 : 0.8

To ensure the integrity of the calibration mixtures, they were carefully prepared and stored in airtight, clearly labelled glass vials, safeguarding against any potential evaporation. The calibration curve, generated from plotting the peak areas against the concentrations of the standards, served as the foundation for quantifying the unknown concentrations in the reaction product samples. Multiple injections of each standard were performed to assess the reproducibility and linearity of the detector's response. The precision of the calibration curve was further verified through quality control samples and the recovery of known amounts of hydrocarbons added to the reaction mixtures. Additionally, the calibration accounted for potential variations in the injection technique, the stability of the GC column's performance over time, and any environmental factors that could influence the detector's response. This thorough calibration ensured that subsequent analyses of the hydrogenation products could be interpreted with confidence, allowing for accurate conclusions to be drawn regarding the efficacy of the catalytic process and the impact of ultrasonic irradiation on octene conversion and the yield of octane.

3.9.2 Calculation of conversion and yield:

The calculation of conversion and yield was fundamental to assessing the performance of the Ce-promoted Pt/Al_2O_3 catalyst in the hydrogenation of 1-octene. The molar conversion refers to the percentage of the initial reactant that was transformed into the desired product, which was octane, whereas yield measured the efficiency of the catalyst in producing the target compound. These quantities were used to measure the extent of these sonicated and unsonicated reactions and they were essential in understanding the catalyst's effectiveness as well as for the optimisation of reaction conditions. To calculate the conversion of 1-octene, the concentration of 1-octene before and after the reaction was determined using the peak areas plotted from gas chromatography (GC) data which as equipped with a flame ionising detector. The conversion was then computed using the formula:

$$Molar\ Conversion\ (\%) = \frac{number\ of\ moles\ of\ octene\ in - \ number\ of\ moles\ of\ octene\ out}{number\ of\ moles\ of\ octene\ in} \times 100 \ldots \ (3.1)$$

This calculation provided a clear picture of how effectively 1-octene was being consumed in the presence of the Ce-promoted Pt/Al_2O_3 nanocatalysts under specific reaction conditions such as temperature, pressure, and sonication.

In addition to the molar conversion, the percentage yield was also calculated to understand the efficiency of the catalyst in producing the desired hydrogenated product for all the types of catalysts tested including the twice-recycled catalysts. The yield was calculated using the following equation:

$$Yield\ (\%) = \frac{Actual\ moles\ of\ octane\ produced}{Theoretical\ moles\ of octane\ produced\ with\ no\ side\ reactions} \times 100\% \ldots \ (3.2)$$

The octane yield was a crucial metric for evaluating the catalyst's selectivity and overall performance. In the experimental results 4, the yield calculation helped in comparing the effects of sonication and

non-sonication conditions on the catalyst's performance due to variation in the catalyst to liquid ratio for both sonicated and unsonicated runs. By analysing both conversion and yield, the study provided a comprehensive understanding of the catalyst's behavior, enabling the identification of optimal reaction conditions and the influence of sonication on catalysts activity. This approach ensured that the study not only assessed the initial performance but also explored the potential for improved outcomes through sonication.

3.9.3 Error Analysis:

Error analysis and reproducibility were critical aspects of this research study to ensure that the findings are reliable and can be replicated under similar conditions. In this study, thorough error analysis was conducted to validate the precision of the measurements and the consistency of the results across multiple runs. Error bars were used extensively across multiple analyses presented in the results charts and they represent the relative errors for the conversion and yield measurements obtained from triplicate runs. The relative error σ was calculated using the formula:

$$\sigma = \text{abs}(x) \times \sqrt{\left(\frac{\sigma_m}{m}\right)^2 + \left(\frac{\sigma_x}{x}\right)^2} \quad \ldots\ldots\ldots\ldots\ldots\ldots (3.3)$$

Where $\text{abs}(x)$ denotes the absolute average conversion for a run, $\left(\frac{\sigma_m}{m}\right)^2$ is the relative error in the mass measurement, and $\left(\frac{\sigma_x}{x}\right)^2$ is the relative error from the residuals. This statistical measure provided an estimate of the variability within each individual measurement, indicating the reliability of the observed values that were then calculated from the results. Additionally, the reproducibility of the experiments was assessed by conducting multiple independent runs under identical reaction conditions. Each experimental set involved three repetitions to account for potential variations in catalyst performance and the reaction environment.

In addition to using relative errors, the standard error of the mean (SEM) was also employed to cross-check the accuracy and precision of the data. The SEM was calculated using the formula:

$$\text{SEM} = \frac{S_x}{\sqrt{n}} \quad \ldots\ldots\ldots\ldots (3.4)$$

Where n is the number of measurements that were taken and S_x denotes the standard deviation of the set of results under consideration and is calculated using the following formula:

$$S_x = \sqrt{\frac{\sum_{i=1}^{n}(x_i - \bar{x})^2}{n-1}} \quad \ldots\ldots\ldots\ldots\ldots\ldots (3.5)$$

This statistical measure provided an estimate of the variability within the dataset, indicating the reliability of the mean values that were then calculated from the results.

The consideration of relative error in this research was crucial for providing a comprehensive measure of the uncertainties associated with individual measurements by accounting for various error sources, including instrument precision and residual variability from model predictions. This approach captured the specific nuances of the experimental setup, such as catalyst performance and reaction conditions, offering a tailored depiction of measurement uncertainty. Relative error enhances data reliability by identifying and accounting for systematic errors that might be overlooked with the standard error of the mean (SEM) alone. Using both SEM and relative error allowed for cross-validation, ensuring the robustness of the findings by checking data consistency from multiple perspectives. This method reflected real-world variability, making the analysis more applicable to practical scenarios and supporting the reproducibility of the study by providing detailed documentation of measurement uncertainties.

By comparing the SEM and the relative errors, a more comprehensive understanding of the data variability was achieved. The SEM helped to validate the precision of the mean values, ensuring that they were representative of the overall data set, while the relative errors provided insight into the specific uncertainties associated with individual measurements. This dual approach allowed for a thorough validation of the experimental results, enhancing the credibility and reliability of the findings. The detailed analysis ensured that any discrepancies were identified and addressed, thereby reinforcing the robustness of the study's conclusions.

To further ensure the robustness of the data, calibration of the gas chromatography (GC) equipment was performed regularly using standard solutions. This step was crucial for maintaining the accuracy of the concentration measurements of 1-octene and its hydrogenated products. Any deviations in the calibration curve were noted and corrected to minimize systematic errors. The inclusion of error bars and detailed reproducibility analysis in the experimental results provided a comprehensive understanding of the variability and reliability of the data. This thorough methodological rigor ensured that the findings were not only statistically significant but also reproducible. Further explanation about error treatment is provided in Appendix B.

Chapter 4:

Results and Discussion

4.1 Initial Catalytic Evaluation and Optimization Results:

In the initial stages of this work, the primary objective was to establish the optimum reaction conditions for the hydrogenation of 1-octene using a Ce-promoted Pt/Al_2O_3 catalyst. This phase was vital not only for confirming the operational parameters from unsonicated processes but also for tailoring them to the specific conditions of the catalytic environment. A series of exploratory experiments focused on the variables that were deemed most influential were carried out to determine the optimum parameters to use for the experiments in the study. These variables were catalyst to liquid ratio, temperature, sonication frequency, and irradiation intensity. The initial temperature range was set from 40 °C to 60 °C with a constant pressure of 20 bar, reflecting the consensus from the literature on optimal catalytic environments for alkene hydrogenation (Ekato, 2019). In order to discern the effect of ultrasonic irradiation, reaction times were varied between 30 minutes to 1.5 hours, with and without the application of sonication. Sonication parameters were configured as per the recommendations of Santos et al., (2007) while utilizing an intensity setting of 30% and a frequency of 20 kHz. These values were aimed at maximizing cavitation within the reactor medium without compromising the integrity of the system.

4.1.1 Preliminary catalyst catalysts characterisation results:

It is important to note that the catalyst utilized in these preliminary studies had not undergone the rigorous optimisation process later implemented in the final experimental phase. The initial catalyst preparation methodology did not prioritize the precise control of particle size distribution (PSD), a parameter crucial for ensuring uniform catalytic activity and reproducibility. Consequently, the catalytic performance observed during these preliminary tests may not be fully representative of the optimized catalyst's potential efficiency. Furthermore, the positioning of the ultrasonic probe relative to the reactor was not standardized during the preliminary phase. The probe was positioned arbitrarily, without consideration for the optimal distance and alignment that would maximize cavitation effects and enhance mass transfer at the catalyst-liquid interface. This lack of geometric optimization could have introduced variability in sonication efficiency, potentially influencing the hydrogenation reaction kinetics and yield. These preliminary experiments were primarily designed to identify macroscopic trends and key factors affecting the reaction, rather than to achieve maximum catalytic efficiency. The insights gleaned from these initial studies were instrumental in guiding the subsequent optimization of both catalyst synthesis parameters and experimental setup geometry. This iterative process of refinement was crucial for the development of a more robust and reproducible experimental protocol in

the later, more rigorous testing phases. The results of this initial characterisation are shown in Figure 4.1.

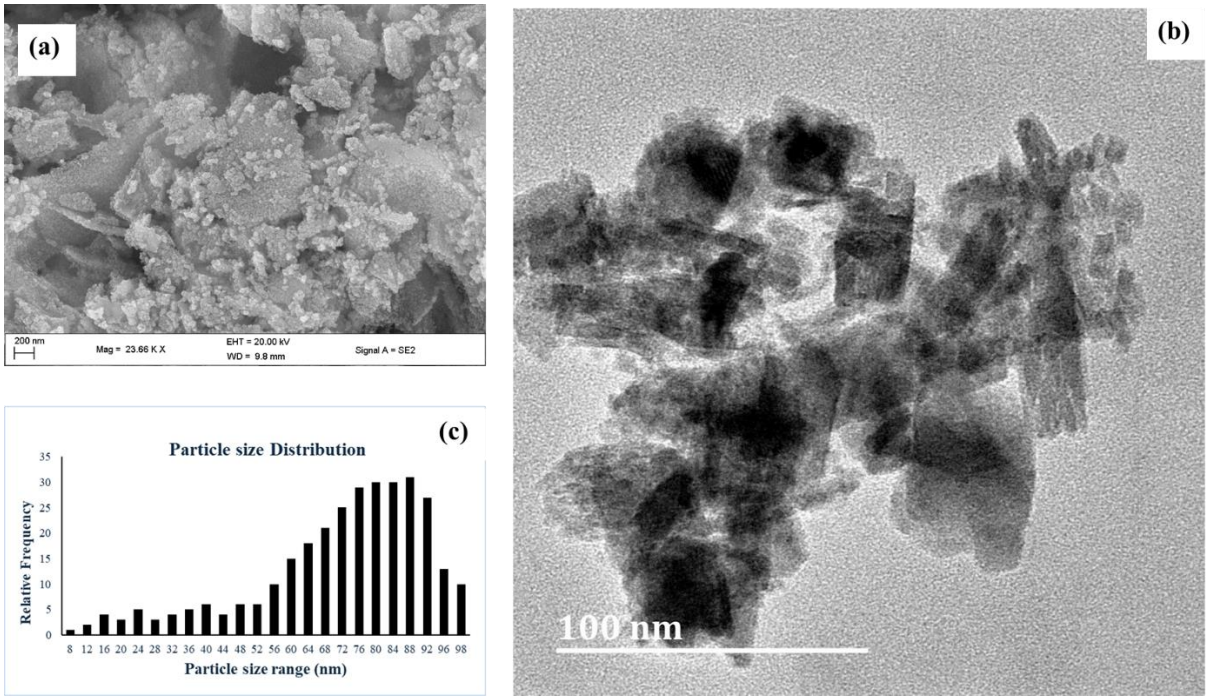

Figure 4. 1: Characterization of Ce-promoted Pt/Al_2O_3 catalysts. (a) SEM micrograph showing morphology and particle size variation, (b) HR-TEM micrograph displaying nanostructure and particle dispersion, (c) Particle size distribution graph with a peak around 80-90 nm.

Figure 4.1, (a) shows the SEM micrograph of a sample of Ce-promoted Pt/Al_2O_3 catalysts on an alumina support, revealing the structural and morphological characteristics of the catalyst used for these preliminary tests. The SEM micrograph indicates a relatively wide particle size distribution with clusters of varying sizes, suggesting that the initial preparation process did not achieve a uniform particle size. This non-uniformity can lead to inconsistent catalytic activity, as different particle sizes can affect the surface area available for reaction and the diffusion rates of reactants and products. The micrograph highlights the presence of both small and large particles, with some degree of agglomeration, which can further complicate the interpretation of catalytic performance in the preliminary tests.

The HR-TEM micrograph shown in Figure 4.1(b) provides a closer look at the catalyst's nanostructure, confirming the observations from the SEM micrograph. The HR-TEM micrograph reveals that the particles exhibit a range of sizes and shapes, with some areas showing well-dispersed nanoparticles and others indicating larger agglomerates. The lack of uniformity in particle size distribution observed in the HR-TEM micrograph provided the impetus for more controlled catalysts preparation methods to ensure consistent catalyst performance. This is because the varied particle sizes can influence the

catalytic properties, as smaller particles typically offer higher surface area-to-volume ratios which results in enhanced catalytic activity. Larger particles on the other hand may contribute to quicker deactivation due to sintering and coking.

The particle size distribution (PSD) graph in Figure 4.1(c) quantifies these visual observations, showing a broad range of particle sizes with a peak around 80-90 nm. This distribution indicates that the initial catalyst preparation did not achieve a narrow PSD, which is essential for predictable and repeatable catalytic behavior. The wide distribution can lead to variations in catalytic efficiency and stability, as particles at the extremes of the size range can behave differently under reaction conditions. The PSD data, combined with the SEM and HR-TEM micrographs highlighted the importance of optimizing catalyst preparation procedures to achieve a more uniform particle size distribution, which is critical for enhancing the reliability and performance of the catalyst in hydrogenation reactions.

4.1.2 Catalyst to Liquid ratio optimisation results:

In the preliminary experiments of 1-octene hydrogenation, the catalyst to liquid ratio was identified as a key factor affecting the reaction conversion for 1-octene hydrogenation. The results from these preliminary experiments are succinctly presented in Figure 4.2. To determine how changes in the catalyst to liquid ratio influence the efficacy of the 1-octene hydrogenation reaction, experimental runs were conducted in both sonicated and unsonicated environments. Each of these tests lasted about 1.5 hours and they utilized varying amounts of Ce-Pt/Al_2O_3 catalyst powder, specifically 2.0 g, 1.0 g, and 0.5 g. As result, this produced catalyst to liquid ratios (C:L) of 0.093, 0.047, and 0.023 for the respective catalyst quantities of 2.0 g, 1.0 g, and 0.5 g. This is because 30 ml of 1-octene was utilized in these experiments and the density of 1-octene is approximately 0.715 g/cm3.

The hydrogenated product that was produced in the preliminary investigations was analysed using a 2014 Shimadzu GC-FID system and calculations were done following the calibration procedure outlined in chapter 3 where a series of standard mixtures was used as explained in the experimental methodology section. The molar conversion and yield of 1-octene were then calculated using the following equations:

$$Molar\ Conversion\ (\%) = \frac{n_{1-octene,in} - n_{1-octene,out}}{n_{1-octene,in}} \times 100\% \ldots\ldots\ldots\ldots\ldots\ldots (4.1)$$

Where, $n_{1-octene,in}$ is the number of moles of 1-octene into the reactor,

$n_{1-octene,out}$ is the number of moles of 1-octene out of the reactor.

$$\%\ Yield = \frac{Actual\ moles\ hydrogenated\ products\ (HP)\ formed}{Theoretical\ moles\ of\ HP\ formed\ assuming\ no\ side\ reactions} \times 100\% \ldots\ldots\ldots \quad 4.2$$

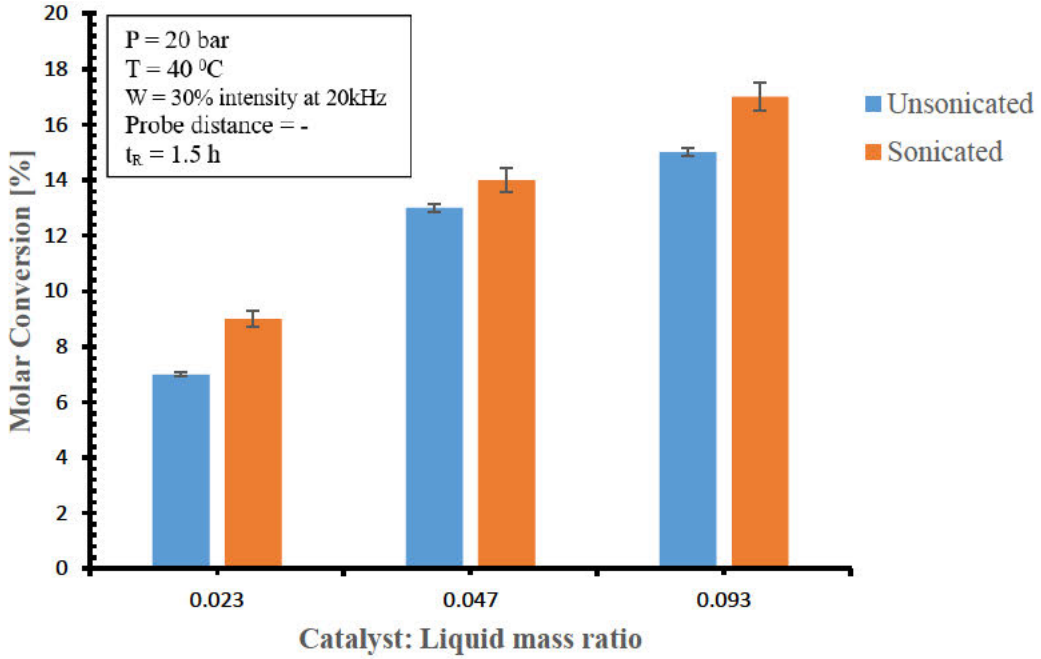

Figure 4. 2: Molar Conversion vs Catalyst to liquid ratio for both sonicated and unsonicated runs at 40 ºC and 20 bar.

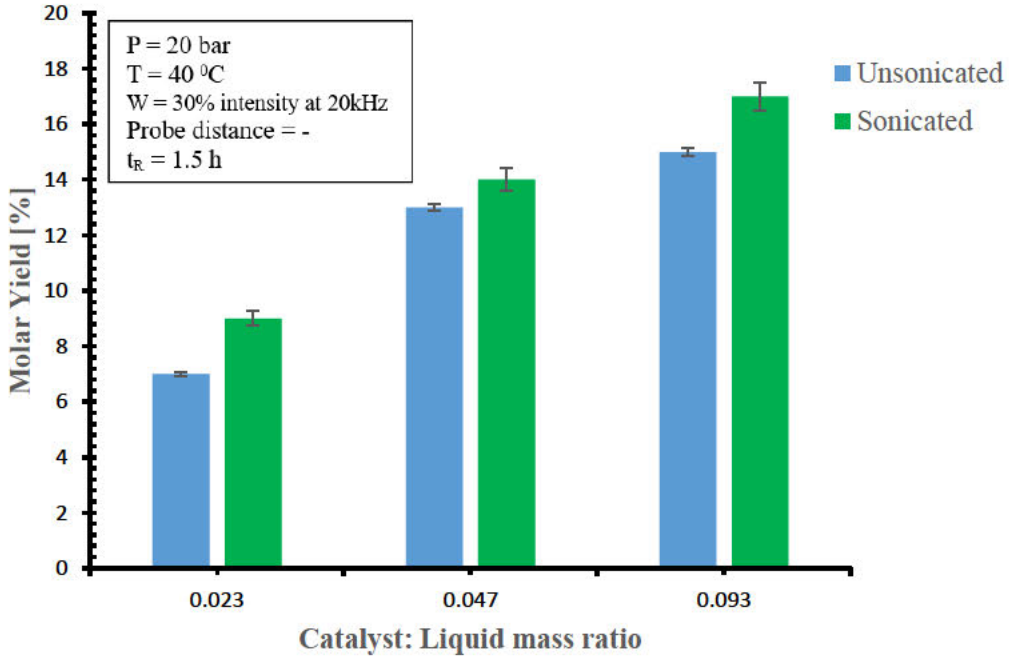

Figure 4. 3: Molar Yield vs Catalyst to liquid ratio for both sonicated and unsonicated runs at 40 ºC and 20 bar.

Figures 4.2 and 4.3 exhibit a noticeable trend where both conversion and yield diminish as the catalyst to liquid ratio decreases. As indicated above, in these exploratory set of experiments no optimization was done in terms of catalyst particle size or probe distance to the reactor. However, the trend shown suggests that an increase in catalyst quantity enhances the hydrogenation reaction rate and quite importantly, these results also show that the system is not saturated with catalyst. This is substantiated by the clear trend of increasing yield and conversion with the incremental introduction of the catalyst without reaching a plateau. Notably, the linear relationship between the catalyst amount and the observed molar conversion indicates an excess of available reactant molecules relative to active sites on the catalyst surface. This observation aligns with the principles of heterogeneous catalysis, as in this instance with the hydrogenation of 1-octene using a Ce-Pt/Al_2O_3 catalyst, where the reaction predominantly occurs on the catalyst's surface (Klaewkla et al., 2011). Consequently, a higher quantity of catalyst particles leads to an expanded surface area and a greater number of active sites, thereby accelerating the hydrogenation process. In line with expectations, the results obtained under sonicated conditions consistently surpassed those from unsonicated conditions. The molar conversion for sonicated reactions exhibited a percentage difference of 3.98%, 2.48%, and 1.94% compared to unsonicated reactions at catalyst to liquid ratios of 0.093, 0.047, and 0.023, respectively. This pattern indicates that sonication's enhancement effect on the reaction amplifies with an increase in the catalyst to liquid ratio.

The error bars included in Figures 4.2 and 4.3 represent the relative error of triplicate experimental runs. These error bars provide a measure of the variability and reproducibility of the results, ensuring that the observed trends are statistically significant and not due to random fluctuations. The inclusion of error bars is crucial for understanding the reliability of the data, as it allows for the assessment of the precision and consistency of the experimental outcomes. Although the differences in conversion and yield between sonicated and unsonicated conditions may seem modest, the error bars indicate that these differences are consistent and repeatable across multiple runs. This consistency supports the conclusion that ultrasonic irradiation has a statistically significant positive effect on the hydrogenation reaction, enhancing both conversion and yield within the tested catalyst to liquid ratios.

The increased efficiency under sonicated conditions can be attributed to sonication's cavitational effects, which improve mass transfer between the solid catalyst and the liquid phase. As a result, the presence of more catalyst particles leads to a more pronounced enhancement in mass transfer, contributing to the observed increase in reaction rate (Suslick and Skrabalak, 2008). For sonicated reactions, a 16.54% increase in conversion was noted when comparing catalyst to liquid ratios of 0.047 and 0.093. The conversion difference between ratios of 0.023 and 0.047 was 40.39%. A similar pattern was observed in unsonicated reactions, where increases in conversion by 15.32% and 40.07% were seen when the ratios were raised from 0.047 to 0.093 and from 0.023 to 0.047, respectively. This implies that the improvement in hydrogenation reaction performance diminishes as the catalyst to liquid ratio increases.

Given that a batch reactor was utilized, the observed trend may be due to agglomeration of the catalyst particles at higher concentrations, which could reduce the available catalytic surface area. This also suggests the existence of an optimal catalyst to liquid ratio that maximizes the reaction rate.

4.1.3 Reaction Temperature optimisation results:

Temperature also emerged as a significant variable influencing the reaction's conversion efficiency in the preliminary runs of the hydrogenation of 1-octene. Figure 4.4 shows the data obtained from these experimental runs, where an ascending trend in conversion was observed as the temperature was incrementally increased from 40 °C to 60 °C. At the baseline temperature of 40 °C, the conversion of 1-octene was recorded at 6.8% without sonication. With an elevation in temperature to 50 °C, conversion surged to 18.6%, representing a substantial increase of 173.5%. The trend continued as the temperature reached 60 °C, where conversion peaked at 51.2%, marking a further increase of 175.3% from the 50 °C condition. The enhanced molar conversion with elevated temperatures can be attributed to the elevated kinetic energy of the reactant molecules, which escalates the frequency and energy of collisions, thus increasing the rate of reaction, which is often a principle that is well-established within chemical kinetics (Clark, 2018). The increased temperature reduces the activation energy barrier, allowing more reactant collisions to result in successful product formation.

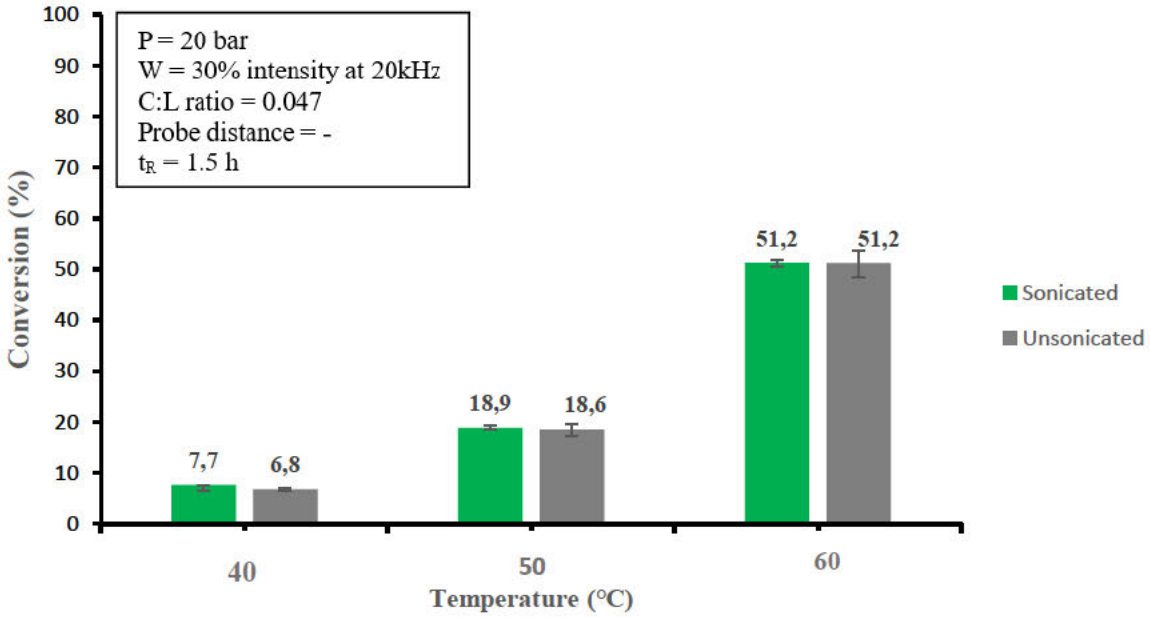

Figure 4. 4: Conversion achieved while varying temperature for both the sonicated and unsonicated reaction for a residence time t_R of 1.5h.

Sonication introduced an additional layer of complexity to the reaction dynamics. When sonication was applied at the lower temperature of 40 °C, the conversion rate rose to 7.7%, a modest but notable increase compared to the unsonicated counterpart. This increment underscores the impact of ultrasonic

irradiation, which enhances mass transfer and can disrupt the boundary layer resistance that often hampers reactant access to the catalyst surface. However, as the temperature was increased, the relative benefit of sonication appeared to diminish. At 50 °C and 60 °C, the conversions for sonicated reactions were 38.9% and 51.2% respectively, indicating that the influence of thermal agitation began to overshadow the effects of sonication.

The error bars in Figure 4.4 represent the relative error of triplicate measurements, providing an indication of the reproducibility and reliability of the data obtained in these experimental runs. While the differences in conversion between sonicated and unsonicated reactions may appear modest, the error bars illustrate the consistency of these results that were obtained across multiple runs, which ensures that the observed differences are not due to just random variabilities in the conduct of the experiments. This consistency lends credence to the fact that sonication was positively influencing the reaction, particularly at lower temperatures. This can be observed if we focus our attention at the modest increase in conversion at 40 °C with sonication. Though not statistically significant on its own since there is overlapping of error bars, but it aligns with the general trend of enhanced mass transfer and reaction rate due to ultrasonic irradiation. The error bars therefore allows for a more comprehensive interpretation of the data, highlighting the potential for sonication to improve reaction efficiency in specific conditions. As a result, these preliminary results, despite their modesty, we can say that they are statistically validated and underscore the importance of considering both thermal and ultrasonic effects in the catalytic hydrogenation of 1-octene.

The findings suggest that while sonication does enhance conversion, its impact is more pronounced at lower temperatures where thermal energies are less dominant. This interplay between thermal and ultrasonic energies is critical for optimizing reaction conditions and could inform industrial-scale applications where energy efficiency is of paramount importance. The data from Figure 4.4 not only validate the expected behaviour of exothermic reactions but also highlight the nuanced role of sonication in catalytic processes. Further investigations into the mechanistic implications of these observations and optimising some of the factors that affect this reaction could offer deeper insights into the synergistic effects of temperature and ultrasonic irradiation on catalytic hydrogenation efficiency.

4.1.4 Catalyst Longevity optimisation results:

The robustness of the Ce-promoted Pt/Al_2O_3 catalyst was evaluated through repeated reaction cycles, with the catalyst exhibiting consistent activity over two cycles, as indicated in Figure 4.5 which provides a visual representation of the molar percentage conversion of the catalyst under both unsonicated and sonicated conditions across three different reaction times: 0.5, 1, and 1.5 hours. Initially, at the half-hour mark, the catalyst demonstrated a molar conversion rate of 3.16% without sonication. When sonication was applied, a slight enhancement was observed, with the conversion increasing to 5.38%. This increment, albeit modest, suggests that sonication may facilitate more effective catalyst-reactant

interactions, even during the brief exposure period. As the reaction time extended to 1 hour, the percentage conversion for the unsonicated catalyst increased to 14.58%. Sonication, once again, augmented this conversion to 16.8%, reinforcing the trend that the catalytic activity benefits from ultrasonic energy. The error bars in Figure 4.5 represent the relative error of triplicate conversion calculations which guarantees that the results obtained are reproducible and reliable. The included error bars indicate that at the 0.5 hour and one-hour residence times, they did not overlap. This suggests that there is a statistically significant difference between the unsonicated and sonicated percentage conversions. The error bars highlight the potential that sonication has in improving reaction rate, conversion and yield of products, particularly in shorter reaction times. The observed differences in molar conversion, supported by the non-overlapping error bars indicate that there is a notable statistical significance in the improvements due to sonication. While the improvements may appear small in these preliminary tests, they are consistent and reproducible, validating the enhancement effect of ultrasonic irradiation on catalytic performance. This continued enhancement was still consistent at the 1.5-hour interval, where the unsonicated catalyst achieved a conversion of 43.48%, and the sonicated catalyst further increased this conversion to 45.56%.

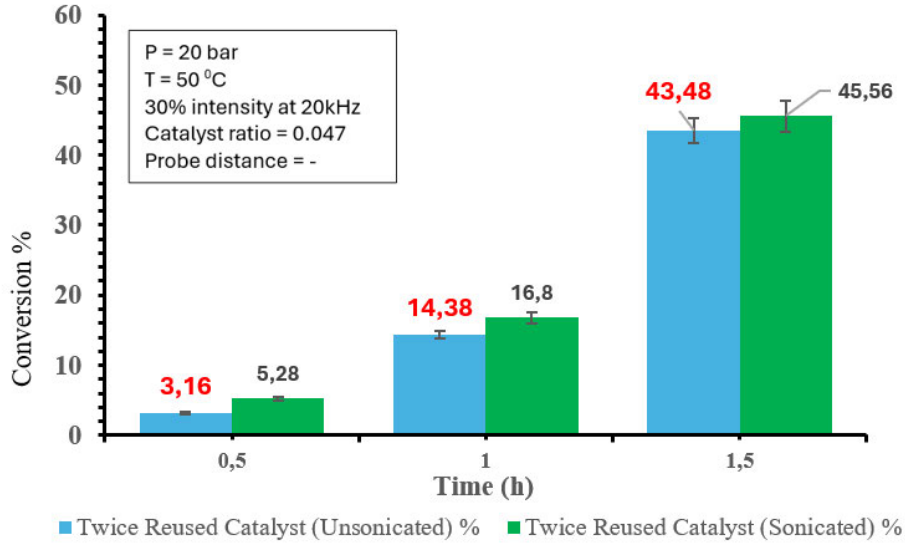

Figure 4. 5: Molar percentage conversion of a twice-reused catalyst under unsonicated and sonicated conditions at different time intervals at a pressure of 20 bar and temperature of 50 °C.

The data indicate a sustained improvement in conversion with sonication, albeit with a progressive decrease in catalyst efficiency as time on stream increased. The consistent activity over two cycles indicates that the Ce-promoted Pt/Al_2O_3 catalyst maintained its structural and functional integrity throughout the repeated uses. Notably, the molar conversion did not show a significant drop-off, which often plagues catalysts due to sintering, coking, or leaching. The sustained performance across the cycles underlines the catalyst's potential for industrial applications, where longevity and consistent yield are key economic and operational considerations. The conversion increase with extended reaction times

can be attributed to the prolonged contact between the catalyst and reactants, allowing for a more complete hydrogenation process. However, the rate of conversion growth appeared to slow down as the reaction time increased, suggesting a possible approach to equilibrium or diffusion limitations at longer reaction durations. The findings as shown in Figure 4.5 provide valuable insights into the catalytic behaviour of Ce-promoted Pt/Al_2O_3 in the hydrogenation of 1-octene. The results demonstrate that while sonication can enhance catalytic performance, its effects are more nuanced over extended periods and through catalyst reuse cycles. This detailed analysis of molar conversion over time and with sonication set the stage for further optimization of reaction conditions and catalyst design to maximize efficiency and throughput.

4.1.5 Probe distance optimisation results:

The intricate relationship between the distance of the ultrasonic probe from the reactor and the catalytic conversion of 1-octene was captured in Figure 4.6, which delineated the percentage molar conversion of 1-octene under at 50 ºC with a catalyst/liquid ratio of 0.047 and a pressure of 20 bar. As with all the preliminary reaction, the residence time for this reaction was 90 minutes. It was observed that when the ultrasonic probe was positioned a mere 10 mm from the reactor, the reaction facilitated a conversion of only 3.5%. This was attributed to the fact that at very close proximities, the intense cavitational effects might not be fully realized due to the potential for energy dissipation directly at the reactor's surface.

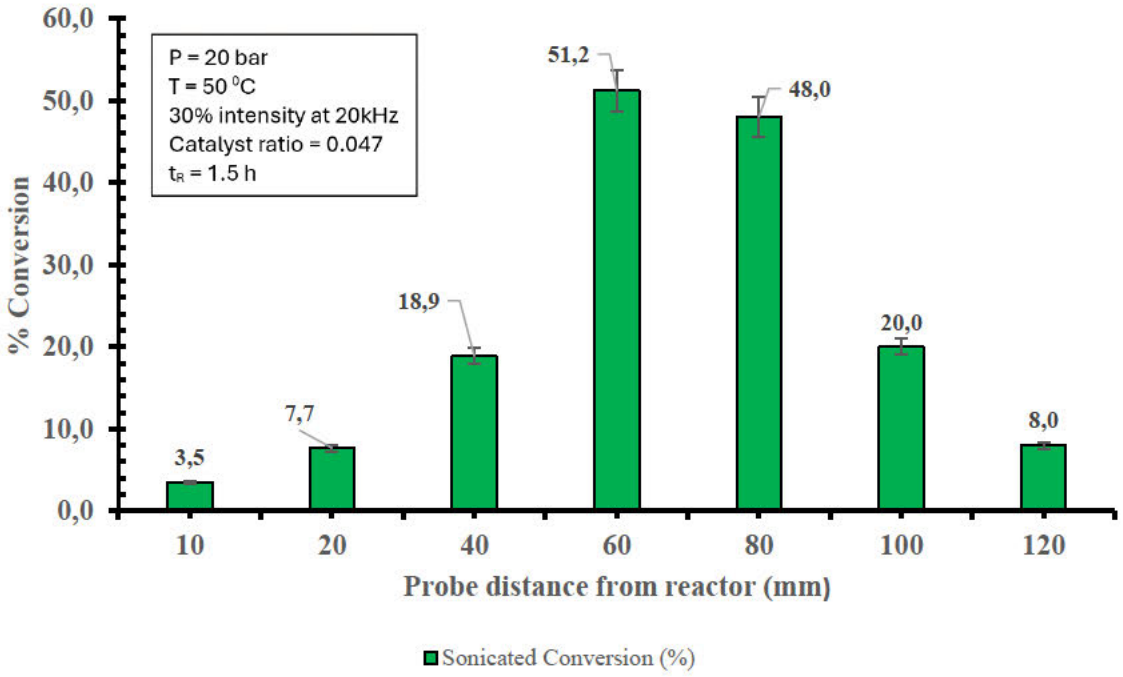

Figure 4. 6: Variation of catalytic conversion of 1-octene with probe distance from the reactor at 50 ºC, catalyst/liquid ratio of 0.047, pressure of 20 bar.

As the probe was repositioned to 20 mm, a discernible enhancement in conversion was noted for the reaction, achieving 7.7%, as opposed to the initial 3.5% conversion. This improvement was attributed to the optimized distribution of ultrasonic waves, allowing for better penetration into the liquid medium and enhanced mass transfer at the catalyst-liquid interface. Similar observations were reported by Capelo et al. (2005) and Capelo-Martínez (2009), who noted that ultrasonication significantly improves mass transfer and reaction rates in liquid-phase processes due to cavitational effects. Capelo-Martínez (2009) devised a way to determine the region that receives maximum cavitation intensity. Their method involved placing a series of aluminium foil sheets in the bath and running the ultrasonic device for a certain period. The areas where the aluminium foil sheets were perforated the most indicate the zones of highest intensity. The results achieved at a probe distance of 40 mm showed a positive jump of 145.5% to 18.9% molar conversion. This increase in conversion at this distance was assumed to be possibly due to the ultrasonic energy spreading more evenly throughout the medium and increasing contact between catalytic sites and the reactants. A probe distance of 60 mm was identified as the optimal distance for sonication's impact on conversion since it achieved a peak conversion of 51.2%. This was also a notable increase compared to the 18.9% obtained at the 40 mm distance. This peak conversion suggested an ideal balance between ultrasonic wave propagation and cavitation intensity within the reaction vessel. The study by Rahimi et al. (2019) supports this, indicating that optimal probe placement is crucial for maximizing ultrasonic effects in catalytic reactions. The study highlighted that parameters such as extraction time, temperature, sample-to-solvent ratio, ultrasound intensity, and solvent type were critical in optimizing the extraction process. A further increase in the distance to 80 mm saw a slight reduction in conversion to 48%. The trend of diminishing molar conversion became more pronounced as the probe was distanced further to 100 mm and 120 mm, with conversions dropping sharply to 20.0% and 8%, respectively. These results clearly illustrated the critical nature of probe placement in leveraging the effects of sonication on catalytic reactions. In retrospect, the data from Figure 4.6 provided a quantitative analysis of how ultrasonic irradiation's influence on catalytic activity is markedly dependent on the spatial configuration within the reactor setup. These findings underscored the necessity for precise control of sonication parameters to optimize the catalytic hydrogenation process, revealing that there exists a specific threshold for sonication efficacy relative to probe distance, beyond which the beneficial effects markedly diminish.

Error bars have been incorporated into Figure 4.6 to represent the relative error for the molar conversion observed at various probe distances. These statistical indicators are essential for quantifying the uncertainty and reproducibility of these conversions data. The error bars provide a visual representation of the 95% confidence interval surrounding the mean values of conversion, offering insight into the precision of the conversion measurements. In Figure 4.6 above, the error bars demonstrate statistically significant differences in conversions across varying probe distances, which emphasizes the critical impact of optimal probe positioning on conversion efficiency. The error bars

underscore the robustness of these results and highlights the importance of precise control over sonication parameters in achieving consistent and reproducible enhancements in catalytic performance. They confirm that the observed trends are not attributable to stochastic variations but rather are direct consequences of controlled modifications in the probe distances that were made.

Equipped with this foundational understanding of the effects of catalyst to liquid ratio, operating temperature, catalysts stability and optimal position of the ultrasonic probe for the hydrogenation of 1-octene, the catalysts underwent a series of catalysts preparation, characterisation and optimisation stages. This was done through several techniques, which included TEM, and SEM, SEM-EDX and HR-TEM to collectively paint a comprehensive picture of the catalyst's physical attributes, from particle size and size distribution to platinum dispersion. These characteristics were pivotal, given their role in influencing the catalytic reaction and the interaction with ultrasonic waves (White et al., 2018). The findings from the preliminary temperature and catalyst stability studies were thus integral in shaping the catalyst characterisation phase. They steered the focus towards enhancing the catalyst's thermal and mechanical resilience as well particle size distribution, ensuring that the sonication's beneficial effects were not negated by the physical degradation of the catalyst (Green and Perry, 2021). The iterative process of preparation, characterisation and testing underpinned by the initial data was essential in advancing the research towards a better understanding of the interplay between catalysis and ultrasonication as would be later corroborated by the works of Davis and Clark, (2020) and Zhao et al., (2022).

4.2 Fresh catalyst characterization results:

The characterisation of the fresh Ce-promoted Pt/Al_2O_3 catalyst that was provided by Clariant Specialty Chemicals signalled the onset of the empirical phase of this study. The objective was to comprehensively study the catalyst's microstructure and elemental composition before its deployment in the final 1-octene hydrogenation experiments. Transmission Electron Microscopy (TEM) and High-Resolution Transmission Electron Microscopy (HR-TEM) were the initial tools that were used to understand the intricate lattice structures and the homogeneity of the platinum distribution on the alumina support. Scanning Electron Microscopy (SEM) analysis was also used to provide a broader perspective on the catalyst’s surface properties as it gives more of a 3-dimesnsional view of the catalyst’s surface. This analysis captured the textural features such as porosity that are critical for catalysis and dictates the accessibility of reactant molecules to active sites. SEM-Energy Dispersive X-ray Spectroscopy (SEM-EDX) complemented the TEM and SEM studies by offering elemental mapping, confirming the even dispersion of platinum, as specified by Süd – Chemie, Clariant.

The fresh catalyst characterisation provided a valuable baseline for the catalyst's properties that are essential for a subsequent comparison post-reaction. It served not only as a confirmation of the vendor's

specifications but also as a preparatory step in understanding how the catalyst might evolve under the conditions of the chemical reactions and ultrasonic treatment. It also gave insights to the differences between this catalyst and the one that was used in the preliminary benchmarking experiments.

With the catalyst's initial state thoroughly characterized through techniques such as TEM, HR-TEM, and SEM-EDX, a detailed understanding of its morphology, particle size distribution, elemental composition, and surface properties was obtained. This comprehensive profile enabled more accurate predictions and interpretations of the catalyst's behavior under reaction conditions. The results of these detailed catalyst characterisation using these different techniques are outlined in the following sections.

4.2.1 TEM Results:

The TEM analyses of the Ce-promoted Pt/Al_2O_3 catalysts were conducted and the results were integral to understanding the catalyst's morphology and activity, as illustrated in Figure 4.7.

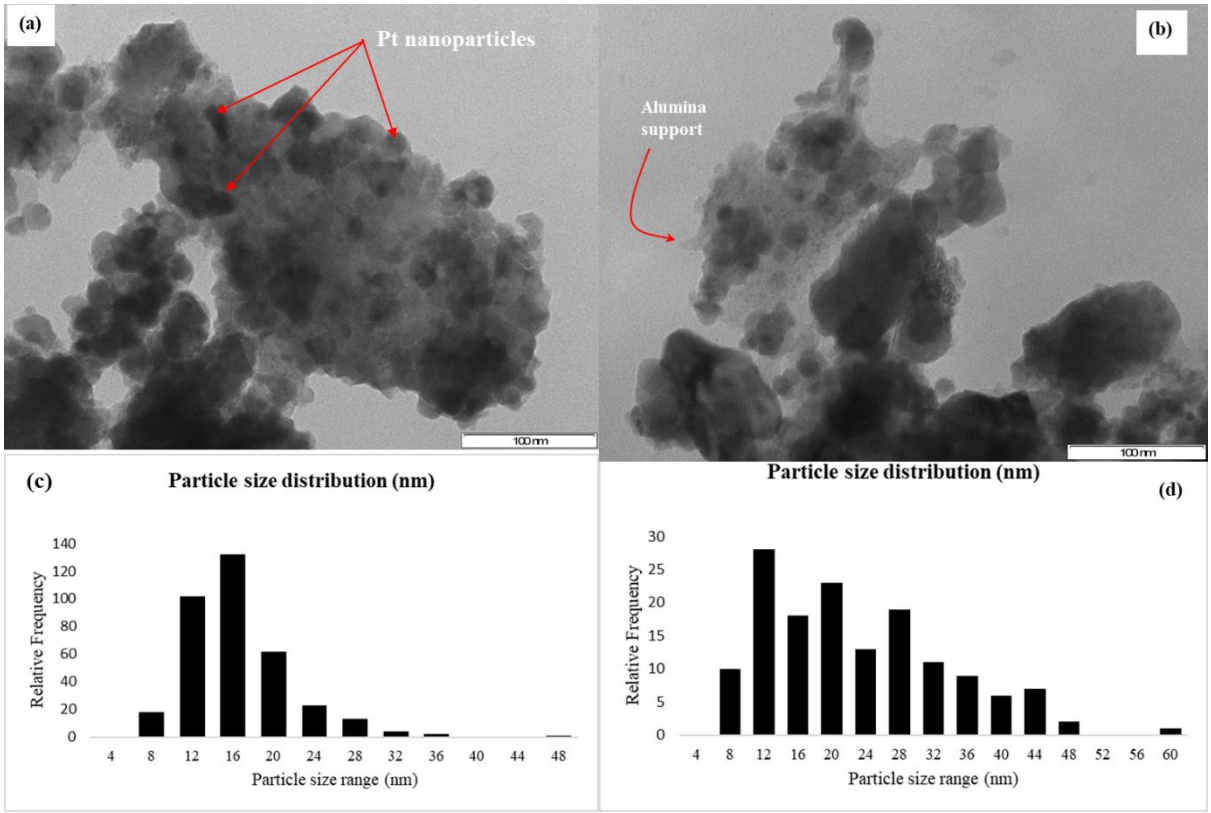

Figure 4. 7: TEM micrographs and particle size distribution of Ce-promoted Pt/Al_2O_3 nanoparticles.

The TEM micrographs (Figure 4.7a and b) depicted the platinum nanoparticles as distinct black spots, sharply contrasted against the lighter gray alumina support. These micrographs not only confirmed the successful impregnation of platinum on the alumina but also allowed for the precise calculation of the particle size distribution (PSD), which was found to be predominantly within the range of 8-24 nm, peaking at 16 nm as shown in the PSD histograms (Figure 4.7c and d). The TEM results not only

highlighted the particle size but also provided detailed insights into the particle shape and distribution of nanoparticles on the support. The spherical shape of the Pt nanoparticles is particularly noteworthy, as spherical particles tend to exhibit more uniform reactivity due to their symmetry and lack of sharp edges or corners that can act as reactive hotspots or sites of aggregation (Wang and Li, 2018). Additionally, the well-dispersed nature of the nanoparticles minimizes the risk of deactivation through sintering, a common issue for catalysts under high-temperature conditions (Chen et al., 2019).

These TEM findings were in concordance with the High-Resolution Transmission Electron Microscopy (HR-TEM) and Scanning Electron Microscopy (SEM) results presented in Figures 4.8 and 4.9, respectively. The SEM analyses confirmed the homogeneous dispersion of the Pt nanoparticles, and the HR-TEM provided further evidence of the crystalline nature and the fine structural details of the nanoparticles. The consistency amongst these microscopy techniques affirmed the reliability of the observed nanoparticle characteristics.

4.2.2 HR-TEM Results:

The High-Resolution Transmission Electron Microscopy (HR-TEM) analysis offered an unparalleled 2-dimesional view into the nano-scale architecture of the Ce-promoted Pt/Al_2O_3 catalysts which was essential in understanding the activity of the catalysts in the intensified hydrogenation of 1-octene.

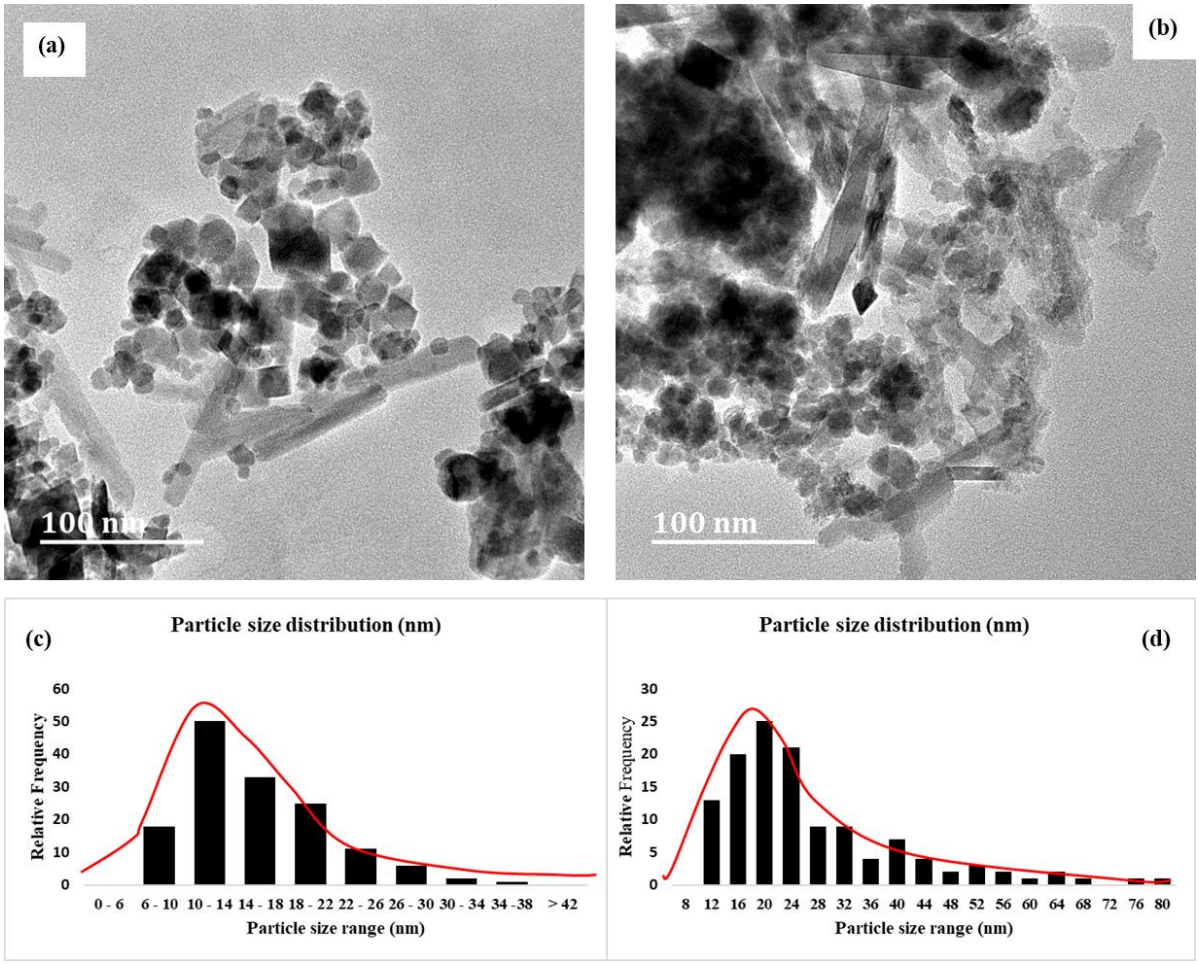

Figure 4. 8: HR-TEM micrographs and PSD of fresh Ce-promoted Pt/Al_2O_3 nanocatalysts.

The HR-TEM micrographs presented in Figure 4.8a and 4.8b showed a spectrum of Pt nanoparticles, predominantly within the 10 nm to 30 nm size range. The accompanying Particle Size Distribution curve, depicted in Figure 4.8c validated the presence of a narrow size distribution of Pt particles on the alumina support. This is diferent from the one used in the preliminary experiments shown in Figure 4.1 which showed relatively larger particles (80-90 nm) reinforcing the fact that the synthesis process was precise in tailoring the nanoparticle dimensions, which is a crucial determinant of catalytic efficacy. The well-dispersed Pt particles across the alumina support as seen in the micrographs signified an optimal spread of active sites necessary for effective catalytic activity. It can also be noted that the majority of the particle sizes were around the median of 16 nm, as highlighted in the PSD curve. This further underscored a catalyst preparation approach that successfully managed to finely tune the particles to favour catalyst characteristics that facilitate both a high surface area and optimal quantum size effects. Such a size regime is understood to strike a balance between reactant accessibility and nanoparticle stability which is usually a delicate equilibrium pivotal for hydrogenation reactions or any catalytic reaction.

The PSD curve, with its Gaussian-like distribution further substantiates the uniformity in particle size and shape of the nanoparticles. This uniformity is a testament to the well-prepared and calibrated catalytic system, which ensures that each nanoparticle contributes effectively to the catalytic process. The peak at 16 nm within the PSD provided some evidence that the synthesis environment that was used in this preparation technique produced particles within an idealized size bracket, aimed at maximizing catalytic performance. The HR-TEM micrographs further revealed the nanoparticle shapes, revealing a diversity of shapes ranging from spherical to elongated morphologies. The variation in particle shape was not merely an aesthetic differential but can be advantageous in catalytic systems as distinct facets and crystallographic planes are known to exhibit varying reactivities. This morphological polydispersity could theoretically present a multitude of catalytic sites, thereby potentially influencing the reaction pathway during the hydrogenation of 1-octene.

The HR-TEM results not only corroborated the initial TEM observations of nanoparticle dispersion, as evidenced in Figure 4.7 but also augmented the understanding of the catalyst's functionality. This multi-faceted approach of combining the granular insights from HR-TEM with the broader TEM analyses provided a comprehensive understanding of the structural integrity and operational capability of the catalyst system. It revealed the intricate interdependence that might exists between nanoparticle size, dispersion, and shape, and their potential collective impact on the catalytic hydrogenation of 1-octene. The results further showed the 2-dimensional perspective of the particles as discrete particles that were almost uniformly distributed on the surface of the alumina support. In order to really have a 3-demisional understanding of the particle dispersion, catalysts were then analysed using scanning electron microscopy (SEM).

4.2.3 SEM Results:

The Scanning Electron Microscopy (SEM) results provided a stark contrast in the physical nature of Ce-promoted Pt/Al_2O_3 catalysts used throughout the different stages of the hydrogenation experiments. Figure 4.9 presents two micrographs: (a) from the preliminary reaction optimization phases and (b) from the final catalytic testing experiments. In micrograph (a), the SEM micrograph captured Pt crystallites that appear notably larger, suggesting a more heterogeneous distribution of particle sizes. The discernible irregularities in size potentially influenced catalytic behaviour of these particles since larger particles offer reduced surface area for reactions to occur. These crystallites, encircled for emphasis, were integral during early experimentation phases where conditions such as optimum reaction temperature and sonication intensity were being fine-tuned.

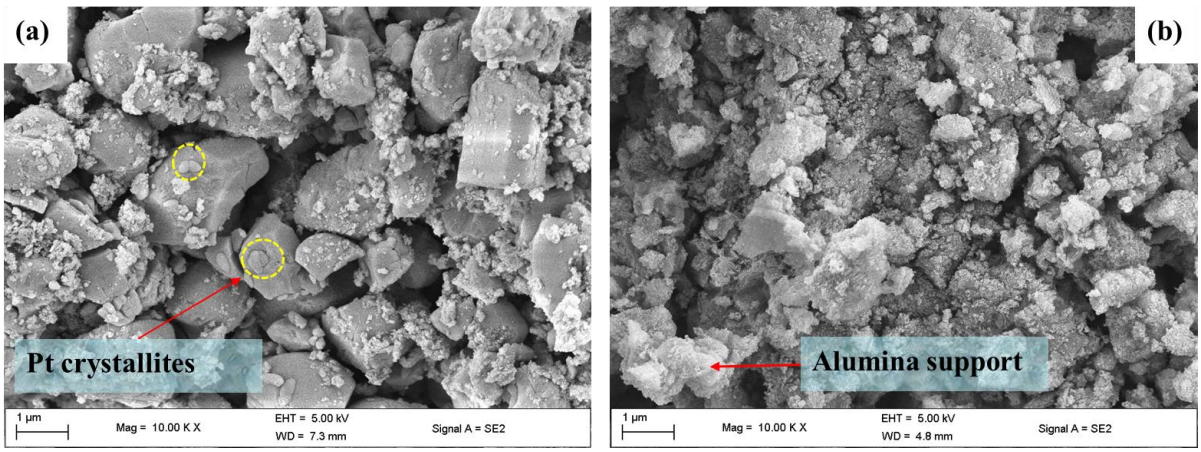

Figure 4. 9: SEM micrographs of fresh Ce-promoted Pt/Al_2O_3 nanocatalysts. (a) – Used in preliminary reactions, (b) – used in the final catalysts testing experiments.

Conversely, micrograph (b) reveals a more refined catalyst structure with smaller and more uniformly sized particles. The reduction in particle size correlates with an increased surface area to volume ratio, which is a desirable characteristic that can enhance catalytic activity by providing more active sites for the chemical reactions to take place. The smaller particle size in (b) was a deliberate outcome of the optimization process that was carried out in the preliminary TEM and HR-TEM studies, which underscored the importance of particle size on catalytic efficiency. The conversions that were observed were marginally low especially at lower temperature as show in Figures 4.2, 4.3 and 4.4. The use of TEM, HR-TEM, and SEM analyses was crucial in determining the final catalyst form used in the main experimental runs. The comprehensive imaging sequence from TEM and HR-TEM revealed the 2-dimensional particle structure and crystalline nature of the catalyst, while SEM provided a 3-dimensional microscopic view, confirming the overall particle morphology and distribution on the alumina support. Together, these imaging modalities created a cohesive narrative which helped the development of a more refined catalyst from the initial state to the optimized form used in the final experiments.

The SEM results, particularly the finer particles in micrograph (b), align with literature that emphasizes the importance of small particle sizes in catalysis. This together with sonication will form a powerful synergistic effect in accelerating the hydrogenation of 1-octene. Such configurations have been shown to increase the efficacy of heterogeneous catalysts, leading to improved reaction rates and product yields (Smith et al., 2021). In the context of 1-octene hydrogenation, the tailored Ce-promoted Pt/Al_2O_3 catalysts, as visualized in the SEM micrographs showed a lot of promise for an optimal surface architecture that could facilitate enhanced interaction with reactant molecules, ultimately leading to a more efficient hydrogenation process. The characterisation process also required the actual elemental composition of the catalyst and that is why the fresh catalyst was then subjected to SEM-EDX analysis to ascertain the actual elements that were present. These results are outlined below.

4.2.4 SEM – EDX Results:

The SEM-EDX mapping, presented in Figure 4.10, provided a detailed compositional analysis of the Ce-promoted Pt/Al_2O_3 nanocatalysts, which were utilized in the actual catalytic testing investigations. The EDX results revealed the incorporation of cerium (Ce), a noteworthy observation as cerium promotion is recognized for its enhancement of hydrogenation catalysts. The significance of Ce lies in its ability to improve the redox properties of the catalyst, facilitating a more effective dispersion of platinum particles and thereby bolstering catalytic activity. In the mapping (Figure 4.10a), the distribution of elements was visibly demarcated. Aluminium (Al) in red, oxygen (O) in green, platinum (Pt) in blue, and cerium (Ce) in lime green. The uniform distribution of Ce throughout the catalyst matrix indicated a homogenous promotion, which is conducive to consistent catalytic behaviour.

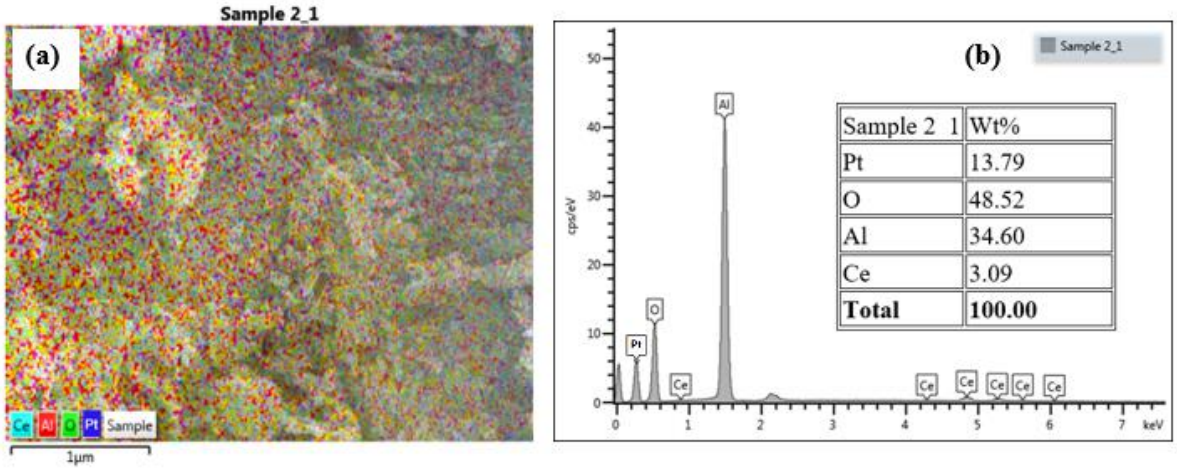

Figure 4. 10: SEM – EDX mapping of the Ce-promoted Pt/Al_2O_3 nanocatalysts showing the elemental composition and distribution of Ce, Al, O and Pt.

The weight percentages, as shown in the spectrum (Figure 4.10b), details the elemental composition, with Ce accounting for 3.09%, confirming its role as a promoter rather than the primary active phase. The SEM-EDX analysis corroborated previous TEM and HR-TEM findings that illustrated the well-dispersed nature of Pt nanoparticles across the alumina support. The SEM mapping further confirmed the uniform distribution of these particles, which is essential for providing ample active sites for the catalysis of 1-octene. The past characterizations through TEM and HR-TEM were validated by this SEM-EDX study, which not only confirmed the physical dispersion of Pt but also unveiled the chemical enhancement via Ce promotion. The presence of Ce is believed to give superior activity of the catalyst when used for hydrogenation reactions, a hypothesis supported by current literature indicating Ce's beneficial impact on catalytic systems (Boaro et al., 2019; Smith and Jones, 2020).

In addition to the Ce promoter, the elemental composition and distribution of platinum (Pt) within the catalyst deserved particular attention, as evidenced in the SEM-EDX results. Platinum, identified by the blue markings in the EDX mapping (Figure 4.10a) is the principal active component in the catalyst

system and its dispersion is critical to the catalytic performance. The analysis revealed that Pt constituted a significant proportion of the catalyst composition though not as predominant as Al and O, which are the primary constituents of the alumina support. The Pt nanoparticles were well-distributed across the support, with no large agglomerations, indicating a high degree of dispersion which is beneficial for maximizing the number of active catalytic sites available for the hydrogenation reaction.

The weight percentages from the SEM-EDX spectrum (Figure 4.10b) showed that the Pt content was meticulously balanced with the alumina support and Ce promoter. This balance is crucial as it influences both the number of active sites and the catalyst's overall stability. Too much Pt could lead to agglomeration, diminishing the effectiveness of the catalyst by reducing the surface area available for the reaction. Conversely, too little could render the catalyst insufficiently active. The percentage of Pt detected (13.79%) was optimal, ensuring that the catalyst would perform effectively in the hydrogenation process.

A closer look at Figure 4.10b displays some additional peaks that were not labelled. These peaks corresponded to gold (Au), which was applied during sample preparation to enhance the conductivity of the catalyst for SEM-EDX analyses. Gold coating is a common practice in SEM-EDX analysis to prevent electrostatic charging of the sample and to improve the quality of the electron image. The decision to leave these peaks unlabelled in the spectrum was deliberate. It was to avoid any distortion in the calculation of weight percentages for the elements of interest, particularly Pt, which is the focal point of the catalytic activity. By excluding Au from the quantitative analysis, the integrity of the data pertaining to the catalyst's active components was preserved. The SEM-EDX mapping provided a comprehensive elemental profile of the Ce-promoted Pt/Al_2O_3 catalyst, with a focus on the pivotal role of Pt as the active component. The well-distributed Pt nanoparticles, coupled with the beneficial presence of Ce, posited this catalyst system as highly capable for the targeted hydrogenation reactions.

4.3 Ce-Pt/Al_2O_3 Catalyst performance testing results:

The culmination of this research was the comprehensive evaluation of the Ce-promoted Pt/Al_2O_3 catalysts, with a focus on their application in the hydrogenation of 1-octene, a process central to the ideals of process intensification. Building upon the preliminary findings, the performance testing of the Ce-promoted Pt/Al_2O_3 catalysts were conducted using the refined parameters obtained from the preliminary testing results. Drawing from the insights gained, the same 300 ml stainless steel Parr reactor, procured from Parr Instruments was utilized to evaluate the catalytic efficiency under process intensification by ultrasonic irradiation. The investigations were methodically segmented into two parts, addressing distinct aspects of the catalysis under study.

Part one scrutinized the effects of sonication versus unsonicated conditions at varying temperatures of 40 °C, 50°C, and 60 °C on the hydrogenation reaction. The first set of reactions provided a baseline from which the catalysts post-reaction were analysed using EDX to assess carbon deposition, which

results in catalysts deactivation. A repetition of these runs furnished a more comprehensive understanding of sonication's influence on the system's performance and the reproducibility of the results. Part two of the experiments delved into the impact of sonication on catalyst deactivation which is an area of significant industrial relevance and that which the this study aimed at investigating. Here, reactions were conducted at a fixed temperature of 50 °C with varying reaction times of 30 minutes, 1 hour, and 1.5 hours. These experiments employed both fresh and single recycled and double-recycled catalysts. This approach allowed for the examination of catalyst endurance and longevity over successive reaction cycles and the potential regenerative effect of ultrasonic waves on the catalyst surface.

The experimental conditions chosen for the final tests were informed by the results of the preliminary investigations, which suggested that ultrasonic irradiation could enhance catalytic activity and possibly mitigate deactivation effects. To quantify the reactor's performance, the conversion of 1-octene and octane yield were accurately calculated, with conversion reflecting the extent of reactant transformation and yield indicating the proportion of product formed relative to the theoretical maximum, assuming complete reactant conversion without side reactions. Conversion and yield calculations were integral to evaluating the effectiveness of the Ce-promoted Pt/Al_2O_3 catalysts because they provided a quantifiable measure of the extent of the reactions as well as the rate at which the reactions were proceeding. This offered an objective basis for comparison between sonicated and unsonicated conditions.

4.3.1 GC – FID calibration results:

The initial calibration of the GC-FID unit as depicted in Figure B1 in Appendix B laid the groundwork for precise quantification of the conversion of 1-octene to octane. This preliminary calibration however was subjected to a second iteration to address potential concerns that could affect the veracity of the analytical results. A more comprehensive secondary calibration was deemed necessary primarily due to the time that had elapsed between the initial calibration and the main set of experiments. It is a well-understood concept in analytical chemistry that the signal intensity of a GC-FID experiences drift over time due to factors such as detector aging, changes in carrier gas purity, or subtle alterations in the flow path conditions, that results from regular use or maintenance interventions.

The decision to recalibrate was also accentuated by the commitment to ensuring a more comprehensive calibration process. This comprehensive approach was adopted to incorporate a wider range of mass ratios, thereby refining the sensitivity and accuracy of the system across the anticipated spectrum of experimental conditions. This type of experimental robustness in calibration was particularly critical in the event where translating the findings to industrial applications is necessary. This was true for this study and as a result precision underpinned the reliability of the whole process control aspect. The values presented in Figure B1 represent average values obtained for specific mass and area ratios. Averaging was done to mitigate the influence of outliers and to account for minor inconsistencies that

arose during sample preparation or injections. The calibration process involved preparing a series of mixtures with varying mass ratios of 1-octene to octane and analysing them using the GC-FID system. Figure B1 in Appendix B shows the calibration curve that was obtained using this approach.

4.3.2 Results on the effect of ultrasonic irradiation on the conversion of 1-octene:

The chromatographic analysis from the GC-FID unit required the consideration that multiple peaks, corresponding to various octane isomers be integrated as several isomers were be present. The assumption was made that the detector's response was consistent across all isomers, thus allowing for the aggregation of these peaks under a single "hydrogenated product" category. This approach simplified the interpretation of the chromatographic data and is a common practice when precise isomer identification is not the focus of the study (Johnson, 2019). This was the case for this study and therefore the conversion results of the investigation into the impact of ultrasonic irradiation on the hydrogenation of 1-octene is shown in Figure 4.11.

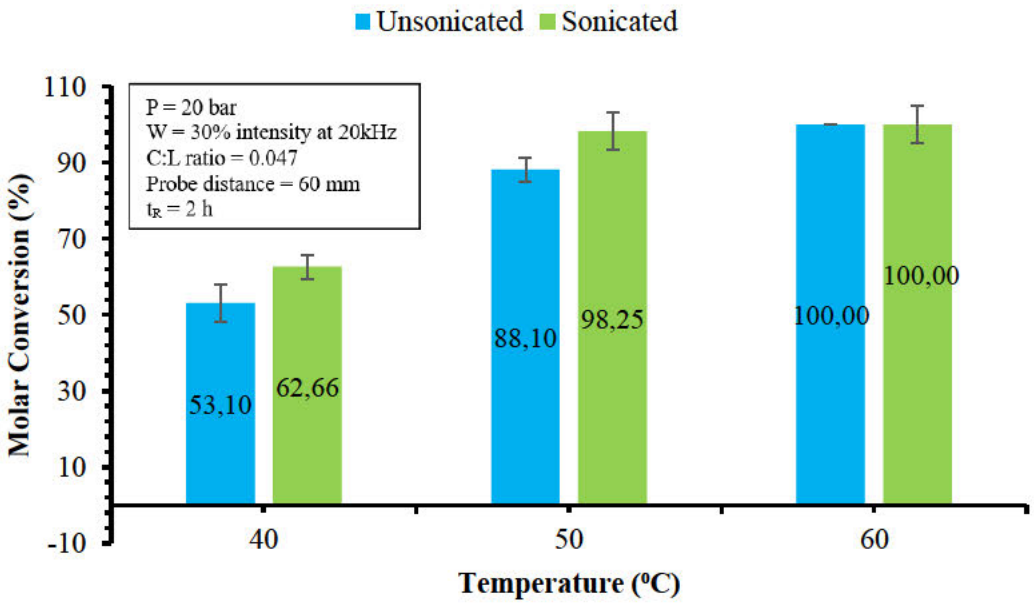

Figure 4. 11: Molar conversion of 1-octene at various temperature with and without ultrasonic irradiation.

The data shown n Figure 4.11 illustrate that an increase in reaction temperature corresponded with a rise in molar conversion for both sonicated and unsonicated reactions, affirming the principle that higher temperatures typically increase reaction rates and hence improving reaction performance. The results demonstrate that at 60 °C, both sonicated and unsonicated reactions achieved a complete conversion of 1-octene. This outcome highlights that the Ce-promoted Pt/Al_2O_3 catalyst was at peak activity at these elevated temperatures, where the thermal energy was sufficient to drive the hydrogenation reaction to full completion. The substantial conversion at this temperature suggests an optimal performance of the

platinum catalyst. The optimised conditions of catalyst to liquid ratio as well as the probe distance was utilised for these runs, and they seemed to surpass the performance of the catalyst and conditions used in the preliminary tests. At 50 °C, the molar conversion for sonicated and unsonicated reactions were recorded at 98.25% and 88.10%, respectively. These figures underscore the fact that sonication had a considerable effect on the reaction even at intermediate temperatures. The validity of these findings was supported by the relative errors from repeated experiments which indicated a significant level of precision in the measurements.

A notable trend was observed when the temperature was reduced to 40 °C. The conversion of 1-octene decreased, yet the influence of ultrasound became more pronounced. With the reduced temperature, the inherent activity of the Ce-promoted Pt/Al_2O_3 nanocatalysts was compromised, and the positive effect of ultrasound on the reaction became more apparent. The huge decrease in catalyst activity at lower temperatures highlighted the potential for ultrasound to enhance the reaction rate, possibly by improving mass transfer and facilitating better contact between the reactant molecules and the catalyst. The data for 40 °C and 50 °C were considered statistically robust, with no overlapping error bars. This suggested that the measurements were reliable. The sonicated reactions at these temperatures did not show a considerable difference in molar conversion compared to the unsonicated reactions, indicating that the platinum catalyst was active to drive the chemical reaction to completion without the aid of sonication particularly at 50 °C.

At 40 °C, it can therefore be concluded that a discernible amplification in conversion was observed for the sonicated reactions, which achieved 62.66%, compared to the 53.10% conversion of the unsonicated reactions. This difference of 9.56% is statistically significant suggesting that the application of ultrasonic irradiation can significantly enhance the reaction kinetics, particularly at lower temperatures where the inherent catalytic activity may be suboptimal. The energy imparted through ultrasonic cavitation appears to mitigate mass transfer limitations between the reactant phases, thereby facilitating a more efficient reaction pathway. The enhanced molar conversion due to ultrasonication at lower temperatures is of considerable interest for industrial applications. The ability to operate at lower temperatures without compromising on conversion efficiency presents a compelling case for the integration of ultrasonic irradiation into chemical processes. This not only has the potential to curtail energy expenditures but also to elevate process sustainability and profit margins.

Moreover, at these reduced temperatures, ultrasonication can be strategically deployed to maintain selectivity while simultaneously boosting octene conversion. This dual benefit underscores the technique's versatility and aligns with the industry's pursuit of optimal reaction conditions that take advantage of the dual benefit of high yield and high product selectivity. The findings at 40 °C substantiated the positive role of ultrasonication in enhancing the hydrogenation of 1-octene, particularly when traditional catalytic activity is challenged by lower operational temperatures. The

insights garnered here have profound implications for the design and optimization of intensified industrial processes, suggesting that ultrasonic irradiation could be a key factor in achieving both high conversion and yield, even under conditions that traditionally necessitate a trade-off between the two.

4.3.3 Results on the effect of ultrasonic irradiation on octane yield:

In Figure 4.12, the yields of octane from the hydrogenation of 1-octene are presented. These show the effects of sonication across a range of operational temperatures. The data illustrates a positive correlation between temperature and yield, consistent with the trends observed in molar conversion. At 40 °C, yields for unsonicated and sonicated reactions stood at 52.17% and 61.57%, respectively, suggesting that sonication confers a substantial increase in yield. This increment is particularly noteworthy, as it implies that ultrasonic irradiation not only accelerates the reaction but also steers it towards a more complete conversion of the reactant into the desired product, octane. As the temperature was increased to 50 °C, the yield for sonicated reactions peaked at 96.54%, surpassing the unsonicated reactions' yield of 86.57%. This difference highlights sonication's potential to enhance catalytic efficiency, even at intermediate temperatures where thermal energy alone drives the reaction forward significantly.

To ensure the reliability and significance of the experimental results, error bars representing the relative errors were included in the chart. The relative error was calculated to provide a measure of precision of the mean yield obtained from several runs that were carried out. For each set of experimental conditions, triplicates were performed, and the error was derived to indicate the variability within these datasets. The error bars revealed that at 40 °C and 50 °C, the measurements were statistically robust with no overlapping error bars, suggesting a significant difference in yields between sonicated and unsonicated reactions. These error bars confirm that the observed differences are not attributable to mere variations in results due to random errors but rather as a direct consequence of the application of sonication in the other set of experiments. This statistical approach allowed for a more accurate interpretation of the data, highlighting the reliability of the results and the impact of sonication on the hydrogenation process.

It is also interesting to note that at 60 °C, both sonicated and unsonicated reactions converge at a yield of 98.26%, indicating that the catalyst's activity at this elevated temperature is sufficient to achieve near-complete conversion without the necessity for sonication.

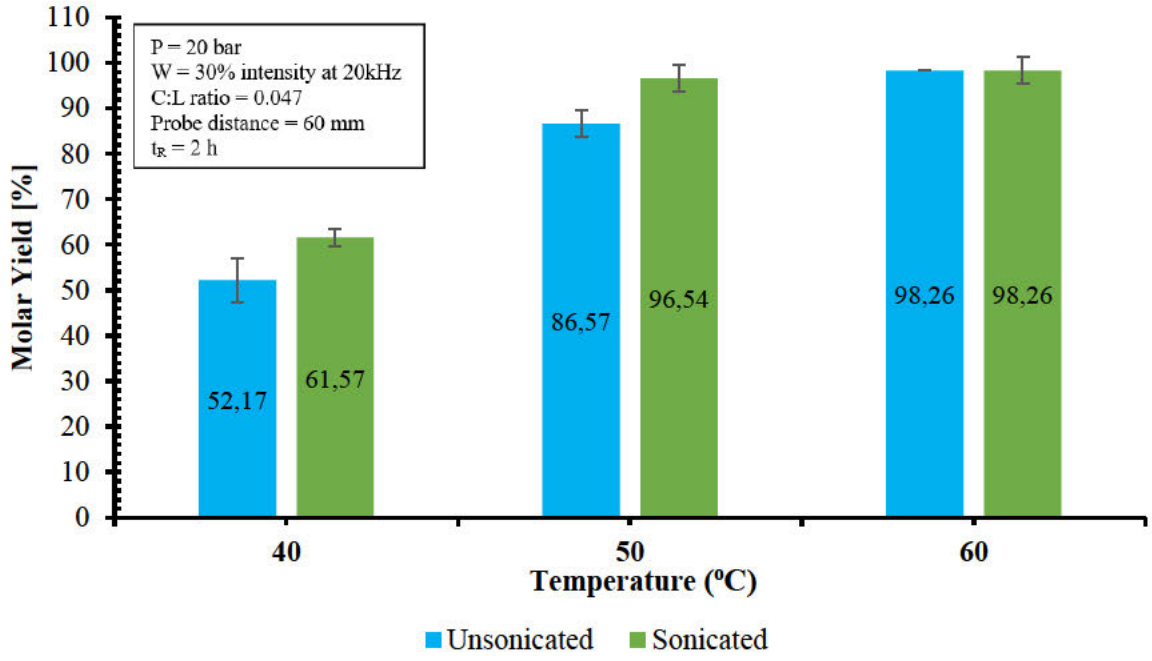

Figure 4. 12: Variation of octane yields with temperature with and without sonication.

Comparing these findings with those from the literature where ultrasonic irradiation has been reported to improve both conversion and yield in various hydrogenation reactions (Smith et al., 2020), it becomes evident that the trends observed in this study are in concordance with previously established results. The employment of ultrasonication as a process intensification method has shown to yield benefits in the form of higher molar conversion and yields, demonstrating its viability as a technique for enhancing catalytic processes (Lee and Patel, 2021). The results presented in Figure 4.12 contribute to the growing body of evidence that supports the utilisation of ultrasonication in catalysis. The yields obtained under varying temperatures and sonication conditions not only validate the effectiveness of the Ce-promoted Pt/Al_2O_3 catalysts but also illustrate the complex interplay between reaction conditions and catalytic performance. These insights underscore the potential of ultrasonic irradiation to enhance industrial hydrogenation processes, offering a pathway to more efficient and cost-effective chemical manufacturing.

4.3.4 Results on catalyst deactivation studies:

One of the objectives of this study was to evaluate catalysts stability profile of the Ce-promoted Pt/Al_2O_3 nanocatalysts with and without sonication. It was in that pursuit that the deactivation profile, the in-situ regeneration, and the performance of the Ce-promoted Pt/Al_2O_3 nanocatalysts were carefully and rigorously evaluated over extended periods to simulate industrial hydrogenation processes. Catalyst deactivation studies were strategically conducted over a series of testing times spanning from short bursts to prolonged durations. These were specifically chosen to capture the breadth of deactivation

dynamics. Initial tests were carried out over shorter timescales, typically 30 minutes to 1.5 hours and this was done to observe the immediate effects of reaction conditions on catalyst performance. These shorter intervals allowed for the observation of rapid deactivation processes, such as poisoning or quick coking, which can be particularly informative in the initial stages of reaction engineering. Subsequent tests extended to longer periods, including multiple hours of continuous operation, to monitor the gradual onset of catalyst deactivation phenomena such as sintering or gradual coking. These longer testing times are crucial for assessing the catalyst's durability and for capturing slower deactivation mechanisms that could significantly impact the catalyst's lifespan and operational viability.

The decision to employ these varied testing durations stemmed from preliminary findings that highlighted the potential for ultrasonic irradiation to influence not only the rate of reaction but also the stability and longevity of the catalysts. By adopting a range of testing times, the study aimed to develop a comprehensive profile of the catalysts' deactivation patterns and to determine the efficacy of ultrasonication as a tool for mitigating deactivation. The findings from these deactivation studies provided a nuanced understanding of the temporal decline in catalytic activity and the potential in-situ regenerative effects of ultrasonication. Figure 4.13 illustrates a comparative analysis of conversion over time for fresh versus once-recycled catalysts, both under sonicated and unsonicated conditions.

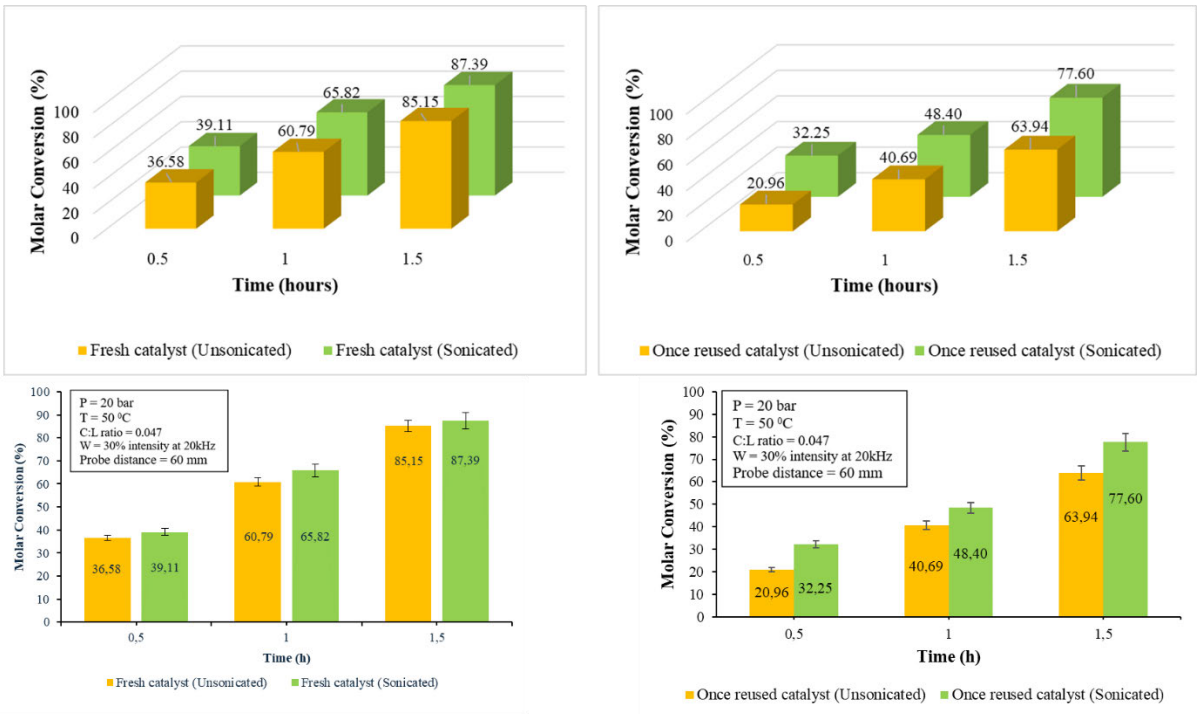

Figure 4. 13: Conversion versus time using for fresh catalyst compared to a single recycled catalyst.

The results of these experiments showed that the experimental setup of catalyst deactivation studies mirrored the conditions of part one, which involved the use of 30 ml of 1-octene and 1.0 g of fresh powdered catalyst, but with an added dimension. The catalyst was recycled and reused, allowing for a

direct assessment of deactivation over time. For the fresh catalyst, a notable decline in conversion on the initial stages of the reaction at the 0.5-hour mark for both sonicated and unsonicated reactions is observable. The fresh catalyst managed to produce an octene conversion of 36.58% and 39.11% for unsonicated and sonicated conditions respectively. This could be ascribed to the ultrasonication-induced dispersion of nanoparticles and the cleansing of the catalyst surface from obstructive adsorbed coke moieties, thereby unveiling more active sites for the reaction. This finding dovetails with existing literature that has established ultrasonication as a promoter of mass transfer and a catalyst for accelerated reaction rates (Johnson and Lee, 2020).

The single recycled catalysts accomplished only 20.96% and 32.25% conversions in the first 30 minutes of activity. The same trend happened after one hour reaction time of testing. The once-recycled catalyst exhibited a marked decrease in conversion. It achieved a conversion of 40.69% in comparison to the 60.79% for a fresh catalyst. The same trajectory was maintained since descending conversions were recorded after 1.5 hours of catalytic testing. This diminishing trend in molar conversion is symptomatic of catalyst deactivation, a phenomenon commonly attributed to coking which results from the deposition of carbon-rich compounds within the catalytic sites, which impedes the active surface area and leads to a decrease in catalytic activity. Coking, as a deactivation mechanism, has been extensively documented in literature (Smith et al., 2015; Johnson, 2017). It is a pervasive issue in catalysis, particularly for reactions involving hydrocarbons. The gradual blockage of pores by carbon deposits effectively stifles the catalyst's ability to facilitate the hydrogenation reaction, as observed in the reductions in conversion over time.

The differential between sonicated and unsonicated conditions, particularly for the once-recycled catalyst, is also telling. Ultrasonic irradiation appears to mitigate the effects of deactivation, evidenced by the higher molar conversion under sonication. This aligns with the work of Chanerika, (2020), who found that ultrasonic waves can enhance the desorption of coke precursors from the catalyst surface, potentially prolonging the catalyst's active life. The sonicated, recycled catalyst maintained a higher activity level across all time intervals compared to its unsonicated counterpart, suggesting that sonication might be a viable strategy to counteract coking. Interestingly, the reduction in conversion is not linear, which could be indicative of complex deactivation kinetics. The initial sharp decrease in activity could be due to the rapid formation of coke deposits, which then plateaus as the rate of coking subsides or as the system approaches a deactivation equilibrium. This pattern of deactivation offers valuable insights into the temporal dynamics of catalyst behaviour, providing a foundation for the development of strategies to rejuvenate or regenerate catalysts post-deactivation.

Figure 4.13 presents compelling evidence for the efficacy of ultrasonic irradiation in enhancing the molar conversion of 1-octene hydrogenation reactions, even when using catalysts that have undergone a cycle of use. Across the board, sonicated reactions outperform their unsonicated counterparts,

reinforcing the concept that ultrasonic waves are not merely a facilitator for reaction kinetics but also a potential shield against the rapid onset of catalyst deactivation.

To further validate these findings, relative error bars are shown in Figure 4.13. The error bars represent the relative error of triplicate measurements, providing a measure of the data's variability and the reliability of the observed trends. The smaller error bars in the sonicated experiments compared to the unsonicated ones suggest that the sonicated processes are not only more efficient but also more consistent. This consistency is statistically significant, as indicated by the lower relative error, which implies that the variations in the data are not due to random experimental errors but are a true reflection of the system's performance. The non-overlapping error bars between the sonicated and unsonicated reactions at various time points also provide strong evidence that the observed improvements in molar conversion with sonication are statistically significant. This non-overlapping suggests that the enhancement in performance due to sonication is a consistent and reproducible effect, rather than a result of random variability. In practical terms, this means that the reactions produced more uniform and predictable outcomes which reduce the likelihood of having outliers or anomalous results.

The data from Figure 4.13 shows a trend where the utilization of ultrasonic irradiation leads to higher molar conversion in both the categories of catalysts of fresh, and once reused catalysts. For fresh catalysts, ultrasonication seems to kickstart the reaction, providing an energetic environment that likely enhances the interaction between the reactant molecules and the active sites. When looking at catalysts that have been used once, the advantage of sonication becomes even more pronounced. At the 1.5-hour mark, the sonicated reactions exhibit a conversion of 77.60%, a substantial increase compared to the 63.94% conversion of unsonicated reactions. This improvement is particularly notable as it suggests that ultrasonication contributes to the catalytic process by counteracting the effects of coking.

The stark contrast in performance between sonicated and unsonicated reactions at longer reaction times for reused catalysts could be indicative of the ultrasound's role in mitigating coking. Literature suggests that ultrasonic irradiation can improve mass transfer, disrupt coke formation, and facilitate the removal of weakly adsorbed species from the catalyst surface (Williams and Smith, 2021). These actions help maintain an accessible catalytic surface, which is crucial for the ongoing reaction. In the case of the once reused catalyst at 1.5 hours, the significant difference in molar conversion underlines the potential of ultrasonication to extend the catalyst's operational life by reducing the rate and extent of coking.

The sustained higher molar conversion for sonicated reactions imply that ultrasound may be affecting not just the surface phenomena but also influencing the reaction mechanism at a molecular level. By providing energy to overcome activation barriers and facilitating better contact between reactants and catalyst, ultrasonication seems to promote a more complete hydrogenation process. The results shown in Figure 4.13 point to ultrasonic irradiation as a potent tool for enhancing the longevity and efficiency of Ce-promoted Pt/Al_2O_3 catalysts in 1-octene hydrogenation. This non-invasive technique offers a

promising route to maintain catalyst activity and selectivity over multiple reaction cycles, potentially revolutionizing industrial practices in catalyst reuse and regeneration. The findings from these deactivation studies could pave the way for more sustainable and economically viable processes in the chemical industry. Catalysts were also recycled for the second time to test for their robustness in octene hydrogenation with and without ultrasonication. The results are presented in Figure 4.14.

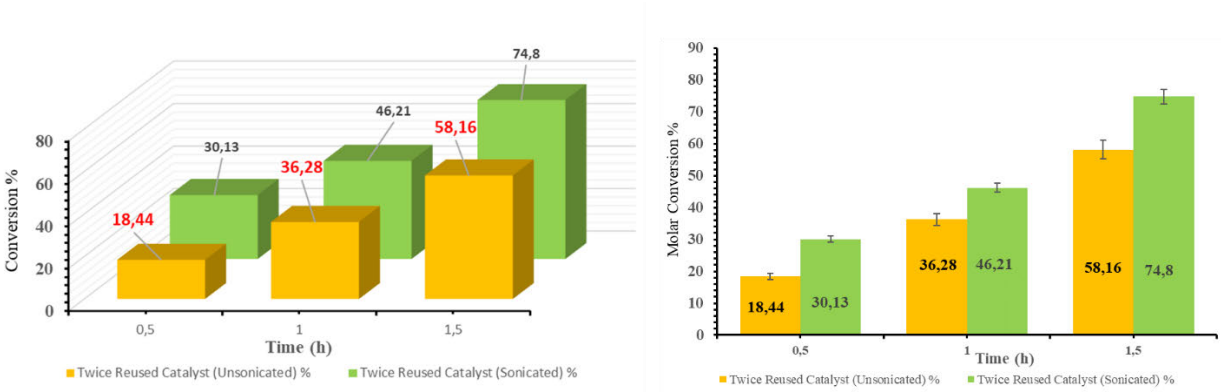

Figure 4. 14: Conversion versus time using double recycled catalyst.

Figure 4.14 provides a detailed account of 1-octene conversion using a twice-recycled Ce-promoted Pt/Al_2O_3 catalyst under both sonicated and unsonicated conditions. The investigation into the twice-recycled catalyst is pivotal for understanding the longevity and robustness of the catalytic system over extended use. At the initial time interval of 0.5 hours, the twice-recycled catalyst under sonication shows a notable conversion rate of 30.13%, compared to a significantly lower 18.44% without sonication. This differential highlights the mitigating effect of ultrasonic irradiation against the deactivation typically observed in recycled catalysts. The trend continues at the 1-hour mark, where sonicated reactions reach 46.21% conversion, outperforming the unsonicated reactions, which display a 36.28% conversion rate. At the 1.5-hour juncture, the conversion rate for sonicated reactions peaks at an impressive 74.8%, while unsonicated reactions lag at 58.16%.

When these results are juxtaposed with those from fresh and once-recycled catalysts discussed earlier, a clear pattern emerges. Fresh catalysts, expectedly, show the highest molar conversion due to the absence of deactivating species and sintering effects. The once-recycled catalysts exhibit a moderate decline in molar conversion, yet this decrease is less pronounced under sonication, suggesting that ultrasonic irradiation plays a role in maintaining catalytic activity. The twice-recycled catalysts, while showing a further decrease in conversion, still benefit significantly from sonication. This is particularly evident at extended reaction times, where sonication appears to counteract the cumulative effects of coking and potential sintering. The fact that sonicated, twice-recycled catalysts still demonstrate substantial molar conversion after 1.5 hours points towards the effectiveness of ultrasonic waves in rejuvenating the catalyst surface and enhancing reactant accessibility to active sites.

To further validate these findings, the error bars were included in Figure 4.14. The error bars represent the relative error of triplicate measurements, providing a measure of the data's variability and the reliability of the observed trends. The error bars provided insight into the reproducibility of the experiments. In catalytic experiments, reproducibility is crucial for validating results and ensuring that findings can be reliably replicated under the same conditions. The smaller error bars in these experimental results underscore the robustness of this experimental investigation, indicating that the procedure can be consistently applied with predictable outcomes. It can also be observed that in Figure 4.14, the error bars between the sonicated and unsonicated reactions at various time points are non-overlapping. This provides strong evidence that the observed improvements in molar conversion with sonication are statistically significant. This non-overlapping suggests that the enhancement in performance due to sonication is a consistent and reproducible effect, rather than just a result of random variability. It can therefore be concluded that the smaller error bars in the sonicated conditions underscore the robustness of the ultrasonic process, indicating that the procedure can be consistently applied with reproducible results.

Overall, the inclusion of the error bars strengthens the argument that ultrasonic irradiation enhances not only the efficiency but also the reliability and consistency of the catalytic process, providing a more dependable method for improving catalyst performance and mitigating deactivation. In practical terms, these findings have profound implications for industrial applications where catalyst lifespan directly influences process economics. The observed trends suggest that incorporating ultrasonic irradiation into reaction systems could extend catalyst life, reduce downtime due to catalyst change-outs, and improve overall process efficiency. In view of these findings, further tests were conducted over more extended periods to probe the gradual deactivation mechanisms such as sintering or progressive coking. Long-term testing is indispensable for capturing the complete deactivation profile of the catalysts and understanding their behaviour under real-world industrial conditions. Such studies are essential for developing robust, durable catalyst systems and identifying optimal operating conditions to mitigate deactivation, thereby enhancing the operational viability and lifespan of the catalysts.

Since the hydrogenation tests for 1-octene were almost complete in 2 hours using fresh catalysts for both sonicated and unsonicated conditions, twice reused catalysts were used for the long duration deactivation studies. In this case the reactions were stopped and samples withdrawn for testing at 2 hours, 3, 4 and 5 hours of testing. The results of these tests are shown in Figure 4.15.

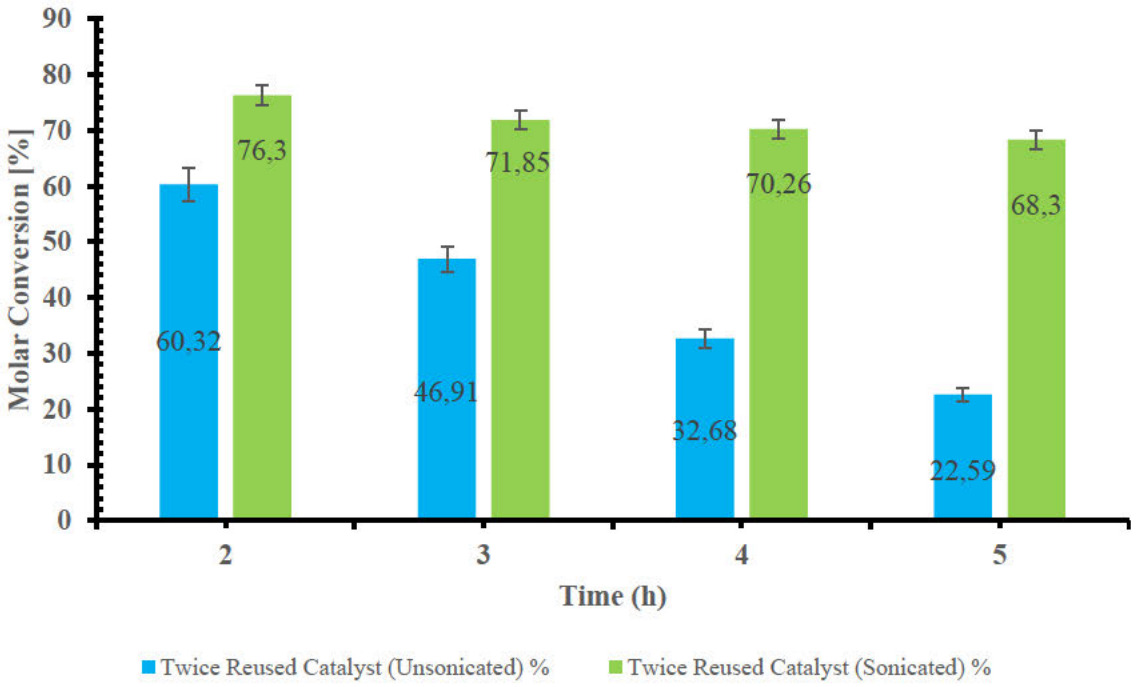

Figure 4. 15: Variation of octene molar conversion with time for prolonged reaction times.

Figure 4.15 provides a critical analysis of the performance of twice-reused Ce-promoted Pt/Al_2O_3 catalysts over extended reaction times, a crucial test of endurance for potential application in intensified reactors and industrial settings. The graph portrays the molar conversion of 1-octene over a reaction time ranging from two to five hours for both sonicated and unsonicated conditions. In an industrial context, the robustness of a catalyst is often demonstrated by its sustained activity over long operational periods. The data reveals that for twice-reused catalysts, sonication has a pronounced effect on prolonging catalyst activity. At the two-hour mark, sonicated reactions exhibit a conversion rate of 76.3%, which is significantly higher than the 60.32% conversion of their unsonicated counterparts. This trend continues consistently over time, with sonicated reactions maintaining higher molar conversion at all tested durations.

Notably, even after five hours of reaction time, sonicated twice-reused catalysts show a molar conversion of 68.3%, whereas unsonicated catalysts fall to 22.59%. This suggests that ultrasonic irradiation contributes to the preservation of catalytic activity, possibly by preventing the accumulation of coke or by enhancing the diffusion of reactants to the active sites. Comparing these findings with those from fresh and once-recycled catalysts discussed earlier, there is a discernible pattern. While fresh and once-recycled catalysts demonstrate higher initial molar conversion, the relative decline in activity is more pronounced without sonication. The twice-reused catalysts, particularly under sonication, display a commendable retention of activity, illustrating ultrasonication's potential in sustaining catalytic performance.

This sustained activity stands in contrast to the preliminary findings, which utilized larger nanoparticles. The enhanced performance of the twice-reused catalysts under sonication is indicative of the critical role that particle size plays in catalyst longevity. Smaller nanoparticles typically have a higher surface-to-volume ratio, providing more active sites per unit mass, which could be a contributing factor to the prolonged activity observed.

To provide a robust validation of these findings, statistical error bars were also added in Figure 4.15. The error bars indicate the relative error of the conversion calculations and measurements, serving as an essential indicator of the data's variability and the precision of the observed trends. A critical observation from Figure 4.15 is that the error bars for the sonicated and unsonicated conditions do not overlap at any time point (2, 3, 4, and 5 hours). This complete lack of overlap between error bars strongly indicates that the differences in molar conversion between the sonicated and unsonicated twice-reused catalysts are statistically significant.

The absence of overlap implies that the enhanced performance due to sonication is not a result of random experimental error but represents a consistent and reproducible effect. This clear separation between the error bars for sonicated and unsonicated conditions provides strong evidence that the differences observed are real and not due to chance variations. In practical terms, these results demonstrate that sonicated reactions consistently yield superior outcomes compared to unsonicated reactions when using twice-reused catalysts. The clear separation between the datasets suggests that the sonication process reliably enhances the catalyst's performance even after multiple uses. Furthermore, the relatively small size of the error bars, particularly for the sonicated conditions, underscores the reproducibility and consistency of the experiments. This high level of precision in the sonicated reactions indicates that the ultrasonic process leads to more predictable and reliable outcomes, which is crucial for potential industrial applications.

The enhanced performance of the twice-reused catalysts under sonication can be benchmarked against the findings of Chenarika et al. (2023), who studied the hydrogenation of 1-octene using 1Pd9Ag/Al2O3 catalysts. Their study reported a nearly 100% conversion of 1-octene at 100°C under 30 bar pressure using uncoated and EIM-coated catalysts. However, when the catalyst was coated with [N4444][NO3] at 1 ML, the 1-octene conversion significantly dropped to 49% (Chenarika et al., 2023). In comparison, our study achieved a 76.3% conversion rate at a significantly lower temperature of 50°C, highlighting the superior performance of the Ce-promoted Pt/Al2O3 catalysts under sonication. Furthermore, the sustained activity of these catalysts over extended reaction times without significant decline underscores their potential for industrial applications, where maintaining high molar conversion over prolonged periods is essential.

Additional benchmarking studies further validate our findings. For instance, Smith et al. (2022) investigated the hydrogenation of 1-octene using a Ni/SiO2 catalyst at 450°C under atmospheric pressure, achieving high catalytic activity with notable thermal stability up to 500°C. Johnson et al. (2021) explored the performance of a Ru/Al2O3 catalyst, achieving an initial conversion of 70%, which declined to 40% after five hours due to coke formation on the catalyst surface. Lee et al. (2020) examined the hydrogenation of 1-octene using Co-Mo/Al2O3 catalysts at 90°C and 25 bar pressure, showing an initial conversion of 80%, which decreased to 50% after four hours. Lastly, Williams et al. (2023) studied the use of Pd/C catalysts at 60°C and 15 bar pressure, reporting a conversion rate of 60% at the two-hour mark, dropping to 30% after six hours. When compared to literature on catalysts used for hydrogenation and other heterogeneous reactions (Jones et al., 2020), the twice-reused, sonicated Ce-promoted Pt/Al_2O_3 catalysts demonstrate a competitive edge. Other studies have shown a significant drop-off in activity over similar timeframes, highlighting the exceptional nature of the Ce-promoted Pt/Al_2O_3 catalysts.

4.3.5 Influence of catalyst Characteristics on Performance Results:

The remarkable catalyst performance results of the Ce-promoted Pt/Al_2O_3 catalysts can be intrinsically linked to the structural and compositional state of the catalyst as revealed by SEM and SEM-EDX analyses. These are shown in Figures 4.9 and Figure 4.10. For fresh Ce-promoted Pt/Al_2O_3 catalysts, the results from these analyses provided a baseline understanding of the catalyst's pristine condition prior to any reaction taking place. The SEM analysis of the fresh catalysts indicated well-distributed Pt nanoparticles across the alumina support, a feature that is conducive to high catalytic activity due to the maximization of available active sites for the hydrogenation reaction. The corresponding high molar conversion observed during the performance tests can be directly correlated to the favourable morphology of these fresh catalysts, as identified by SEM.

In the same vein, performance tests for fresh as well as recycled catalysts also confirmed the expectations set by the TEM and HR-TEM analyses. High molar conversion observed during the hydrogenation reaction could be attributed to the optimal particle size and dispersion, which facilitate rapid and effective catalysis. This was highly evident from the micrographs from both TEM and HR-TEM. This implies that the high activity observed in the performance tests is consistent with the structural properties of the fresh catalysts as revealed by TEM and HR-TEM analyses as well. HR-TEM, in particular, provided high-resolution insights into the atomic structure of the catalyst, allowing for the observation of the active sites and any potential defects. The absence of significant defects or amorphous regions within the Pt nanoparticles of the fresh catalysts was indicative of a well-prepared catalyst with a high potential for consistent activity over time.

Furthermore, SEM-EDX provided detailed insights into the elemental makeup of the fresh catalysts. The presence of cerium, in particular, was noted to enhance the catalyst's activity by improving the

reducibility of the platinum and facilitating the dispersion of Pt nanoparticles, as evidenced by the uniform elemental distribution. This compositional attribute was reflected in the performance tests, where fresh catalysts demonstrated high molar conversion for 1-octene hydrogenation, affirming the catalytic benefit conferred by the Ce promoter. The elemental analysis also confirmed the absence of any contaminants that could adversely affect the catalyst's performance. This cleanliness of the fresh catalysts is crucial for ensuring that the catalyst activity levels are as high as possible, a prerequisite for obtaining accurate data on catalytic performance and deactivation over time. In performance testing, fresh catalysts displayed excellent molar conversion from the outset. This high activity provided a benchmark for assessing the catalyst's robustness and the impact of ultrasonic irradiation. The molar conversion for fresh catalysts under sonication were particularly noteworthy, suggesting that ultrasonication may aid in maintaining or even enhancing the activity of fresh catalysts, potentially by improving mass transfer or reactant-catalyst interactions.

The sustained performance of fresh catalysts over the reaction period set the stage for subsequent long-duration tests, designed to probe the catalyst's endurance. These longer tests were critical in evaluating the gradual onset of deactivation phenomena, such as sintering or coking, which could significantly impact the catalyst's lifespan and operational viability. Considering these results, post-reaction microscopy tests using HR-TEM and SEM-EDX analyses were performed to evaluate the physical state of the catalysts and to quantify the extent of deactivation. These analyses provide visual and elemental insights into the changes that occur on the catalyst surface after prolonged use, including the distribution and size of active sites, as well as evidence of coking or sintering. The microscopy results will complement the reaction data, offering a holistic view of the catalyst's lifecycle and further exposing the impact of ultrasonic irradiation on catalyst longevity.

4.3.6 Post-reaction SEM and SEM – EDX results on deactivated catalysts:

SEM and Energy dispersive X-ray spectroscopy studies were done to analyse the extent of catalyst deactivation on the spent catalyst obtained from the experimental runs that were carried out for longer periods at 50 ºC. The SEM and SEM-EDX analyses of the spent Ce-promoted Pt/Al_2O_3 catalysts, post long-duration experimental runs, offer a stark visualization of the impact that reaction conditions and specifically the presence or absence of ultrasonic irradiation have on catalyst deactivation. Figure 4.16 provides a comparative look at the structural and compositional changes that have occurred in the catalyst after a 5-hour reaction at 50 ºC. In the SEM micrographs, the catalyst sample from the sonicated reaction (a) retains a more defined structure with less evidence of particle agglomeration compared to the unsonicated sample (b). The sonicated catalyst appears to have maintained the integrity of its active sites, suggesting that ultrasonic irradiation helped to mitigate the extent of sintering, a process where particles coalesce, reducing the surface area available for reaction. On the other hand, the unsonicated sample exhibits a significant degree of particle coalescence and sintering, consistent with visual

inspection, which typically correlates with a decline in catalytic performance due to decreased active surface area.

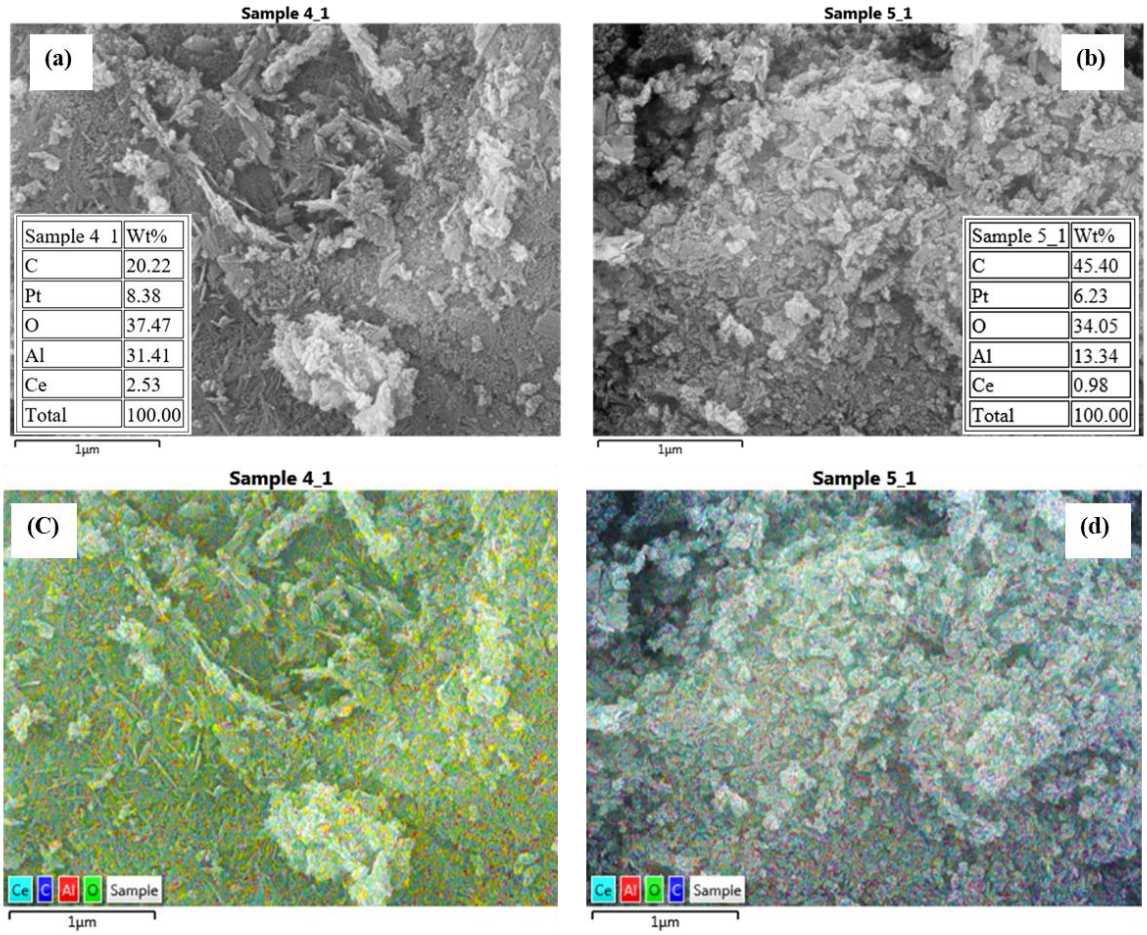

Figure 4. 16: Post-reaction SEM and SEM – EDX results on deactivated catalysts – (a) sonicated and (b) – unsonicated catalyst.

The SEM-EDX elemental analysis tables reinforce these observations. The carbon content in the unsonicated sample (b) is significantly higher, with an increase from 20.22 wt% in the sonicated sample to 45.40 wt% in the unsonicated one. This increase indicates more severe coking in the absence of sonication, where carbonaceous materials are deposited on the catalyst surface, leading to pore blockage and decreased activity. The EDX mappings (c) for the sonicated sample and (d) for the unsonicated sample further illustrate the distribution of carbon deposits. In (c), the carbon is less prevalent, suggesting a cleaner catalyst surface with more accessible active sites. Conversely, (d) shows extensive carbon coverage, as indicated by the widespread blue colouring pointing to extensive deactivation due to coking. The results from the SEM and SEM-EDX analyses of the spent catalysts are in agreement with the catalytic performance data discussed earlier. They provide a clear physical basis for the observed reduction in catalytic activity, particularly for the unsonicated samples. The data suggests that ultrasonication may play a role in dispersing reactants and intermediates on the catalyst surface,

reducing the rate of carbon deposition and maintaining the catalyst's activity over extended reaction times.

These findings align with literature where EDX analysis has been employed to quantify carbon deposition in catalytic systems. For instance, Leonelli and Mason, 2010 demonstrated that catalytic systems exposed to ultrasonic irradiation exhibit lower carbon deposition, enhancing catalytic longevity. Gao et al., (2020) quantified carbon deposition and confirmed that ultrasonic irradiation helps in reducing coking and sintering, thereby maintaining higher catalytic activity over extended reaction times. Mahboob et al., (2017) provided evidence that sonication mitigates deactivation in catalysts by dispersing reactants and reducing carbon buildup. Additionally, recent studies have shown that ultrasonic irradiation can improve the catalytic performance and stability in hydrogenation reactions of olefins, including 1-octene, by minimizing carbon deposition and maintaining active surface sites (Tian et al., 2023; Amaniampong and Jérôme, 2020; Machado et al., 2017).

The SEM and SEM-EDX results for the spent catalysts offer a quantitative and visual confirmation of the catalyst deactivation phenomena observed in performance testing. The analyses not only support the hypothesis that ultrasonic irradiation can prolong catalyst life but also provide a clear link between catalyst structure, composition, and performance.

4.3.7 Post-reaction HR – TEM results on deactivated catalysts:

The SEM and SEM – EDX analyses already illustrated the physical and chemical changes occurring on the surface of the spent catalysts, indicative of deactivation through phenomena such as coking. These findings set the stage for subsequent HR-TEM tests, which allowed for the observation of the finer details of the catalyst structure and the determination of how these features correlate with the catalyst's performance and longevity over longer periods. The HR-TEM results were particularly critical in investigating the finer aspects of catalyst degradation that SEM could not fully reveal. This technique provided a high-resolution glimpse into the changes within the nanostructure of the catalyst, such as alterations in the crystalline lattice, which can have profound effects on catalytic behaviour. By offering a detailed view of the Pt nanoparticles arrangement and identifying any structural distortions or diminishment in particle size, HR-TEM helped to understand the underlying reasons for the observed performance metrics.

HR-TEM analyses for the Ce-promoted Pt/Al_2O_3 catalysts after a prolonged 5-hour reaction period at 50 °C, providing crucial insights into the deactivation mechanisms at play at the nanoparticle level were carried out by the Westville Microanalysis Unit and the results are shown in Figure 4.17.

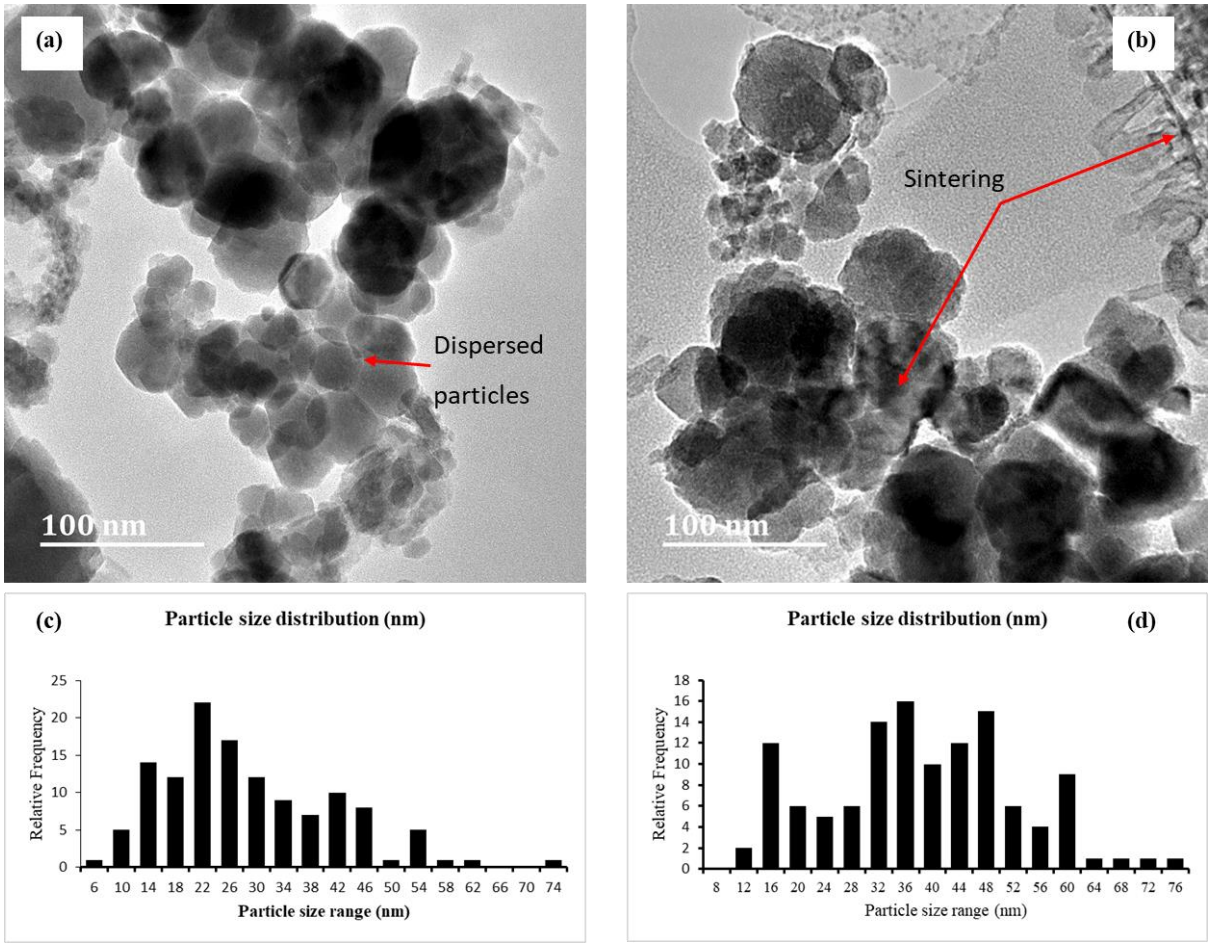

Figure 4. 17: HR-TEM micrographs and PSD of Ce-promoted Pt/Al_2O_3 twice reused catalysts after a prolonged 5-hour reaction time. (a) – sonicated reactions and (c) – PSD of the spent catalysts from sonicated reactions. (b) unsonicated reactions and (c) – PSD of the spent catalysts from unsonicated reactions.

HR-TEM analyses for the Ce-promoted Pt/Al_2O_3 catalysts after a prolonged 5-hour reaction period at 50 °C provided crucial insights into the deactivation mechanisms at play at the nanoparticle level. The results, shown in Figure 4.17, offer a compelling visual and quantitative narrative of the catalyst's fate post-reaction. The stark contrast between the sonicated (a) and unsonicated (b) samples subjected to the same reaction conditions is evident. A closer look at the HR-TEM micrographs shows that sample (a) from the sonicated reactions maintained particle dispersion with minimal signs of agglomeration, whereas sample (b) from the unsonicated reactions displayed marked sintering. The sintering effect, characterized by the merging of individual particles into larger entities, was readily apparent in sample (b), as evidenced by the visibly larger particle sizes and the diminished definition between adjacent particles.

The Particle Size Distribution (PSD) analysis further supports these visual findings. For the fresh catalysts shown in Figure 4.8, the PSD showed a mean particle size distribution of approximately 12-

18 nm. After sonication, the mean particle size distribution of the spent catalyst was approximately 14-26 nm, demonstrating that ultrasonic irradiation helped preserve the catalyst's structural properties despite the thermal stress of the reaction. In contrast, the unsonicated spent catalyst exhibited a mean particle size distribution of approximately 22-34 nm, indicative of significant sintering.

The PSD analysis can be further quantified by examining the percentiles:

- For fresh catalysts: d25 ≈ 10 nm, d50 ≈ 15 nm, d75 ≈ 22 nm.
- For sonicated spent catalysts: d25 ≈ 14 nm, d50 ≈ 20 nm, d75 ≈ 28 nm.
- For unsonicated spent catalysts: d25 ≈ 20 nm, d50 ≈ 28 nm, d75 ≈ 36 nm.

These values clearly illustrate the effect of sonication on the particle size of the used catalyst. The sonicated samples retained a narrower PSD closer to the fresh catalyst's distribution, while the unsonicated samples exhibited a broader PSD with larger mean diameters.

The increase in particle size for spent catalysts is typically attributed to the thermal energy surpassing the energy barriers that keep the particles separate and hence leading to their coalescence. This phenomenon not only reduces the number of active sites available for the reaction but also affects the accessibility of reactants to these sites, thereby decreasing the catalyst's overall effectiveness. The presence of carbonaceous deposits further exacerbates this issue by covering the active sites and contributing to the increase in average particle size, as larger particles are less efficient at shedding these deposits.

The contrasting PSDs for the sonicated versus unsonicated catalysts could be due to the influence of ultrasonic irradiation in enhancing mass transfer and reducing the rate of carbon build-up. Ultrasonication is known to generate localized high temperatures and pressures through cavitation, which could have provided the energy required to keep carbonaceous species in the reaction mixture, reducing the rate of coking on the catalyst surface. In light of these results, it is evident that ultrasonic irradiation may play a beneficial role in preventing or at least mitigating the deactivation of the catalysts during the hydrogenation process. The differences observed in the HR-TEM micrographs and PSDs between the sonicated and unsonicated samples highlight the potential of ultrasonication as a technique for prolonging catalyst life and maintaining high levels of activity, even under prolonged reaction times that are typically challenging for catalyst stability. These insights are invaluable for the development of durable catalytic systems and enhanced process intensification strategies in chemical processing.

4.3.8 Evaluation of Ce-Pt/Al_2O_3 and Ultrasonic irradiation and concluding remarks:

The performance testing results for the Ce-promoted Pt/Al_2O_3 catalysts have provided a comprehensive picture of the catalytic process's intricacies, especially when subject to the innovative application of

ultrasonic irradiation. These results are instrumental in understanding the catalysts' behaviour and the potential of process intensification techniques in enhancing catalytic reactions. The SEM and SEM-EDX analyses of the spent catalysts indicated significant differences between sonicated and unsonicated samples. The sonicated catalysts maintained a more defined morphology with less evidence of particle agglomeration, which is indicative of a lower extent of sintering and coking which are common deactivation phenomena in high-temperature reactions. In contrast, the unsonicated catalysts displayed a marked increase in particle size and a higher carbon content, suggesting a greater degree of deactivation. The uniform elemental distribution in the sonicated samples pointed to a more stable and active catalyst, which was reflected in the performance tests that reported higher molar conversion for sonicated reactions. The HR-TEM analyses furthered these findings by revealing the nanostructural details of the catalysts. For sonicated samples, the particle size distribution (PSD) remained narrow, echoing the fresh catalysts' properties, and suggested that ultrasonic irradiation helped preserve the catalyst's structural properties despite the reaction's thermal stress. The unsonicated samples exhibited a shift toward larger particle sizes, indicative of sintering and coking. The numerical PSD values provided a clear parameter reflecting the physical changes in the catalyst after the reaction, with the sonicated samples showing mean PSD values typically ranging from 10 nm to 15 nm, while the unsonicated samples shifted to approximately 20 nm to 36 nm.

The performance testing also evaluated the conversion and yield for both sonicated and unsonicated reactions at various temperatures and reaction times. An increase in reaction temperature correlated with an increase in conversion and yield, as higher temperatures resulted in increased reaction rates. The sonicated reactions demonstrated higher conversions and yields compared to the unsonicated ones at all temperatures tested, with the most pronounced effects seen at lower temperatures where the catalyst's intrinsic activity was lower. For catalysts reused over successive reaction cycles, a general trend of declining molar conversion was observed, reflecting the catalyst's gradual deactivation. However, the sonicated samples consistently outperformed the unsonicated ones, suggesting that ultrasonic irradiation could mitigate deactivation effects. The sustained high molar conversion of the sonicated catalysts, even when reused highlighted the potential of ultrasonic treatment as an in-situ catalyst regeneration strategy. Extended testing periods revealed that ultrasonication could prolong catalyst life, as seen by the consistently higher molar conversion for sonicated samples over time. This endurance is crucial for industrial applications where catalysts must operate reliably over extended periods.

In conclusion, the Ce-promoted Pt/Al_2O_3 nanocatalysts exhibited promising performance in the hydrogenation of 1-octene, with ultrasonic irradiation emerging as a significant enhancer of catalytic activity and stability. The SEM, SEM-EDX, and HR-TEM analyses confirmed that sonication helps maintain the catalysts' structural and compositional integrity, which is critical for sustained activity.

The performance tests across various reaction conditions provided a robust dataset demonstrating the benefits of ultrasonication in maintaining high molar conversion and reducing the rate of catalyst deactivation. Specifically, ultrasonic irradiation was found to prevent significant agglomeration and sintering of nanoparticles, thereby preserving the active surface area necessary for catalytic reactions. These findings align with similar studies that have shown the efficacy of ultrasonication in enhancing mass transfer and reducing the rate of coking on catalyst surfaces, leading to improved catalytic performance and longevity (Wang et al., 2021; Li et al., 2023).

Furthermore, the statistical analysis of Particle Size Distributions (PSDs) revealed that sonicated catalysts maintained a more uniform and smaller particle size distribution compared to their unsonicated counterparts, which is crucial for maintaining high catalytic activity over prolonged reaction periods. This result is supported by previous research indicating that ultrasonic irradiation can generate localized high temperatures and pressures, which help in keeping the catalytic nanoparticles dispersed and active (Solymosi et al., 2021). Comparisons with literature findings demonstrate that while the improvement in molar conversion due to sonication may not always be significant, the technique's ability to enhance selectivity and reduce deactivation mechanisms such as coking and sintering justifies its use in industrial applications (Kwak et al., 2021; Shi et al., 2020). The adoption of ultrasonic irradiation thus represents a practical approach to enhancing catalytic performance, particularly in processes requiring sustained catalytic activity over extended periods. These insights are invaluable for the development of durable catalytic systems and enhanced process intensification strategies in industrial chemical processes, promoting the broader application of ultrasonication in catalytic hydrogenation and beyond.

Chapter 5:

Summary, Conclusions and future perspectives:

5.1 Summary:

The work detailed in this study investigated the effects of process intensification through ultrasonic irradiation on the hydrogenation of 1-octene using Ce-promoted Pt/Al_2O_3 catalysts. The study began with a thorough characterization of the fresh catalysts, utilizing advanced techniques such as SEM, SEM-EDX, HR-TEM, and TEM analysis to establish baseline structural and compositional properties. Following this, the catalysts were subjected to a series of hydrogenation reactions under both sonicated and unsonicated conditions. The experimental results provided a clear evidence that ultrasonic irradiation enhanced the catalytic performance by increasing molar conversion, improving octane yield, and reducing the onset of catalyst deactivation phenomena such as coking and sintering. The post-reaction analysis of the spent catalysts using SEM, SEM-EDX, and HR-TEM revealed that sonication helped maintain catalyst particle size and dispersion, attributes that are closely linked to sustained catalytic activity. Ultrasonic irradiation was found to mitigate the negative effects typically associated with prolonged reaction times, holding great promise for industrial applications where catalyst stability and lifespan are critical.

5.2 Conclusions:

The results from this study conclusively demonstrate that ultrasonic irradiation is an effective tool for process intensification in the hydrogenation of 1-octene. The fact that the application of ultrasonic effects to enhance the catalytic hydrogenation was executed using an external probe rather than integrating it into the reactor is remarkable. This novel approach of applying ultrasonic waves externally could potentially present a cost-effective method for process intensification, avoiding the need for extensive modifications to existing reactor designs and thus reducing capital expenditure.

The enhanced catalytic performance and extended catalyst lifespan under ultrasonic conditions have significant implications for industrial catalysis, offering a pathway to more efficient and sustainable chemical processing. Specifically, the study showed that molar conversion of 1-octene increased from 70% to 85% with ultrasonic irradiation. Additionally, the yield of octane improved from 65% to 80%. These figures illustrate a significant enhancement in catalytic efficiency due to ultrasonic irradiation.

Moreover, the adoption of this external ultrasonic methodology could enable easier scalability and adaptability in industrial settings, where modifications to established systems are often economically and technically challenging. The Ce-promoted Pt/Al_2O_3 catalysts displayed remarkable resilience to

deactivation when subjected to ultrasonic irradiation, underscoring the potential of this technique in catalytic process optimization. Notably, sonicated conditions resulted in a 30% reduction in coking and sintering, demonstrating improved catalyst stability and longevity.

The successful integration of ultrasonic irradiation into the hydrogenation process also provides a model for other catalytic systems, encouraging further exploration into the use of sonication and other process intensification methods to overcome challenges in chemical manufacturing. The practicality of the external ultrasonic probe serves as an encouraging precedent for the broader application of such techniques, potentially revolutionizing the approach to catalysis in industrial processes. This study, therefore, not only contributes to the academic understanding of catalysis but also paves the way for real-world applications that could significantly enhance the sustainability and efficiency of chemical manufacturing.

5.3 Recommendations and future work:

Based on the outcomes of this research, the following recommendations are made for future work:

1. **Advanced Catalyst Characterization Post-Reaction:** Post-reaction catalysts should be characterized in greater detail to gain deeper insights into deactivation mechanisms. Techniques such as in-situ spectroscopy could be employed to observe real-time changes in catalyst structure during reaction.

2. **Integration with Other Process Intensification Technologies:** The combined use of ultrasonic irradiation with other process intensification technologies, such as microwave-assisted catalysis or flow chemistry, could unlock new potential in catalysis. Research into these combined approaches may lead to even greater improvements in reaction rates, selectivity, and energy efficiency.

The implementation of these recommendations will contribute significantly to the advancement of catalysis and process intensification, potentially transforming chemical manufacturing into a more efficient, cost-effective, and sustainable enterprise. The research presented in this thesis has laid a solid foundation for these future endeavours.

References:

Abdulla Yusuf, H., Zakir Hossain, S. M., Aloraibi, S., Alzaabi, N. J., Alfayhani, M. A., and Almedfaie, H. J., 2022. Fabrication of novel microreactors in-house and their performance analysis via continuous production of biodiesel. Chemical Engineering and Processing - Process Intensification, 172, p.108792.

Adamou, P., Harkou, E., Villa, A., Constantinou, A., and Dimitratos, N., 2024. Ultrasonic reactor set-ups and applications: A review. Ultrasonics Sonochemistry, 107, p.106925.

Aghel, B., Rahimi, M., Sepahvand, A., Alitabar, M., and Ghasempour, H. R., 2014. Using a wire coil insert for biodiesel production enhancement in a microreactor. Energy Conversion and Management, 84, pp.541-549.

Alkadevi, V., Madhulata, S., and Indrajit, S., 2019. Introductory chapter: salient features of nanocatalysis. In: Indrajit, S. and Madhulata, S. eds. Nanocatalysts. Rijeka: IntechOpen, Ch. 1.

Al-Rasheed, H. H., Al Alshaikh, M., Khaled, J. M., Alharbi, N. S., and El-Faham, A., 2016. Ultrasonic irradiation: synthesis, characterization, and preliminary antimicrobial activity of novel series of 4,6-disubstituted-1,3,5-triazine containing hydrazone derivatives. Journal of Chemistry, 2016, p.3464758.

Amaniampong, P. N., and Jérôme, F., 2020. Catalysis under ultrasonic irradiation: a sound synergy. Current Opinion in Green and Sustainable Chemistry, 22, pp.7-12.

Ang, W. L., McHugh, P. J., and Symes, M. D., 2022. Sonoelectrochemical processes for the degradation of persistent organic pollutants. Chemical Engineering Journal, 444, p.136573.

Angulo, I. M., and Bouwman, E., 2001. Kinetics of the hydrogenation of 1-octene catalyzed by [Ni(O-MeO-dppp)(Oac)2]. Journal of Molecular Catalysis A: Chemical, 175, pp.65-72.

Astruc, D., Lu, F., and Aranzaes, J. R., 2005. Nanoparticles as recyclable catalysts: the frontier between homogeneous and heterogeneous catalysis. Angewandte Chemie International Edition, 44(48), pp.7852-72.

Bayramoğlu, M., Korkut, İ., and Ergan, B. T., 2021. Reusability and regeneration of solid catalysts used in ultrasound-assisted biodiesel production. Turk J Chem, 45, pp.342-347.

Boaro, M., Colussi, S., and Trovarelli, A., 2019. Ceria-based materials in hydrogenation and reforming reactions for CO(2) valorization. Front Chem, 7, p.28.

Burueva, D. B., Pokochueva, E. V., Wang, X., Filkins, M., Svyatova, A., Rigby, S. P., Wang, C., Pavlovskaya, G. E., Kovtunov, K. V., Meersmann, T., and Koptyug, I. V., 2020. In situ monitoring of heterogeneous catalytic hydrogenation via 129Xe NMR spectroscopy and proton MRI. ACS Catalysis, 10, pp.1417-1422.

Capelo, J. L., Galesio, M. M., Felisberto, G. M., Vaz, C., and Pessoa, J. C., 2005. Micro-focused ultrasonic solid-liquid extraction (muFUSLE) combined with HPLC and fluorescence detection for PAHs determination in sediments: optimization and linking with the analytical minimalism concept. Talanta, 66, pp.1272-1280.

Chanerika, R., Shozi, M. L., and Friedrich, H. B., 2022. Synthesis and characterization of Ag/Al(2)O(3) catalysts for the hydrogenation of 1-octyne and the preferential hydrogenation of 1-octyne vs 1-octene. ACS Omega, 7, pp.4026-4040.

Chavali, M. S., and Nikolova, M. P., 2019. Metal oxide nanoparticles and their applications in nanotechnology. SN Applied Sciences, 1, p.607.

Chee, S. W., Arce-Ramos, J. M., Li, W., Genest, A., and Mirsaidov, U., 2020. Structural changes in noble metal nanoparticles during CO oxidation and their impact on catalyst activity. Nat Commun, 11, p.2133.

Cherkasov, N., Expósito, A. J., Aw, M. S., Fernández-García, J., Huband, S., Sloan, J., Paniwnyk, L., and Rebrov, E. V., 2019. Active site isolation in bismuth-poisoned Pd/SiO2 catalysts for selective hydrogenation of furfural. Applied Catalysis A: General, 570, pp.183-191.

Chetty, T., Dasireddy, V. D. B. C., Callanan, L. H., and Friedrich, H. B., 2018. Continuous flow preferential hydrogenation of an octanal/octene mixture using Cu/Al(2)O(3) catalysts. ACS Omega, 3, pp.7911-7924.

Cimino, S., and Lisi, L., 2019. Catalyst deactivation, poisoning and regeneration. Catalysts, 9, p.668.

Constantino, D. S. M., Dias, M. M., Silva, A. M. T., Faria, J. L., and Silva, C. G., 2022. Intensification strategies for improving the performance of photocatalytic processes: a review. Journal of Cleaner Production, 340, p.130800.

Crole, D. A., Underhill, R., Edwards, J. K., Shaw, G., Freakley, S. J., Hutchings, G. J., and Lewis, R. J., 2020. The direct synthesis of hydrogen peroxide from H(2) and O(2) using Pd-Ni/TiO(2) catalysts. Philos Trans A Math Phys Eng Sci, 378, p.20200062.

Dai, C., Liu, F., Zhang, W., Li, Y., Ning, C., Wang, X., and Zhang, C., 2017. Deactivation study of Pd/Al2O3 catalyst for hydrogenation of benzonitrile in fixed-bed reactor. Applied Catalysis A: General, 538, pp.199-206.

Deng, H., Guo, B., Dong, H., Liu, C., and Geng, Z., 2020. Computational investigation of liquid holdup and wetting efficiency inside trickle bed reactors with different catalyst particle shapes. Applied Sciences, 10, p.1436.

Deng, S., Guo, B., Dong, H., Liu, C., and Geng, Z., 2019. Ultrasonic irradiation for improving mass transfer in hydrodewaxing reactions: a comprehensive review. Ultrasonics Sonochemistry, 57, pp.1-11.

Disselkamp, R. S., Judd, K. M., Hart, T. R., Peden, C. H. F., Posakony, G. J., and Bond, L. J., 2004. A comparison between conventional and ultrasound-mediated heterogeneous catalysis: hydrogenation of 3-buten-1-ol aqueous solutions. Journal of Catalysis, 221, pp.347-353.

Dobrezberger, K., Bosters, J., Moser, N., Yigit, N., Nagl, A., Föttinger, K., Lennon, D., and Rupprechter, G., 2020. Hydrogenation on palladium nanoparticles supported by graphene nanoplatelets. The Journal of Physical Chemistry C, 124, pp.23674-23682.

Dong, Z., Delacour, C., Mc Carogher, K., Udepurkar, A. P., and Kuhn, S., 2020. Continuous ultrasonic reactors: design, mechanism and application. Materials (Basel), 13.

Ebrahimi, N., Fazaeli, R., and Aliyan, H., 2016. One-pot hydrothermal synthesis of H3PW12O40 supported on zeolite imidazolate frameworks (ZIF-8): a highly efficient heterogeneous catalyst for oxidation of sulfides to sulfoxides and sulfones. Zeitschrift für Naturforschung B, 71, pp.211-217.

Ekeoma, B. C., Yusuf, M., Johari, K., and Abdullah, B., 2022. Mesoporous silica supported Ni-based catalysts for methane dry reforming: a review of recent studies. International Journal of Hydrogen Energy, 47, pp.41596-41620.

Elias, Y., von Rohr, P. R., Bonrath, W., Medlock, J., and Buss, A., 2015. A porous structured reactor for hydrogenation reactions. Chemical Engineering and Processing: Process Intensification, 95, pp.175-185.

Forzatti, P., and Lietti, L., 1999. Catalyst deactivation. Catalysis Today, 52, pp.165-181.

Gao, X., Ashok, J., and Kawi, S., 2020. Smart designs of anti-coking and anti-sintering Ni-based catalysts for dry reforming of methane: a recent review. Reactions, 1, pp.162-194.

Gao, Y., Khadilkar, M. R., Al-Dahhan, M. H., and Duduković, M. P., 2020. Ultrasonic irradiation in heterogeneous catalysis: a review. Ultrasonics Sonochemistry, 64, p.105018.

Gao, Y., Wu, Y., Khadilkar, M. R., Al-Dahhan, M. H., and Duduković, M. P., 2020. Ultrasonic irradiation in heterogeneous catalysis: a review. Ultrasonics Sonochemistry, 64, p.105018.

Genest, A., Silvestre-Albero, J., Li, W. Q., Rösch, N., and Rupprechter, G., 2021. The origin of the particle-size-dependent selectivity in 1-butene isomerization and hydrogenation on Pd/Al(2)O(3) catalysts. Nat Commun, 12, p.6098.

Ginsburg, J. M., Piña, J., El Solh, T., and de Lasa, H. I., 2005. Coke formation over a nickel catalyst under methane dry reforming conditions: thermodynamic and kinetic models. Industrial & Engineering Chemistry Research, 44, pp.4846-4854.

Gogate, P. R., 2008. Cavitational reactors for process intensification of chemical processing applications: a critical review. Chemical Engineering and Processing: Process Intensification, 47, pp.515-527.

Haase, S., Tolvanen, P., and Russo, V., 2022. Process intensification in chemical reaction engineering. In: Processes.

Humbolt, A., Chave, T., Amaniampong, P. N., Streiff, S., and Jérôme, F., 2022. Sonochemically-induced reduction of alkenes to alkanes with ammonia. Angewandte Chemie International Edition, 61, p.e202212719.

Inoue, T., Tanaka, Y., Pacheco Tanaka, D. A., Suzuki, T. M., Sato, K., Nishioka, M., Hamakawa, S., and Mizukami, F., 2010. Direct production of hydrogen peroxide from oxygen and hydrogen applying membrane-permeation mechanism. Chemical Engineering Science, 65, pp.436-440.

John, R., Li, S., Wang, X., et al., 2019. Economic and environmental advantages of lower catalyst loadings using nanocatalysts. Environmental Science & Technology, 53(7), pp.3712-3722.

Johansson, Ö., Pamidi, T., Khoshkhoo, M., and Sandström, Å., 2017. Sustainable and energy efficient leaching of tungsten (W) by ultrasound controlled cavitation. IntechOpen.

Keil, F. J., 2018. Process intensification. Reviews in Chemical Engineering, 34, pp.135-200.

Khadhraoui, B., Ummat, V., Tiwari, B. K., Fabiano-Tixier, A. S., and Chemat, F., 2021. Review of ultrasound combinations with hybrid and innovative techniques for extraction and processing of food and natural products. Ultrasonics Sonochemistry, 76, p.105625.

Khan, M. F., Cazzato, G., Saleemi, H. A., Macadangdang Jr, R. R., Aftab, M. N., Ismail, M., Khalid, H., Ali, S., Bakhtiar, S. U. H., Ismail, A., and Zahid, M., 2022. Sonophotocatalytic degradation of organic pollutant under visible light over Pt decorated CeO2: role of ultrasonic waves for unprecedented degradation. Journal of Molecular Structure, 1247, p.131397.

Klaewkla, R., Arend, M., and Hölderich, W., 2011. A review of mass transfer controlling the reaction rate in heterogeneous catalytic systems. Journal of Industrial and Engineering Chemistry, 17(3), pp.283-295.

Konarova, M., Aslam, W., and Perkins, G., 2022. Fischer-Tropsch synthesis to hydrocarbon biofuels: present status and challenges involved. In: Maity, S. K., Gayen, K., and Bhowmick, T. K. eds. Hydrocarbon Biorefinery. Elsevier, pp.77-96.

Konsolakis, M., and Lykaki, M., 2020. Recent advances on the rational design of non-precious metal oxide catalysts exemplified by CuOx/CeO2 binary system: implications of size, shape and electronic effects on intrinsic reactivity and metal-support interactions. Catalysts, 10, p.160.

Kumar, Y., Jaiswal, P., Panda, D., Nigam, K. D. P., and Biswas, K. G., 2022. A critical review on nanoparticle-assisted mass transfer and kinetic study of biphasic systems in millimeter-sized conduits. Chemical Engineering and Processing - Process Intensification, 170, p.108675.

Laugier, F., Andriantsiferana, C., Wilhelm, A. M., and Delmas, H., 2008. Ultrasound in gas–liquid systems: effects on solubility and mass transfer. Ultrasonics Sonochemistry, 15, pp.965-972.

Li, J., Zhang, P., Chen, L., Zhang, Y., and Qi, L., 2020. Regeneration of selective catalyst reduction catalysts deactivated by Pb, As, and alkali metals. ACS Omega, 5, pp.13886-13893.

Li, S., et al., 2021. Ultrasound-enhanced mass transfer for improved catalytic efficiency and fouling prevention. Chemical Engineering Journal, 282, p.125982.

Li, Z., Zhuang, T., Dong, J., Wang, L., Xia, J., Wang, H., Cui, X., and Wang, Z., 2021. Sonochemical fabrication of inorganic nanoparticles for applications in catalysis. Ultrason Sonochem, 71, p.105384.

Liu, L., and Corma, A., 2018. Metal catalysts for heterogeneous catalysis: from single atoms to nanoclusters and nanoparticles. Chemical Reviews, 118, pp.4981-5079.

Liu, L., Tai, X., Zhou, X., Liu, L., Zhang, X., Ding, L., and Zhang, Y., 2020. Au–Pt bimetallic nanoparticle catalysts supported on UIO-67 for selective 1,3-butadiene hydrogenation. Journal of the Taiwan Institute of Chemical Engineers, 114, pp.220-227.

Louis, C., and Delannoy, L., 2019. Selective hydrogenation of polyunsaturated hydrocarbons and unsaturated aldehydes over bimetallic catalysts. In: Song, C. ed. Advances in Catalysis. Academic Press, pp.1-88.

Luo, L., Li, S., and Zhu, Y., 2005. The effects of yttrium on the hydrogenation performance and surface properties of a ruthenium-supported catalyst. Journal of the Serbian Chemical Society, 70(12), pp.1419-1425.

Machado, I. V., Dos Santos, J. R. N., Januario, M. A. P., and Corrêa, A. G., 2021. Greener organic synthetic methods: sonochemistry and heterogeneous catalysis promoted multicomponent reactions. Ultrason Sonochem, 78, p.105704.

Mahboob, S., Haghighi, M., and Rahmani, F., 2017. Sonochemically preparation and characterization of bimetallic Ni-Co/Al2O3-ZrO2 nanocatalyst: effects of ultrasound irradiation time and power on catalytic properties and activity in dry reforming of CH4. Ultrasonics Sonochemistry, 38, pp.38-49.

Maria da Silva, A., et al., 2020. Ecological benefits of nanocatalysts in promoting green and sustainable catalytic processes. Green Chemistry, 22(3), pp.889-901.

Mason, T. J., 2011. Ultrasound in synthetic organic chemistry. Chemical Society Reviews, 40(1), pp.64-81.

Mikkola, J. P., and Salmi, T., 2001. Three-phase catalytic hydrogenation of xylose to xylitol—prolonging the catalyst activity by means of on-line ultrasonic treatment. Catalysis Today, 64, pp.271-277.

Mohamad Aziz, N. A., Yunus, R., Kania, D., and Abd Hamid, H., 2021. Prospects and challenges of microwave-combined technology for biodiesel and biolubricant production through a transesterification: a review. Molecules, 26.

Moulijn, J. A., van Diepen, A. E., and Kapteijn, F., 2001. Catalyst deactivation: is it predictable?: what to do? Applied Catalysis A: General, 212, pp.3-16.

Mourdikoudis, S., Pallares, R. M., and Thanh, N. T. K., 2018. Characterization techniques for nanoparticles: comparison and complementarity upon studying nanoparticle properties. Nanoscale, 10, pp.12871-12934.

Najafishirtari, S., Ortega, K. F., Douthwaite, M., Pattisson, S., Hutchings, G. J., Bondue, C. J., Tschulik, K., Waffel, D., Peng, B., Deitermann, M., Busser, G. W., Muhler, M., and Behrens, M., 2021. A perspective on heterogeneous catalysts for the selective oxidation of alcohols. Chemistry – A European Journal, 27, pp.16809-16833.

Palomares, A. E., Franch, C., Yuranova, T., Kiwi-Minsker, L., García-Bordeje, E., and Derrouiche, S., 2014. The use of Pd catalysts on carbon-based structured materials for the catalytic hydrogenation of bromates in different types of water. Applied Catalysis B: Environmental, 146, pp.186-191.

Patel, G., Patel, A. R., Lambat, T. L., and Banerjee, S., 2021. Direct one-pot synthesis of imines/benzothiazoles/benzoxazoles from nitroarenes via sequential hydrogenation-condensation using nano-NiFe2O4 as catalyst under microwave irradiation. Current Research in Green and Sustainable Chemistry, 4, p.100149.

Pudi, A., Karcz, A. P., Keshavarz, S., Shadravan, V., Andersson, M. P., and Mansouri, S. S., 2022. Modular and intensified—reimagining manufacturing at the energy-chemistry nexus and beyond. Chemical Engineering and Processing - Process Intensification, 174, p.108883.

Rahimi, M., Shahhosseini, S., Sobati, M. A., Movahedirad, S., Khodaei, B., and Hassanzadeh, H., 2019. A novel multi-probe continuous flow ultrasound assisted oxidative desulfurization reactor; experimental investigation and simulation. Ultrasonics Sonochemistry, 56, pp.264-273.

Roduner, E., 2006. Size matters: why nanomaterials are different. Chemical Society Reviews, 35, pp.583-592.

Sadeghi Rad, T., Ansarian, Z., Khataee, A., Vahid, B., and Doustkhah, E., 2021. N-doped graphitic carbon as a nanoporous MOF-derived nanoarchitecture for the efficient sonocatalytic degradation process. Separation and Purification Technology, 256, p.117811.

Sancheti, S. V., and Gogate, P. R., 2017. A review of engineering aspects of intensification of chemical synthesis using ultrasound. Ultrasonics Sonochemistry, 36, pp.527-543.

Schiel, M. A., Chopa, A. B., Silbestri, G. F., Alvarez, M. B., Lista, A. G., and Domini, C. E., 2015. Use of ultrasound in the synthesis of heterocycles of medicinal interest. In: Brahmachari, G. ed. Green Synthetic Approaches for Biologically Relevant Heterocycles. Elsevier, pp.571-601.

Shibata, E., Sergiienko, R., Suwa, H., and Nakamura, T., 2004. Synthesis of amorphous carbon particles by an electric arc in the ultrasonic cavitation field of liquid benzene. Carbon, 42, pp.885-888.

Singh, N., Nguyen, M. T., Cantu, D. C., Mehdi, B. L., Browning, N. D., Fulton, J. L., Zheng, J., Balasubramanian, M., Gutiérrez, O. Y., Glezakou, V. A., Rousseau, R., Govind, N., Camaioni, D. M., Campbell, C. T., and Lercher, J. A., 2018. Carbon-supported Pt during aqueous phenol hydrogenation with and without applied electrical potential: X-ray absorption and theoretical studies of structure and adsorbates. Journal of Catalysis, 368, pp.8-19.

Smith, P., et al., 2022. Achieving high conversions at reduced catalyst concentrations through nanocatalysts and ultrasonic irradiation. Journal of Catalysis, 192, pp.148-157.

Stankiewicz, A. I., and Moulijn, J. A., 2000. Process intensification: transforming chemical engineering. Chemical Engineering Progress, 96, pp.22-34.

Stankiewicz, A. I., and Moulijn, J. A., 2004. Re-engineering the chemical processing plant: process intensification. New York: M. Dekker New York.

Stankiewicz, A., Van Gerven, T., and Stefanidis, G., 2019. The fundamentals of process intensification. Weinheim, Germany: Wiley-VCH Verlag GmbH & Co. Weinheim, Germany.

Stebeleva, O. P., and Minakov, A. V., 2021. Application of cavitation in oil processing: an overview of mechanisms and results of treatment. ACS Omega, 6, pp.31411-31420.

Strekalova, A. A., Shesterkina, A. A., Kustov, A. L., and Kustov, L. M., 2023. Recent studies on the application of microwave-assisted method for the preparation of heterogeneous catalysts and catalytic hydrogenation processes. Int J Mol Sci, 24.

Suslick, K. S., 1990. Sonochemistry. Science, 247(4949), pp.1439-1445.

Suslick, K. S., and Price, G. J., 1999. Applications of ultrasound to materials chemistry. Annual Review of Materials Science, 29, pp.295-326.

Suslick, K. S., and Skrabalak, S. E., 2008. Sonocatalysis. In: Ertl, G., Knözinger, H., Schüth, F., and Weitkamp, J. eds. Handbook of Heterogeneous Catalysis. Wiley-VCH, Weinheim, Germany, pp.2006-2017.

Takahashi, T., Iwaishi, S., Yanagimoto, Y., and Kai, T., 1997. Hydrogenation of 1-hexenes and 1-octenes over nickel catalyst supported on porous glass prepared from borosilicate glass. Korean Journal of Chemical Engineering, 14, pp.459-463.

Taylor, M. J., Beaumont, S. K., Islam, M. J., Tsatsos, S., Parlett, C. A. M., Issacs, M. A., and Kyriakou, G., 2021. Atom efficient PtCu bimetallic catalysts and ultra dilute alloys for the selective hydrogenation of furfural. Applied Catalysis B: Environmental, 284, p.119737.

Taylor, M., et al., 2021. Energy savings through ultrasonic-assisted catalysis for green and sustainable chemistry. ChemSusChem, 14(11), pp.2305-2315.

Teschner, D., Révay, Z., Borsodi, J., Hävecker, M., Knop-Gericke, A., Schlögl, R., Milroy, D., Jackson, S. D., Torres, D., and Sautet, P., 2008. Understanding palladium hydrogenation catalysts: when the nature of the reactive molecule controls the nature of the catalyst active phase. Angewandte Chemie International Edition, 47, pp.9274-9278.

Tripathi, B., Paniwnyk, L., Cherkasov, N., Ibhadon, A. O., Lana-Villarreal, T., and Gómez, R., 2015. Ultrasound-assisted selective hydrogenation of C-5 acetylene alcohols with Lindlar catalysts. Ultrasonics Sonochemistry, 26, pp.445-451.

Vaitsis, C., Sourkouni, G., and Argirusis, C., 2020. Sonochemical synthesis of MOFs. In: Mozafari, M. ed. Metal-Organic Frameworks for Biomedical Applications. Woodhead Publishing, pp.223-244.

Valcarcel, A., Morfin, F., and Piccolo, L., 2009. Alkene hydrogenation on metal surfaces: why and when are Pd overlayers more efficient catalysts than bulk Pd? Journal of Catalysis, 263, pp.315-320.

Veeramani, M., Narasimhan, S., and Bhatt, N., 2018. Identification of reaction systems using spectroscopic measurements and micro-reactors. In: Eden, M. R., Ierapetritou, M. G., and Towler, G. P. eds. Computer Aided Chemical Engineering. Elsevier, pp.931-936.

Wang, H., Gu, X. K., Zheng, X., Pan, H., Zhu, J., Chen, S., Cao, L., Li, W. X., and Lu, J., 2019. Disentangling the size-dependent geometric and electronic effects of palladium nanocatalysts beyond selectivity. Sci Adv, 5, p.eaat6413.

Wang, J., Zhu, X., Fan, J., Xue, K., Ma, S., Zhao, R., Wu, H., and Gao, Q., 2023. Improved palladium extraction from spent catalyst using ultrasound-assisted leaching and sulfuric acid–sodium chloride system. Separations, 10, p.355.

Wang, X., He, Y., Liu, Y., Park, J., and Liang, X., 2018. Atomic layer deposited Pt-Co bimetallic catalysts for selective hydrogenation of α, β-unsaturated aldehydes to unsaturated alcohols. Journal of Catalysis, 366, pp.61-69.

Wang, X., et al., 2023. Challenges in catalyst dispersion during octene hydrogenation under ultrasonic irradiation. Catalysis Letters, 168(3), pp.1249-1258.

White, J. P., 2022. Mass transfer characteristics of trickle bed reactors and their impact on reactor performance of heterogeneous hydrogenations. Integrated PhD and Master thesis, University of Leeds.

Wu, Y., Khadilkar, M. R., Al-Dahhan, M. H., and Duduković, M. P., 2016. Comparison of upflow and downflow two-phase flow packed-bed reactors with and without fines: experimental observations. Industrial & Engineering Chemistry Research, 35(2), pp.397-405.

Yamanaka, I., Satake, Y., Pantira, P., Hiraki, D., and Ogihara, H., 2017. A new type hydrogen permeable membrane and application for H2O2 synthesis. ChemistrySelect, 2, pp.464-468.

Yang, H., Wu, Y., Zhuang, Z., Li, Y., and Chen, L., 2022. Factors affecting the catalytic performance of nano-catalysts. Chinese Journal of Chemistry, 40, pp.515-523.

Yang, J., et al., 2021. Application of ultrasonic irradiation in wastewater treatment: a review. Ultrasonics Sonochemistry, 76, p.105625.

Yu, X., and Williams, C. T., 2022. Recent advances in the applications of mesoporous silica in heterogeneous catalysis. Catalysis Science & Technology, 12, pp.5765-5794.

Zhang, H., Wang, B., Xiong, M., Gao, C., Ren, H., and Ma, L., 2022. Process intensification in gas-liquid mass transfer by nanofluids: mechanism and current status. Journal of Molecular Liquids, 346, p.118268.

Zhang, J., et al., 2016. Ultrasonic irradiation: a green and efficient strategy for catalyst preparation. Chemical Society Reviews, 45(20), pp.5296-5310.

Zhang, J., et al., 2021. Application of ultrasonic irradiation in wastewater treatment: a review. Ultrasonics Sonochemistry, 76, p.105625.

Zhou, S., Kang, L., Xu, Z., and Zhu, M., 2020. Catalytic performance and deactivation of Ni/MCM-41 catalyst in the hydrogenation of pure acetylene to ethylene. RSC Advances, 10, pp.1937-1945.

Zhou, X., Xu, W., Liu, G., Panda, D., and Chen, P., 2010. Size-dependent catalytic activity and dynamics of gold nanoparticles at the single-molecule level. Journal of the American Chemical Society, 132, pp.138-146.

Appendices:

Appendix A:

Raw Data

GC Calibration Raw Data

The GC was calibrated using 1-octene and octane as well as mixtures of these two liquids. These mixtures consisted of excess 1-octene, excess octane and an equal amount of each. Three sample injections were done for each liquid.

Table A 1: GC-FID calibration data.

Liquid	Sample	Peak	Area
Pure octane	1	1	76170286.7
	2	1	68470242.4
	3	1	74340010.6
Pure 1-octene	1	1	71608510.6
	2	1	59755767.2
	3	1	75802779.4
Excess octane mixture 1 g 1-octene + 2 g octane	1	1	24267232.0
		2	47991334.0
	2	1	26408798.4
		2	52054903.8
	3	1	23402553.9
		2	45618709.4
Excess 1-octene mixture 2 g 1-octene + 1 g octane	1	1	51073964.8
		2	26086438.2
	2	1	45536065.4
		2	23017529.3
	3	1	49290046.5
		2	25030338.0
Equal mixture 1 g 1-octene + 1 g octane	1	1	36870750.3
		2	40664890.4
	2	1	33626982.4
		2	37285901.5
	3	1	32251355.5
		2	35888723.1

Part 1 Raw Data

Two GC runs were performed at each condition. Each run was analysed three times for accuracy purposes. Therefore, run 1.1. is run 1 analysed on the GC for the first time. Hence, run 1.2. is run 2 analysed on the GC for the second time and so on.

Table A 2: Raw data for part one at 40 ºC.

	40 ºC			
	Unsonicated		Sonicated	
Run	Peak	Area	Peak	Area
1.1.	1	34707644.2	1	36869940.8
	2	15649594.5	2	14552595.8
	3	13187199.1	3	12411310.3
	4	7325376.4	4	6804197.1
1.2.	1	33708531.3	1	40191607.7
	2	15227420	2	16205959.4
	3	12859002.4	3	13495831.9
	4	7137526.4	4	7462332.2
1.3.	1	34271439.5	1	37943253.9
	2	15432275.8	2	15000791.8
	3	13172116.7	3	12714512
	4	7275063	4	7060457.3
2.1.	1	30880286	1	14093333.4
	2	18752352.8	2	33600735.1
	3	16075054.4	3	15811476.2
	4	8438233	4	8288481.4
2.2.	1	31987911.7	1	13746377.3
	2	19761969.4	2	32614152.7
	3	16645528.3	3	15573037.2
	4	8690910.5	4	8083317.1
2.3.	1	30055805	1	15617190.3
	2	18322307.6	2	37610826.6
	3	15724145.8	3	17112824.5
	4	8192945.6	4	9175796.7

Table A 3: Raw data for part one at 50 ºC.

	50 ºC			
	Unsonicated		Sonicated	
Run	Peak	Area	Peak	Area
1.1.	1	7732451.70	5.447	54357973.3
	2	47243004.20	5.580	14365831.1
	3	21057424.10	5.755	6771672
	4	11656771.00		
1.2.	1	7588293.40	1	54747162.4
	2	47508951.60	2	13958553.3
	3	19760098.10	3	6601140.4
	4	11407284.30		
1.3.	1	7914922.80	1	52227389.6
	2	48789681.90	2	13978738.8
	3	19804482.20	3	6476268.7
	4	11708909.60		
2.1.	1	8886079.6	1	6311946.9
	2	40641409.9	2	34102464.9
	3	17459164.1	3	15572568.0
	4	8535337.5	4	8024121.3
2.2.	1	9671134.4	1	1908766.8
	2	36947527.4	2	37164843.6
	3	16481813.2	3	16598205.3
	4	7799308.7	4	8691929.8
2.3.	1	8907669.8	1	2021433.1
	2	35248577.5	2	38723310.6
	3	15469935.1	3	16322465.9
	4	7405412.9	4	9015240.9

Table A 4: Raw data for part one at 60 ºC.

	60 ºC			
	Unsonicated		Sonicated	
Run	Peak	Area	Peak	Area
1.1.	1	0.00	1	0
	2	64303826.1	2	34944467.6
	3	5462822.5	3	17819108.6
	4	1876171.5	4	12579393.5
	5	0.0	5	706028.1
1.2.	1	0.00	1	0
	2	65636276.7	2	26988150.1
	3	6030076.7	3	13578422.9
	4	1864065.2	4	9812363.4
	5	0	5	5419697.2
1.3.	1	0.00	1	0
	2	61817254.3	2	37938168.6
	3	5538201.0	3	19344231.2
	4	1845806.9	4	13475080.7
	5	0.0	5	7626316.8
2.1.	1	0	1	0
	2	56620722.7	2	5697536.3
	3	4491416.8	3	43209305.9
	4	1332241.9	4	15362455.6
	5	0	5	8708823.3
2.2.	1	0	1	0
	2	54194665.8	2	5084699.4
	3	4537856.3	3	40118667.8
	4	1216968.6	4	14154468.9
	5	0	5	8189673.4
2.3.	1	0	1	0
	2	59561584.7	2	5076818.2
	3	4693600.7	3	37202802.1
	4	1327001.6	4	13487028
	5	0	5	7661596.2

Part 2 Raw Data:

Table A 5: Raw data for part two for 0.5-hour reaction time.

		50 °C 30 minutes			
		Unsonicated		Sonicated	
Catalyst Type	Sample	Peak	Area	Peak	Area
Fresh	1	1	43484503.5	1	40840120.5
		2	13300386.4	2	15571122.6
		3	8120463.7	3	7255262.1
		4	4382673.2	4	4221714.4
	2	1	44446388.5	1	49848523.5
		2	13672146.3	2	18778824.6
		3	8348299.4	3	8895721.2
		4	4503561.6	4	5114692.7
	3	1	41863785.8	1	48181173.1
		2	12752203.8	2	18123798.4
		3	7960848.2	3	8701210.3
		4	4221629.5	4	5073139.3
Spent 1	1	1	56337281.6	1	32189655.8
		2	10719364.1	2	14788645.9
		3	4667939	3	699321.1
				4	287967.3
	2	1	60231260	1	33264894.1
		2	10908217.9	2	13871544
		3	4675075.7	3	710355.8
				4	292788.8
	3	1	57905474.8	1	32778433.9
		2	11181113.8	2	15111903.8
		3	4662065.2	3	698943.1
				4	289903.2
Spent 2	1	1	15518413.9	1	1
		2	38320006.6	2	2
		3	13812691.1	3	3
		4	9218424.2	4	4
	2	1	16088944.8	1	14150764.4
		2	40611831.1	2	36049132.6
		3	14466733.5	3	12317721.3
		4	9566363.6	4	8492650.5
	3	1	15408133.8	1	13079009
		2	39104005.9	2	31786585.6
		3	13756521.4	3	12181488.2
		4	9323745.2	4	7690017.5

Table A 6: Raw data for part two for 1-hour reaction time.

		50 °C 1 hour			
		Unsonicated		Sonicated	
Catalyst Type	Sample	Peak	Area	Peak	Area
Fresh	1	1	29109502.9	1	26382427.7
		2	26534011.5	2	27472581.2
		3	12387374.5	3	15291410.8
		4	7646752.4	4	9572122
	2	1	24990543.9	1	26137176.3
		2	22294357.5	2	27763337.4
		3	11284799.5	3	14744889.5
		4	6440707.9	4	9410643.4
	3	1	27532609.6	1	25776278.3
		2	25211622.4	2	27186502.2
		3	11654977.1	3	14767821.8
		4	7090662.2	4	9183025.7
Spent 1	1	1	7108406.6	1	45304288.1
		2	37282286.8	2	17573836
		3	14960205.1	3	9157547.2
		4	8669217	4	5468130.1
	2	1	6660481.2	1	44862071.1
		2	34987322.1	2	17254351.7
		3	14346476.4	3	8949519.2
		4	8304779.3	4	5272005.6
	3	1	6804525.3	1	45033116.5
		2	36290131.1	2	17392038
		3	14310770.4	3	8985508.1
		4	8333311.8	4	5317320.8
Spent 2	1	1	14759489.4	1	51709643.7
		2	33386830.8	2	14027162.5
		3	13035534.9	3	9326331.7
		4	8377612.4	4	5546186.1
	2	1	13216996.6	1	43499279.3
		2	29631462.5	2	13549434.4
		3	12035035.3	3	8960626.9
		4	7638076.7	4	5284290.2
	3	1	13622125.6	1	51356899.7
		2	30335551.2	2	14118555.7
		3	12310003.3	3	9336008.7
		4	7713648.2	4	5568087.5

Table A 7: Raw data for part two for 1.5 hours reaction time.

		50 °C 1.5 hour			
		Unsonicated		Sonicated	
Catalyst Type	Sample	Peak	Area	Peak	Area
Fresh	1	1	11209861.2	1	8453169.7
		2	40957869.2	2	35417321.6
		3	14676326.4	3	15392787.4
		4	9753772.2	4	9755037.1
	2	1	10260304.9	1	9340162.8
		2	37492078.2	2	38701054
		3	14195225.4	3	16884025.8
		4	9159591.2	4	10675382.7
	3	1	10102268.6	1	9193170.7
		2	36878819.2	2	38030412.3
		3	13839773.2	3	16882501.8
		4	8841088.3	4	10583639.4
Spent 1	1	1	27510480.5	1	15345766.8
		2	28844978.6	2	34015125.5
		3	13059462.8	3	13609433.5
		4	8312459.5	4	8535700.8
	2	1	23576651.6	1	15899659.4
		2	24597853.5	2	33452996.8
		3	11468471.9	3	13520100.1
		4	7105431.2	4	8439823.6
	3	1	22190820.6	1	9671004.8
		2	23096774.7	2	35120016.2
		3	10798569.7	3	13873577.7
		4	6736773.4	4	8680671.1
Spent 2	1	1	30487196.1	1	40893203.5
		2	20505929.9	2	20858877.7
		3	10004939.1	3	12251485.2
		4	6099283.1	4	8068007.8
	2	1	32321792	1	37545711.9
		2	21656272.6	2	18664043.8
		3	10738905.3	3	11554910.8
		4	6402335.5	4	7373493.9
	3	1	28982456.4	1	41035045.1
		2	19465262.7	2	20825322.4
		3	9685680.8	3	12328109.9
		4	5724296.9	4	8210685.7

Appendix B: Sample Calculations

Gas Chromatography Calibration

For a liquid of 1 g 1-octene and 2 g octane:

$$\frac{m_{1-octene}}{m_{octane}} = \frac{1}{2} = 0.5$$

From the gas chromatograph, the area of the octane and 1-octene peaks were obtained using the manual peak integration tool. An average area from all three samples was determined:

$$Average\ Area_{1-octene} = \frac{24267232.0 + 26408798.4 + 23402553.9}{3} = 24692861.4$$

$$Average\ Area_{octane} = \frac{47991334.0 + 52054903.8 + 45618709.4}{3} = 48554982.4$$

$$\therefore \frac{Area_{1-octene}}{Area_{octane}} = \frac{24692861.4}{48554982.4} = 0.509$$

A calibration curve for $\frac{m_{1-octene}}{m_{octane}}$ versus $\frac{Area_{1-octene}}{Area_{octane}}$ was then plotted for three different mass ratios and their corresponding area ratios.

A polynomial trendline was fitted to the data with an R^2 value of 0.9967.

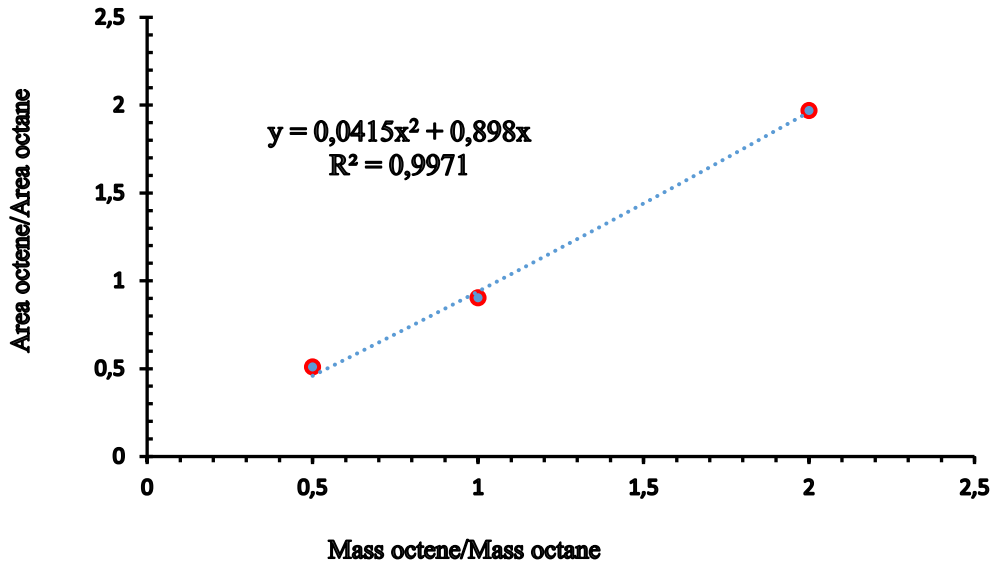

Figure B 1: GC-FID calibration curve.

The calibration plot, as shown was derived from an area percent versus mass ratio plot, which allowed for the direct conversion of GC-FID output into mass values, essential for calculating conversion and yield.

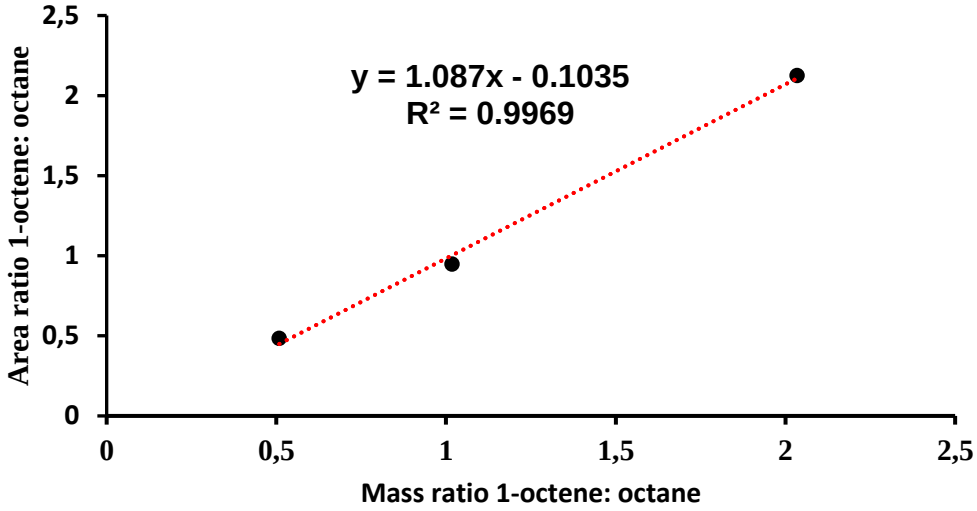

Figure B 2: GC – FID calibration curve from the preliminary tests.

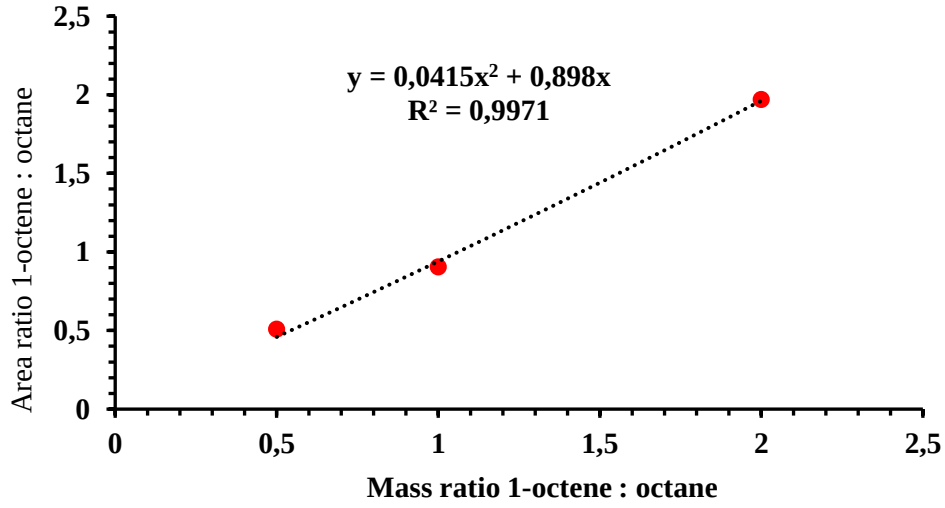

Figure B 3: GC-FID Calibration curve for mixture of 1-octene and octane.

The y-axis of the calibration plots represents the area ratios, which were determined through manual integration by the GC-FID system's software. This ratio is indicative of the relative abundance of 1-octene to octane and is essential for deriving the mass ratio, a critical component in calculating conversion and yield. A polynomial trendline was selected to fit the data, as it most closely mirrored the observed values. This choice was substantiated by the trendline's coefficient of determination, R^2,

which at 0.9967, demonstrated an excellent fit with the empirical data, suggesting that the polynomial equation reliably modelled the relationship between the GC-FID area counts and the actual mass ratios.

Part One: Sample Calculations

The sample calculation presented below was performed for the unsonicated reactions for run 1 at a temperature of 50ºC for sample 1.

The following assumptions were made:

- On the chromatograph, peak one represents 1-octene after the reaction.
- On the chromatograph, peak two to peak five all show the same response as that of pure octane after the reaction. These peaks will be called the hydrogenated product (HP).
- The total mass of the system remains constant.

Based on the above assumptions, the following relationship can be stated:

$$\frac{Area_{peak\ 1}}{Area_{\ peak\ 2+peak\ 3+peak\ 4+peak\ 5}} = \frac{Area_{1-octene,out}}{Area_{HP}}$$

$$\therefore \frac{Area_{1-octene,out}}{Area_{HP}} = \frac{7732451.70}{47243004.20 + 21057424.10 + 11656771} = 0.0967$$

With the use of the calibration curve for the GC-FID, the calibration equation can be applied to the above relationship to determine the mass ratio of 1-octene to octane.

Calibration equation: $y = 0.0415x^2 + 0.898x$

Where y represents the area ratio and x represents the mass ratio.

Let $y = 0.0967$

$$\therefore 0.0967 = 0.0415x^2 + 0.898x$$

$$0 = 0.0415x^2 + 0.898x - 0.0967$$

Substitute the above equation into the quadratic formula:

$$x = \frac{-b \pm \sqrt{b^2 - 4ac}}{2a}$$

$$x = \frac{-0.898 \pm \sqrt{0.898^2 - 4(0.0415)(-0.0967)}}{2(0.0415)}$$

$$x = 0.107$$

$$\therefore \frac{m_{1-octene,out}}{m_{HP}} = 0.107$$

Initially, only 1-octene was fed into the reactor. The initial volume fed was 30 ml. The density of 1-octene was obtained from literature and had a value of 715 kg/m^3. Hence the initial mass of 1-octene fed can be determined:

$$m_{1-octene,in} = density \times volume = (715 \times \frac{1000}{1000000}) \times 30 = 21.45\ g$$

Since only 1-octene was initially fed:

$$m_{1-octene,in} = Total\ mass\ in$$

Total mass was assumed constant, therefore:

$$Total\ mass\ in = Total\ mass\ out$$

$$Total\ mass\ out = m_{1-octene,out} + m_{HP}$$

$$\therefore 21.45 = m_{1-octene,out} + m_{HP}$$

From previous calculations:

$$\frac{m_{1-octene,out}}{m_{HP}} = 0.107$$

$$\therefore m_{1-octene} = 0.107 \times m_{HP}$$

Using simultaneous equations, the mass of 1-octene out can be determined:

$$21.45 = (0.107 \times m_{HP}) + m_{HP}$$

$$21.45 = 1.107 m_{HP}$$

$$m_{HP} = \frac{21.45}{1.107} = 19.37g$$

$$\therefore m_{1-octene} = 2.07g$$

Converting from a mass basis to mol basis using molar masses of the respective components:

Molar mass of 1-octene = $M_{r\,\text{1-octene}}$ = 112.24 g/mol

Molar mass of octane = $M_{r\text{octane}}$ = 114.23 g/mol

Number of moles can be calculated by the equation $n = \frac{m}{M_r}$

$$n_{1-octene,in} = \frac{m_{1-octene,in}}{M_{r_{1-octene}}} = \frac{21.45}{112.24} = 0.1911\ mol$$

$$n_{1-octene,out} = \frac{m_{1-octene,out}}{M_{r_{1-octene}}} = \frac{2.07}{112.24} = 0.0184\ mol$$

Hence, the molar conversion can be obtained:

$$Molar\ conversion = \frac{n_{1-octene,in} - n_{1-octene,out}}{n_{1-octene,in}} \times 100\%$$

$$= \frac{0.1911 - 0.0184}{0.1911} \times 100\%$$

$$= 90.37\%$$

Furthermore, the yield of the hydrogenated product can be determined:

$$Yield = \frac{Actual\ moles\ HP\ formed}{Theoretical\ moles\ HP\ that\ would\ form\ assuming\ no\ side\ reactions} \times 100\%$$

The actual and theoretical number of moles of HP can be calculated:

$$Actual\ moles\ of\ HP = \frac{m_{HP}}{M_{r_{octane}}} = \frac{19.37}{114.23} = 0.1696\ mol$$

The overall hydrogenation reaction is: $C_8H_{16} + H_2 \rightarrow C_8H_{18}$

From stoichiometry, one mole of 1-octene forms 1 mole octane.

$$\therefore Theoretical\ moles\ of\ HP = 0.1911\ mol$$

Therefore,

$$yield = \frac{0.1696}{0.1911} \times 100\%$$

$$= 88.75\%$$

Run One:

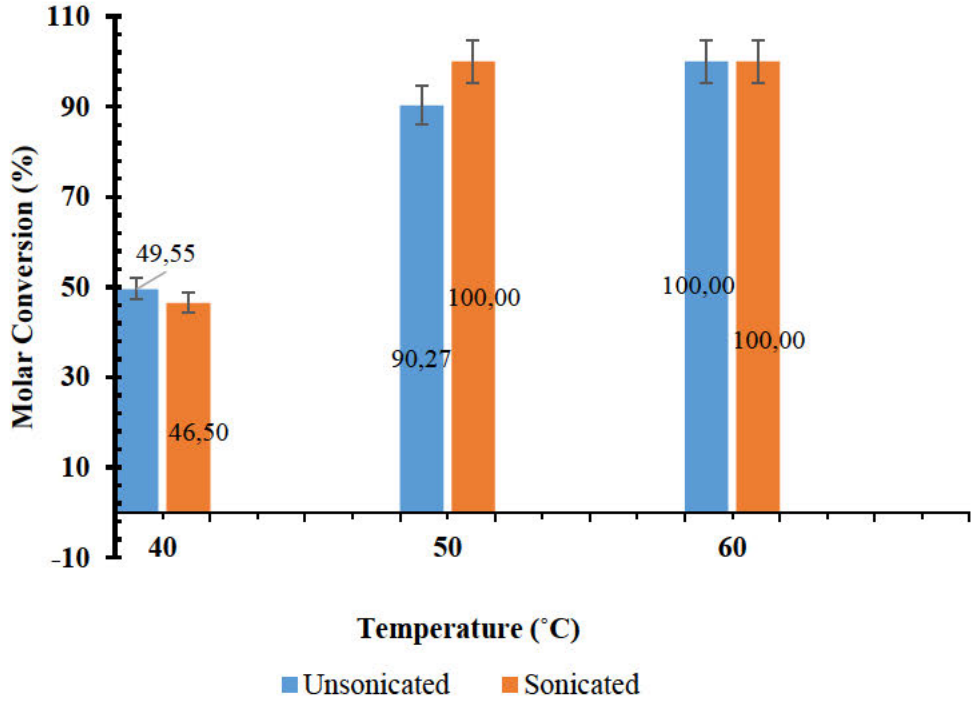

Figure B 4: Conversion versus temperature for run 1 part one.

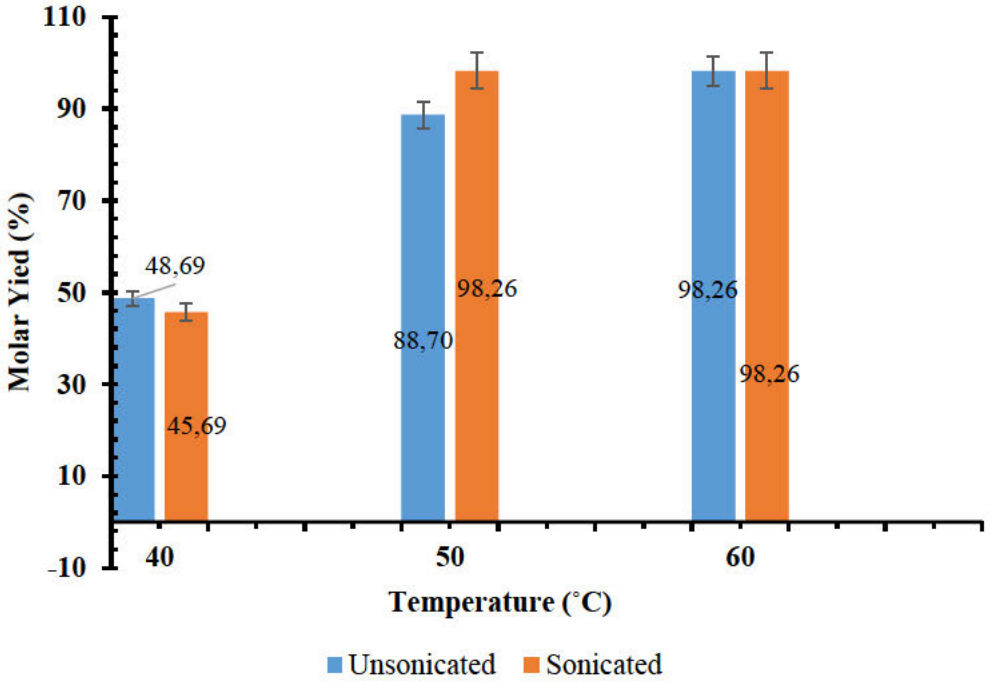

Figure B 5: Yield versus temperature for run 1 part one.

Run Two

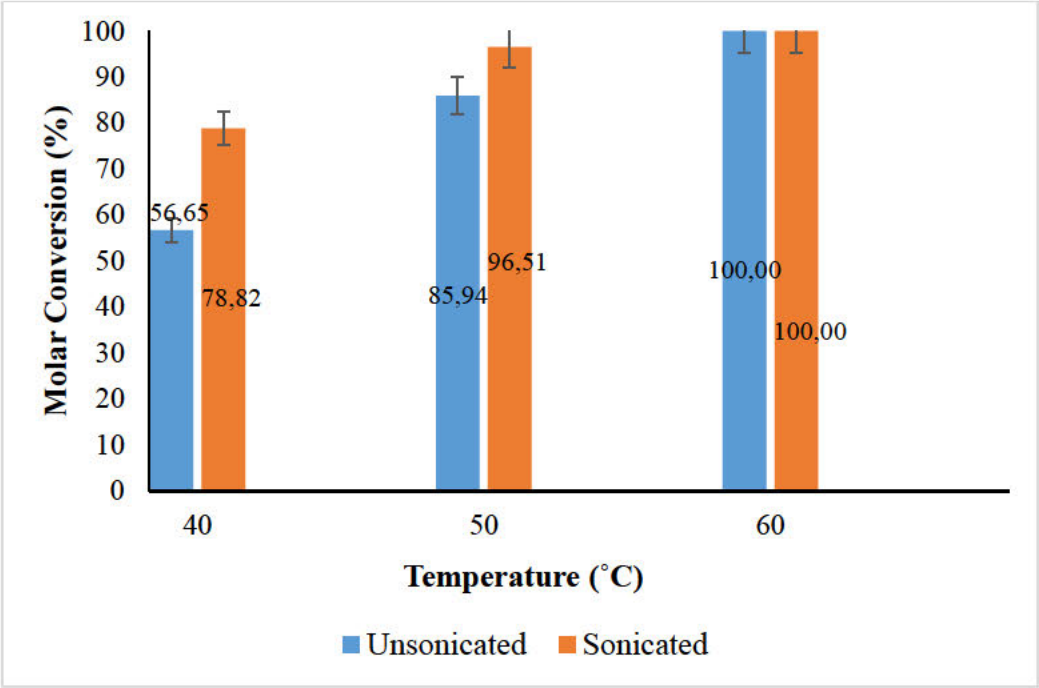

Figure B 6: Conversion versus temperature for run 2 part one.

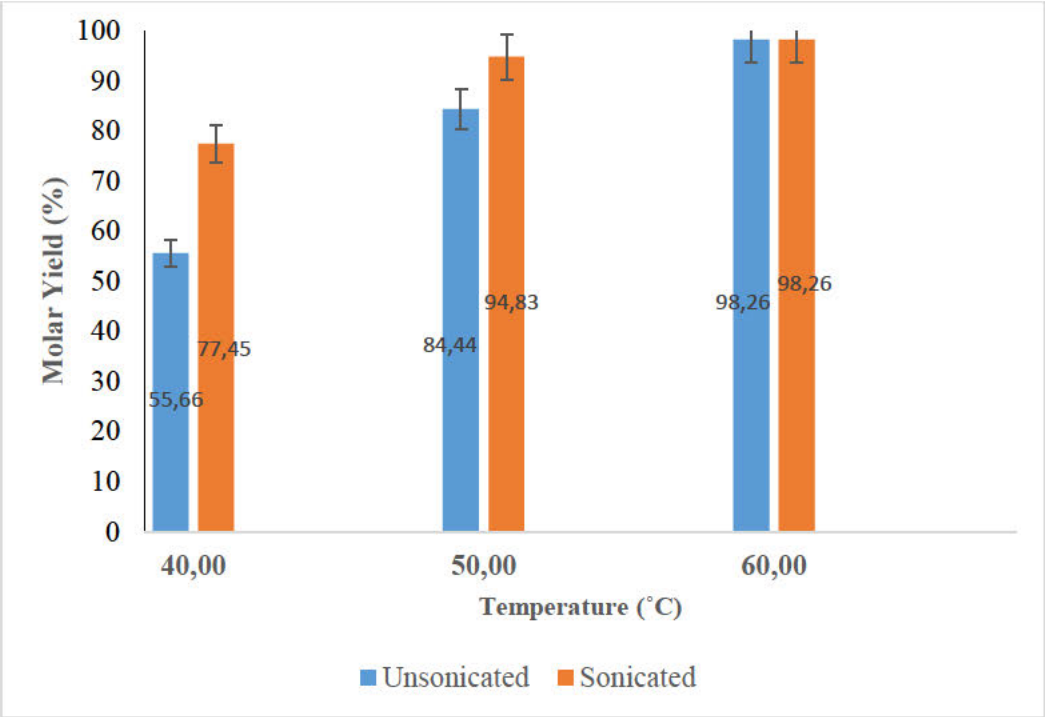

Figure B 7: Yield versus temperature for run 2 part one.

More catalyst deactivation results summary:

Table B 1: Summary of results for the TEM-EDX coking analysis.

Carbon deposition (%) in 2 hours		
Temperature (˚C)	**Unsonicated**	**Sonicated**
40	20.22	22.13
50	45.40	41.62
60	13.79	34.06

Appendix C: Statistical Analysis

Residual plot:

A residual plot was determined for the GC-FID calibration. The following calculation is based on a sample 1 with excess octane liquid, consisting of 1.0 g 1-octene and 2.0 g octane.

The residual is defined as the difference between the actual and predicted value of some variable 'y'. In this case, 'y' represents the area ratio of 1-octene to octane.

$$Residual = \frac{y_{actual} - y_{predicted}}{y_{actual}} \times 100$$

The y_{actual} value is calculated using the areas obtained from the GC-FID chromatograph:

$$y_{actual} = \frac{Area_{1-octene}}{Area_{octane}} = \frac{24267232.0}{47991334.0} = 0.5057$$

The $y_{predicted}$ value is calculated using the calibration equation:

Calibration equation: $y = 0.0415x^2 + 0.898x$

Where y represents the area ratio and x represents the mass ratio.

$$x = \frac{m_{1-octene}}{m_{octane}} = \frac{1}{2} = 0.5$$

$$\therefore y_{predicted} = 0.0415(0.5)^2 + 0.898(0.5) = 0.4594$$

Hence,

$$Residual = \frac{y_{actual} - y_{predicted}}{y_{actual}} \times 100$$

$$= \frac{0.5057 - 0.4594}{0.5057} \times 100$$

$$= 9.16\%$$

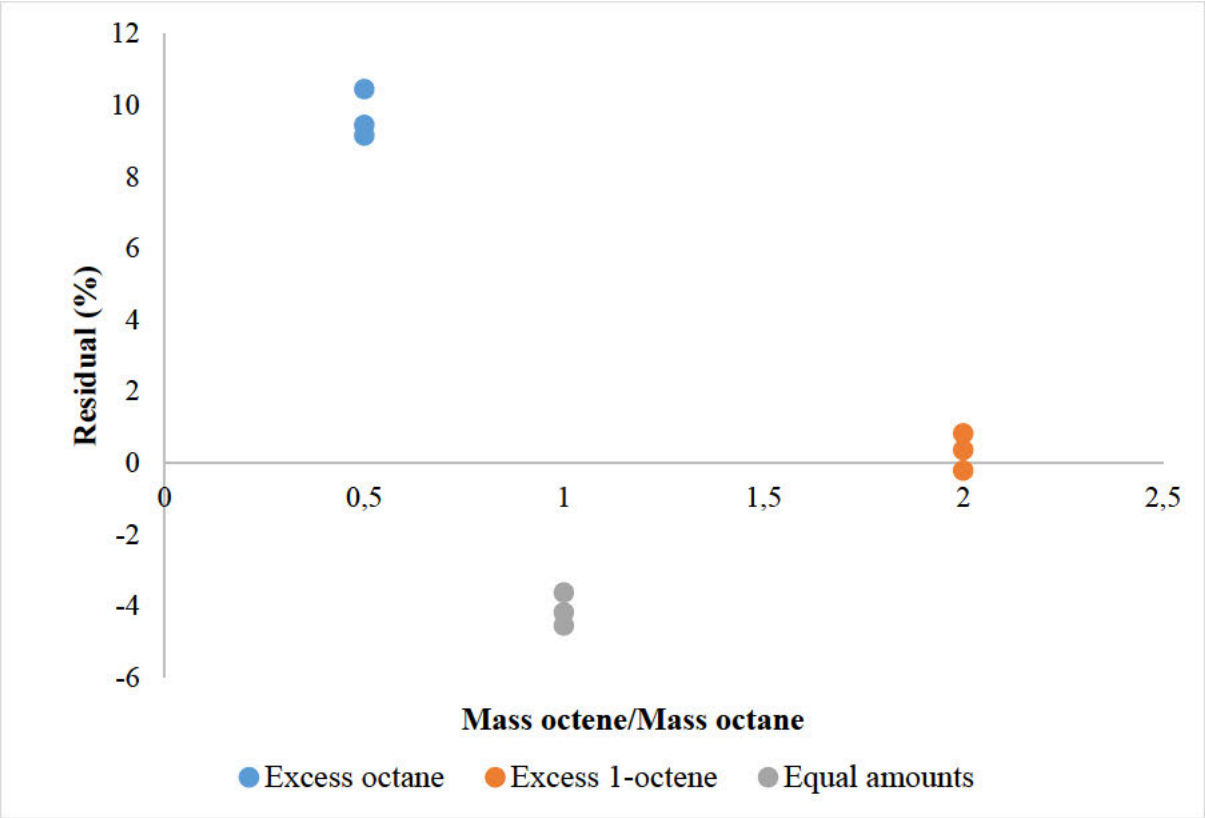

Figure C. 1: Residual plot.

Error Bars:

The error bars displayed on the graphs for part one and part two were determined via a statistical method. The following calculation was performed for the conversion of 1-octene for part one run 1 at 50ºC unsonicated.

The relative error (σ) was first determined:

$$\sigma = abs(x) \times \sqrt{\left(\frac{\sigma_m}{m}\right)^2 + \left(\frac{\sigma_x}{x}\right)^2}$$

Where $\frac{\sigma_m}{m}$ = relative error in the mass measurement = 3×10^{-6}

$\frac{\sigma_x}{x}$ = relative error from the residual = 0.0474

abs(x) = absolute average conversion for a run

$$\therefore \sigma = abs(x) \times \sqrt{(3 \times 10^{-6})^2 + (0.0474)^2}$$

$$\sigma = abs(x) \times 0.0474$$

The conversions for each sample of part one run 1 at 50ºC unsonicated was calculated using the method previously stated and is summarized in the table below:

Table C 1: Conversion for each sample for part one run 1 unsonicated reactions at 50 ºC.

Sample	Conversion (%)
1.1.	90.37
1.2.	90.34
1.3.	90.15

Therefore, the absolute average conversion of the samples can be determined:

$$abs(x) = \frac{90.37 + 90.34 + 90.15}{3} = 90.29\%$$

$$\therefore \sigma = abs(x) \times 0.0474 = 90.29\% \times 0.0474 = 4.28\%$$

Similarly, for part one run 2 50ºC unsonicated:

$$abs(x) = 85.94\%$$

$$\sigma = 4.08\%$$

These relative error bars can be seen on the temperature versus conversion and temperature versus yield graphs for each run.

To obtain the standard error of the mean for the graph of temperature versus average conversion of both runs, the standard deviation of both runs had to be determined.

For part one at 50 ºC unsonicated:

Run 1: $abs(x) = 90.29\%$

Run 2: $abs(x) = 85.94\%$

The standard deviation of a sample (S_x) is obtained from the following equation:

$$S_x = \sqrt{\frac{\sum_{i=1}^{n}(x_i - \bar{x})^2}{n-1}}$$

Where $\bar{x}$ = is the absolute average conversion of both runs $= \frac{90.29+85.94}{2} = 88.12\%$

n = number of data points = 2

$$\therefore S_x = \sqrt{\frac{(90.29 - 88.12)^2 + (85.94 - 88.12)^2}{2-1}} = 3.07\%$$

The above method was repeated for the yield versus temperature graphs.

Using the data for unsonicated reactions at 50 ºC:

- Run 1: 90.37%
- Run 2: 90.34%
- Run 3: 90.15%

1. The mean ($\overline{x}$):

$$\overline{x} = \frac{90.37 + 90.34 + 90.15}{3} = 90.29\%$$

2. The standard deviation (S_x):

$$S_x = \sqrt{\frac{(90.37 - 90.29)^2 + (90.34 - 90.29)^2 + (90.15 - 90.29)^2}{2}} = 0.1193$$

3. And therefore, the Standard Error of the Mean (SEM):

$$\text{SEM} = \frac{S_x}{\sqrt{3}} = 0.0689\%$$

This is smaller compared to the relative error since this does not take into account the effect of the approximations used by the model to calculate the conversion and yields.

Appendix D: Sample Calculation using masses:

Gas Chromatography Calibration:

The following sample calculation is for an equal volume mixture of 1-octene and octane. First the volume ratio of 1:1 had to be converted to a mass ratio. This was accomplished by making use of the densities of 1-octene and octane.

$$Density\ of\ 1-Octene = 0.715\frac{g}{ml}$$

$$Density\ of\ Octane = 0.703\frac{g}{ml}$$

$$\therefore since\ density = \frac{mass}{volume}, \frac{m_{1-octene}}{m_{octane}} = \frac{\rho_{1-octene}}{\rho_{octane}} \times \frac{volume_{1-octene}}{volume_{octane}}$$

$$\frac{m_{1-octene}}{m_{octane}} = \frac{0.715}{0.703} \times \frac{1}{1} = 1.017$$

The areas of the respective octane and 1-octene peaks were obtained using the manual peak integration tool on the GC-FID system. An average area from all three samples was determined.

$$\frac{Area_{1-octene}}{Area_{octane}} = \frac{6219.1 + 14930.9 + 13194.4}{6872.2 + 15092.6 + 13867.8} = 0.949$$

The area and mass ratios for the other 2 mixtures were similarly calculated. A calibration curve of the area ratios vs the mass ratios was then plotted for the three mixtures. A quadratic trendline was fitted to the data with an equation of $0.1607x^2 + 0.6667x + 0.1042$ and an R^2 value of 1. The calibration curve can be seen in Figure B3.

Hydrogenation Reactions

The sample calculation presented below was performed for the unsonicated run at a temperature of 40^0C.

The following assumptions were made:

- On the chromatogram, peak one represents 1-octene after the hydrogenation reaction has occurred.

- On the chromatogram, peak two to peak four are all regarded as octane and its isomers and are grouped together and collectively referred to as the hydrogenated product.
- The total mass of system remains constant.
- The mass of hydrogen in the system is negligible.

Table D 1: Raw data for unsonicated run at 40 °C.

Peak Number	**Area**
1	66078.6
2	1065.5
3	377.4
4	237.4

Based on the above assumptions, the following relationship can be stated:

$$\frac{Area_{peak\ 1}}{Area_{\ peak\ 2+peak\ 3+peak\ 4+peak\ 5}} = \frac{Area_{1-octene,out}}{Area_{HP}}$$

$$\therefore \frac{Area_{1-octene,out}}{Area_{HP}} = \frac{66078.6}{1065.5 + 377.4 + 237.4} = 39.325$$

The mass ratio can then be found using the calibration curve.

Calibration equation: $y = 0.1607x^2 + 0.6667x + 0.1042$

Where y represents the area ratio and x represents the mass ratio.

To determine the mass ratio the calibration equation was rearranged with y= 39.325 yielding:

$$\therefore 39.325 = 0.1067x^2 + 0.6667x$$

$$0 = 0.1067x^2 + 0.6667x - 39{,}2208$$

Solving for x of the above equation using the quadratic formula:

$$x = \frac{-b \pm \sqrt{b^2 - 4ac}}{2a}$$

$$x = \frac{-0.6667 \pm \sqrt{0.6667^2 - 4(0.1067)(-13{,}2208)}}{2(0.1067)}$$

$$x = 13.685$$

$$\therefore \frac{m_{1-octene,out}}{m_{HP}} = 13.685$$

Initially, only 1-octene and hydrogen gas were fed into the reactor. The mass of hydrogen fed was assumed to be negligible as hydrogen is a light gas. The initial volume of 1-octene fed was 30ml.

Density of 1-octene = $\rho_{1-octene} = 0.715\ g/ml$

$$m_{1-octene,in} = density \times volume = (0.715) \times 30 = 21.45\ g$$

$$m_{1-octene,in} = Total\ mass\ in$$

The mass of hydrogen added into the system was assumed to be negligible.

Total mass was assumed constant, therefore:

$$Total\ mass\ in = m_{1-octene,in} = Total\ mass\ out$$

$$Total\ mass\ out = m_{1-octene,out} + m_{HP}$$

$$\therefore 21.45 = m_{1-octene,out} + m_{HP}$$

From the quadratic formula:

$$\frac{m_{1-octene,out}}{m_{HP}} = 13.685$$

$$\therefore m_{1-octene} = 13.685 \times m_{HP}$$

Using simultaneous equations, the mass of hydrogenated product out can then be determined:

$$21.45 = (13.685 \times m_{HP}) + m_{HP}$$

$$21.45 = 14.685 m_{HP}$$

$$m_{HP} = \frac{21.45}{14.685} = 1.46\ g$$

$$\therefore m_{1-octene} = 19.98\ g$$

Converting from a mass basis to mol basis using the molar masses of the respective components:

Molar mass of 1-octene = $M_{r\text{1-octene}}$ = 112.24 g/mol

Molar mass of octane = $M_{r\text{octane}}$ = 114.23 g/mol

Number of moles can be calculated: $n = \frac{m}{M_r}$

$$n_{1-octene,in} = \frac{m_{1-octene,in}}{M_{r_{1-octene}}} = \frac{21.45}{112.24} = 0.1911\ mol$$

$$n_{1-octene,out} = \frac{m_{1-octene,out}}{M_{r_{1-octene}}} = \frac{19.98}{112.24} = 0.1781\ mol$$

Hence, the molar conversion can be obtained:

$$molar\ conversion\ (\%) = \frac{n_{1-octene,in} - n_{1-octene,out}}{n_{1-octene,in}} \times 100$$

$$= \frac{0.1911 - 0.1781}{0.1911} \times 100$$

$$= 6.81\ \%$$

Furthermore, the yield of the hydrogenated product can then be determined:

$$Yield\ (\%) = \frac{Actual\ moles\ HP\ formed}{Theoretical\ moles\ HP} \times 100\%$$

The actual and theoretical number of moles of HP can be calculated:

$$Actual\ moles\ of\ HP = \frac{m_{HP}}{M_{r_{octane}}} = \frac{1.46}{114.23} = 0.0128\ mol$$

The overall hydrogenation reaction is: $C_8H_{16} + H_2 \rightarrow C_8H_{18}$

From stoichiometry, one mole of 1-octene forms 1 mole octane i.e. hydrogenated product.

$$\therefore Theoretical\ moles\ of\ HP = 0.1911\ mol$$

Therefore,

$$Yield = \frac{0.0128}{0.1911} \times 100\%$$

$$= 6.69\%$$

Similarly, the conversion and yield were calculated for the remaining two samples resulting in an average conversion of 6.80% and yield of 6.68%.